1993

Petrography and inorganic geochemistry of the Rosebud coal seam at the Absaloka, Big Sky and Rosebud mines, Powder River Basin, Montana

Lingbu Kong
University of North Dakota

PETROGRAPHY AND INORGANIC GEOCHEMISTRY OF THE ROSEBUD COAL SEAM AT THE ABSALOKA, BIG SKY AND ROSEBUD MINES, POWDER RIVER BASIN, MONTANA

by

Lingbu Kong
Bachelor of Science, Hebei College of Geology, 1982
Master of Science, Chinese Academy of Geological Sciences, 1985

A Thesis

Submitted to the Graduate Faculty

of the

University of North Dakota

in partial fulfillment of the requirements

for the degree of

Master of Science

Grand Forks, North Dakota
May
1993

This thesis, submitted by Lingbu Kong in partial fulfillment of the requirements for the Degree of Master of Science from the University of North Dakota, has been read by the Faculty Advisory Committee under whom the work has been done and is hereby approved.

(Chairman)

This thesis meets the standards for appearance, conforms to the style and format requirements of the Graduate School of the University of North Dakota, and is hereby approved.

Dean of the Graduate School

4-29-93

PERMISSION

Title Petrography and Inorganic Geochemistry of the Rosebud Seam at the Absaloka, Big Sky and Rosebud Mines, Powder River Basin, Montana

Department Geology and Geological Engineering

Degree Master of Science

In presenting this thesis in partial fulfillment of the requirements for a graduate degree from the University of North Dakota, I agree that the library of this University shall make it freely available for inspection. I further agree that permission for extensive copying for scholarly purposes may be granted by the professor who supervise my thesis work or, in his absence, the Chairperson of the department or the Dean of the Graduate School. It is understood that any copying or publication or other use of this thesis or part thereof for financial gain shall not be allowed without my written permission. It is also understood that due recognition shall be given to me and to the University of North Dakota in any scholarly use which may be made of any material in my thesis.

Signature _____

Date _____

TABLE OF CONTENTS

LIST OF ILLUSTRATIONS

Figures

LIST OF TABLES

ACKNOWLEDGMENTS

This study was funded by Fuels and Materials Science Group of the University of North Dakota Energy and Environmental Research Center (EERC).

I would like to extend my appreciation to my thesis committee members, Dr. Frank Karner (chairman), Dr. Steven Benson, and Dr. Ronald Matheny, who gave unselfishly of their time, wisdom, and support through this project, to Mr. Edward Steadman, who gave valuble advices and support in the development of this project and to Dr. James Hower of the Center for Applied Energy Research, University of Kentucky, who trained me in maceral analysis.

I acknowledge the cooperation and help in sampling from Mr. Bill Weaver of the Absaloka mine, Mr. Michael Altavilla of the Big Sky mine, and Ms. Kathy Dorin of the Rosebud mine.

I would also like to thank Mr. Bruce Folkedahl, Mr. David Brekke and Mr. Kevin Galbreath for their help in SEM lab work, and Mr. Stoney Gan (U.T. Austin) for field assistance.

ABSTRACT

Quantitative maceral and microlithotype analyses, huminite reflectance measurements and inorganic constituent analyses of the samples of the Rosebud subbituminous coal seam from the Absaloka, Big Sky and Rosebud Mines were used in the interpretation of the depositional environment of the seam and for prediction of ash formation during combustion. The mean huminite reflectance varies from 0.31% at the Rosebud Mine to 0.34% at the Absaloka Mine and 0.39% at the Big Sky Mine, indicating that the coal rank is transitional from lignite to subbituminous C. Despite the variation in huminite reflectance, samples from the three mines are similar in mean content of huminite (76 to 81 vol%), liptinite (4 to 6 vol%) and minerals (3 to 4 vol%), but somewhat variable in inertinite (10 to 16 vol%). A direct correlation of mean huminite reflectance with mean huminite abundance and an inverse correlation with mean inertinite abundance suggests a possible correlation between coalification and floral precursors.

Within-seam variations in petrographic composition and huminite reflectance are high. Lithologic layering with similar sequence and thickness in the Absaloka and Big Sky profiles is delineated by petrographic variation, suggesting similar geological histories for the two sites. A depositional environment transitional between reed

marsh and forest swamp in a fluvial-deltaic system, is suggested for the Rosebud seam based on interpretation of microlithotype and maceral compositions.

Clay minerals, quartz and calcite are the most abundant mineral phases in the Rosebud seam. Except for the top 0.3 m, the seam at the Big Sky Mine has mean pyrite content as low as 0.4 wt%. A phosphate mineral, crandallite(?), occurs as an abundant authigenic mineral in some layers. Crandallite and associated kaolinite, quartz, zircon, rutile and apatite, may have originated from volcanic ash.

Maceral-associated inorganic elements have significant abundance in ulminite, fusinite and detrogelinite. The most abundant element is Ca, followed by Al, S, Mg, Si, Cl and Na. These elements in macerals are interpreted either as ions associated with carboxylate groups or as coordination complexes in the maceral molecular structure and are a major contributor to low-temperature fouling deposits in utility boilers firing the Rosebud coal.

1. INTRODUCTION

This investigation integrates optical maceral analysis, vitrinite (huminite) reflectance measurement and chemical analysis of inorganic constituents using scanning electron microscopy/electron probe microanalysis (SEM/EPMA) to characterize the petrography and inorganic geochemistry of the Rosebud subbituminous coal seam. The results of these analyses are used for geological interpretation and for prediction of coal ash formation and deposition during combustion. This research was coordinated with studies of U. S. western low-rank coals undertaken by the Fuels and Materials Science Research Group of the University of North Dakota Energy and Environmental Research Center (UNDEERC).

The Rosebud seam at Absaloka, Big Sky and Rosebud mines, Montana, was selected because the Powder River Basin is one of the most important U. S. western low-rank coal reserves. The Tertiary Powder River Basin in southeastern Montana and northern Wyoming (Figure 1) contains over 20 subbituminous coal seams, 10 of which are mined at 24 sites, 7 in Montana and 17 in Wyoming (Energy Resources Co. Inc., 1980). In Montana, over 90 percent of the present coal production is from the Powder River Basin, where these coals which have low sulfur content and high reactivity are of great commercial value for generation of electrical power by

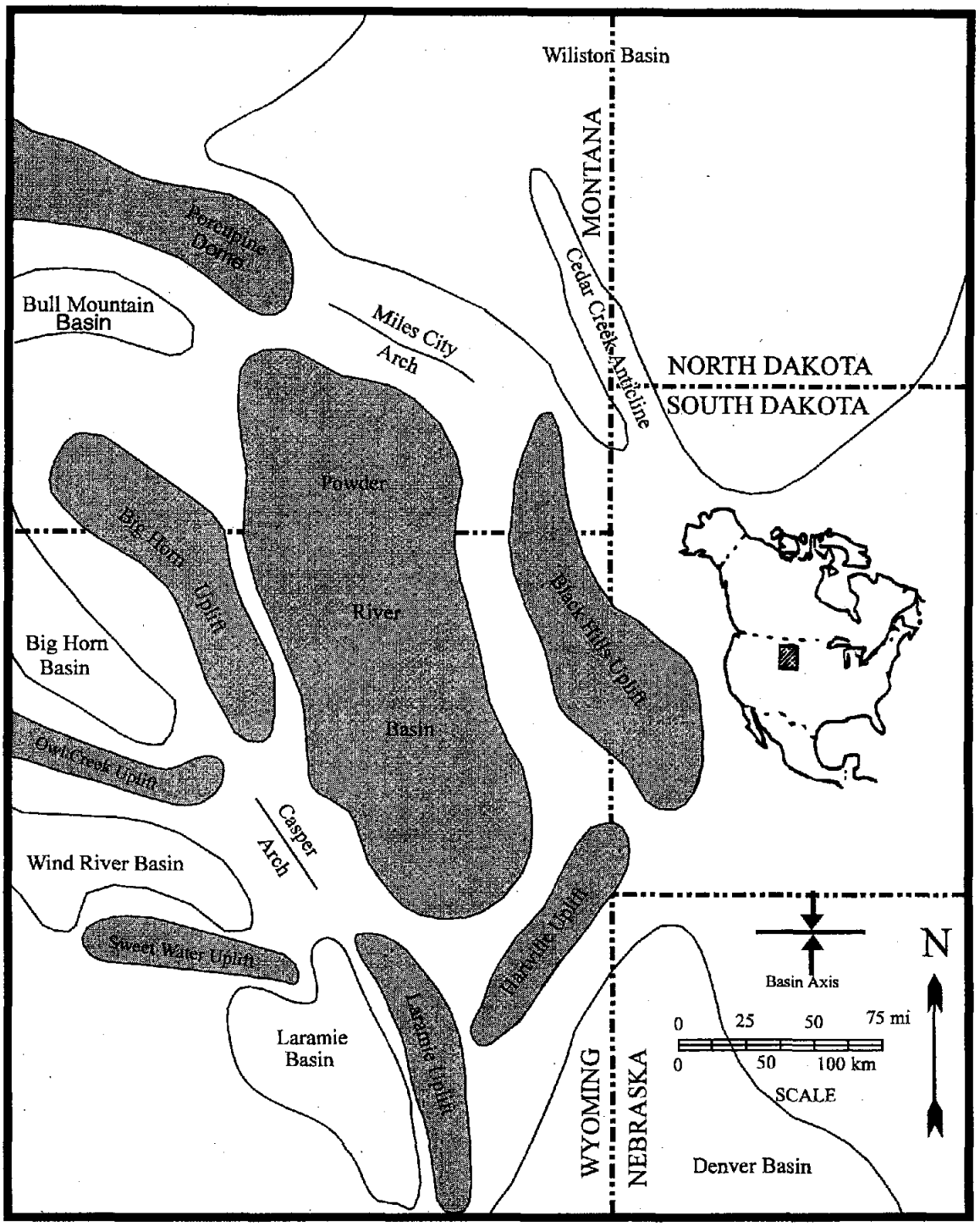

Figure 1. Index map showing the location of the Powder River Basin and present tectonic elements (from Ayers and Kaiser, 1984).

combustion. Although the Powder River Basin coals are expected to continue as an important part of the nation's energy supply and have general geologic significance, a relatively small number of studies on the petrography and geochemistry have been done (Chao and others, 1984; Crowley and others, 1992; Moore, 1986, 1991; Moore and others, 1990; Rich and others, 1988; Stanton and others, 1989; Warwick and Stanton, 1988). Continued extensive use of these coals as well as the development of advanced utilization processes require more complete understanding of their physical and chemical characteristics.

The specific objectives of this research are: 1) to characterize the Rosebud seam by coal petrography using combined maceral and microlithotype analyses and vitrinite (huminite) reflectance measurements; 2) to characterize the inorganic constituents, including both minerals and inorganic elements associated in major macerals; 3) to interpret the data geologically; and 4) to provide petrographic and geochemical data that can be used to predict the effects of coal quality on coal utilization system performance.

Macerals are direct indicators of ancient flora. Detailed physical and chemical characterization of both macerals and inorganic constituents can aid in the interpretation of depositional environments and associated chemical processes, diagenesis, and coalification history of low-rank coals. Detailed coal petrography and inorganic geochemistry are also important for utilization. Maceral composition is the primary factor affecting coal reactivity, which is important in understanding coal combustion, gasification and liquefaction. Inorganic constituents often cause

environmental and operational problems during coal utilization. Western low-rank coals contain a large proportion of organically bound inorganic elements in addition to mineral phases. Both minerals and organically bound inorganic elements are important in determining ash formation and deposition behavior in utility boilers fired by low-rank coals. Trace metals such as As, Se, Co, Ni, Cd, Hg and Pb in coals may produce toxic emissions from coal power plants. Investigations of the distribution of these elements in coal and their behavior during combustion have been an ongoing project.

2. PREVIOUS WORK

2.1 Coal Petrography

Previous work in coal petrography is reviewed by Stach and others (1982) and by Bustin and others (1983). The information in this section is derived from these two references unless noted otherwise.

Coal microscopy forms the basis for coal petrography. Though coals had been microscopically studied by the end of nineteenth century, the most significant pioneering contributions to coal microscopy were made in the early 1900's. White and Thiessen (1913) published the first comprehensive treatise of coal microscopy. Thiessen (1920) published his most important work with 160 plates showing numerous photomicrographs of thin-sections of coal. Stopes (1919) described four rock types in bituminous coal, making distinctions between vitrain, clarain, durain and fusain; in 1935, she suggested using "maceral" for the microscopically discernible constituents of coal. This has become the primary basis of coal petrography.

Stach pioneered the application of reflected light with oil immersion to coal petrography. He introduced polished blocks and their microscopic examination using oil immersion objectives in 1927, and in 1928, developed a method of preparing polished surfaces of ground coal samples which has become standard method for coal petrographic analysis. Because oil immersion greatly enhances microscopic resolution,

examination of polished surfaces has been commonly used in coal petrographic research since the 1930's, so that now thin-section study is no longer recommended, except for special purposes.

The International Committee for Coal Petrology (ICCP) was formed in 1953 and began to work for standardization of nomenclature. The European nomenclature, known as Stopes--Heerlen System, has been accepted as standard nomenclature (ICCP, 1957, 1963, 1971, 1975). The American nomenclature, known as Thiessen--Bureau of Mines and Spackman System, has also been included in the International Handbook of Coal Petrography and related to the Stopes--Heerlen System.

Since the 1960's, coal petrography has expanded to include many specialized areas with significant applications to coal origin and use. It is now a multi-faceted discipline, including research on the chemical and physical properties of macerals, the petrography of peat, the source materials (kerogen) of oil and gas, relationship of petrography to the sedimentology and coalification of coal seams, and relationship to technological applications such as coking, liquefaction and combustion.

2.2 Inorganic Constituents in Coal

Inorganic constituents include minerals and organically bound inorganic elements. Only about 15 minerals are abundant in coals, although over 100 are known to occur (Harvey and Ruch, 1984). Typically three to four phases make up most of the minerals (Zygarlicke and Steadman, 1990). Common phases include clay minerals, carbonates, oxides, hydroxides, sulfides, sulfates, phosphates, silicates and

salts (Stach and others, 1982). Maceral-associated inorganic elements are abundant in low-rank coals. These elements are most probably as cations associated with oxygen functional group or/and as coordination complexes in maceral molecular structure (Given, 1984; Given and Miller, 1987).

Previous work on coal minerals was reviewed by Zygarlicke (1987). The literature pertaining to coal minerals is voluminous but primarily focused on high-rank coals. Parr (1932) used total sulfur and ash contents to calculate the percent of minerals in coal. Comprehensive, pioneering studies of minerals in coal were done by Ball (1935) on the Herrin coal seam of the Illinois Basin, and Sprunk and O'Donnell (1942) who petrographically examined over 3,000 thin sections from about 100 coals.

Much earlier work simply determined the types and relative abundance of minerals. More recently, research on coal mineralogy has emphasized mineral origins (Cecil and others, 1978; Davis, 1984; Karner and others, 1984; Zygarlicke, 1987) and ash transformation in combustion systems (Sarofim and others, 1977; Jones and Benson, 1987; Zygarlicke, 1987; Weisbecker and others, 1992;). Previous studies suggested that minerals in coal be classified as detrital, syngenetic, and epigenetic (Mackowsky, 1968). Detrital minerals are those that were deposited in the early swamp environment by wind or water. Syngenetic minerals formed during early peat stages or before seam compaction and consolidation was complete. Epigenetic minerals are mainly those that formed in pores, cavities, and fractures in coal, after compaction and consolidation (Harvey and Ruch, 1984; Mackowsky, 1968).

Usually minerals make up several volume percent of coal composition. The paucity, dissemination and generally small size of the minerals in coal has made identification difficult. The development of analytical tools such as scanning electron microscope/electron probe microanalysis systems (SEM/EPMA) allows direct quantitative analysis. Computer-controlled scanning electron microscopy (CCSEM) has been used to determine quantitatively the abundance, size, and association of minerals in coal (Zygarlicke and Steadman, 1990). Detailed information from CCSEM is being used for input into computer codes to predict coal ash formation and behavior during combustion (Benson and others, 1992).

Extensive use of U. S. western lignite and subbituminous coals in recent years has led to increased studies of inorganic constituents of low-rank coals. Fowkes (1978) investigated the inorganic constituents of 22 lignite and subbituminous coal samples from the Montana-Wyoming-Dakota region and concluded that most of the inorganic constituents were fixed in coal as "organometallic" components by chelation or by ionic bonding. He noted that high-rank coals had more discrete mineral inclusions than low-rank coal and usually exhibited a very small inorganic fraction that was bound to the coal by chelation or ionic forces. He assumed that, given the correct conditions for coalification, young coals through time lose their sites for ionic or chelation bonding of metallic ions and, therefore, high-rank coals which have undergone extensive coalification have less organically bound inorganic matter.

Additional studies on inorganic constituents of U. S. western low-rank coals include those by Benson and others (1984), Benson and Holm (1985), Karner and

others (1982, 1984, 1986a), and Zygarlicke (1987). These studies focused on North Dakota lignite. Little work has been done on subbituminous coal. Zygarlicke (1987), from study of minerals in the Harmon lignite, concluded that most minerals in the lignite were detrital and that variable ash deposition during combustion might be caused by variations in types and quantities of minerals.

As organically bound inorganic elements play an important role in prediction of ash behavior during combustion of low-rank coals, scientists working on coal geology and utilization began to investigate the elements associated with low-rank coal macerals in late 1970's. Previous workers used chemical fractionation techniques to analyze organically bound inorganic elements of bulk samples (Benson and Holm, 1985). The limitation of this method is that it can not provide any information on the relationship between elements and macerals. SEM/EPMA has been applied to inorganic elements in macerals (Harris and others 1977; Raymond and Gooley, 1978; Karner and others, 1986b, 1987; Harrison, 1991; Demir and Harvey, 1991; Folkedahl and others, 1992). The current analytical procedure is to obtain optical photographs and identify the macerals before doing SEM/EPMA. The macerals can then be located using backscattered electron-imaging. This procedure is done manually at present and automation is under development.

2.3 Powder River Basin Subbituminous Coal

Investigations of the geology of the Powder River Basin subbituminous coals began in hte 1920's (Rogers and Lee, 1923; Baker, 1928; Dobbin, 1930; Knappen and

Moulton, 1930; Bass, 1931; Pierce, 1936), but studies on the depositional environment of the coal bearing formations and the coal petrography were not done until the 1980's. Studies on the depositional environment of Fort Union and Wasach Formations by Flores (1981, 1982, 1986), Flores and Ethridge (1985), Ayers (1986), and Ayers and Kaiser (1984) concluded that the coal-bearing sequence was deposited in a lacustraine and fluvial-deltaic depositional system.

Several studies of the petrography and inorganic geochemistry of Powder River Basin subbituminous coals have been published. Kanza (1983) analyzed maceral composition for a sample from the Rosebud mine, Montana. Chao and others (1984) studied the petrography of the Big George coal bed in Wyoming. Chao and other used maceral nomenclature of high-rank coal in their study, which is not recommended by the International Committee for Coal Petrology (ICCP) for the study of subbituminous coal. More detailed work on the coal petrography of the Smith, Wyodak and Anderson-Dietz seams was done by Moore (1986, 1990), Warwick and Stanton (1988), Stanton and others (1989) and Moore and others (1990). In addition to using the ICCP recommended maceral classification system, Moore (1990) regrouped the maceral types into genetic categories on the basis of their inferred origin and statistical association with one another.

Even fewer studies have been completed on inorganic constituents of the Powder River Basin subbituminous coals. Benson and Holm (1985) studied one Rosebud coal sample using chemical fractionation. Triplehorn and others (1991) found minerals derived from air-fall volcanic ash in two mineral-rich layers in the

Wyodak-Anderson seam in the Wyoming part of the Powder River Basin. Crowley and others (1992) studied the distribution of 46 elements in 76 coal and rock samples of the Anderson-Dietz seam and determined the relation of these elements with detrital and volcanic ash components by cluster analysis. Quantitative mineral analysis for five Powder River Basin coal samples was done by Weisbecker and others (1992) using CCSEM. Their results show that in addition to clay minerals, quartz and pyrite, a calcium-aluminum phosphate mineral (crandallite?) is abundant in these samples.

3. GENERAL GEOLOGY OF THE POWDER RIVER BASIN

3.1 Geologic and Structural Setting

The Powder River Basin is an asymmetrical broad syncline with its axis along the western side (Figure 1). Geology, stratigraphy and coal resources of the basin were described by Dobbin (1930), Noyes (1978), Energy Resource Co. Inc. (1980), Ayers and Kaiser (1984), Flores and Ethridge (1985), Ayers (1986) and Flores (1986).

More than 3900 m of Phanerozoic sediments overlie the Precambrian basement in the Powder River basin (Ayers, 1986). In the Early Cretaceous, stable marine shelf conditions were dominant, but by Late Cretaceous the Fox Hills and Hell Creek (Lance in Wyoming) Formations (Figure 3) recorded a shift toward paralic environments as the epicontinental sea retreated in response to the Laramide orogeny. The Laramie uplifts provided immediate source areas for more than 1500 m of lacustrine and fluvial-deltaic Paleocene Fort Union sediments (Ayers, 1986). The Fort Union Formation crops out around most of the margin of the basin (Figure 2); it is overlain by the predominantly fluvial Eocene Wasatch Formation, which exceeds 300 m in thickness along the basin axis (Ayers, 1986; Flores, 1986). Both Fort Union and Wasatch Formations host commercial coal seams.

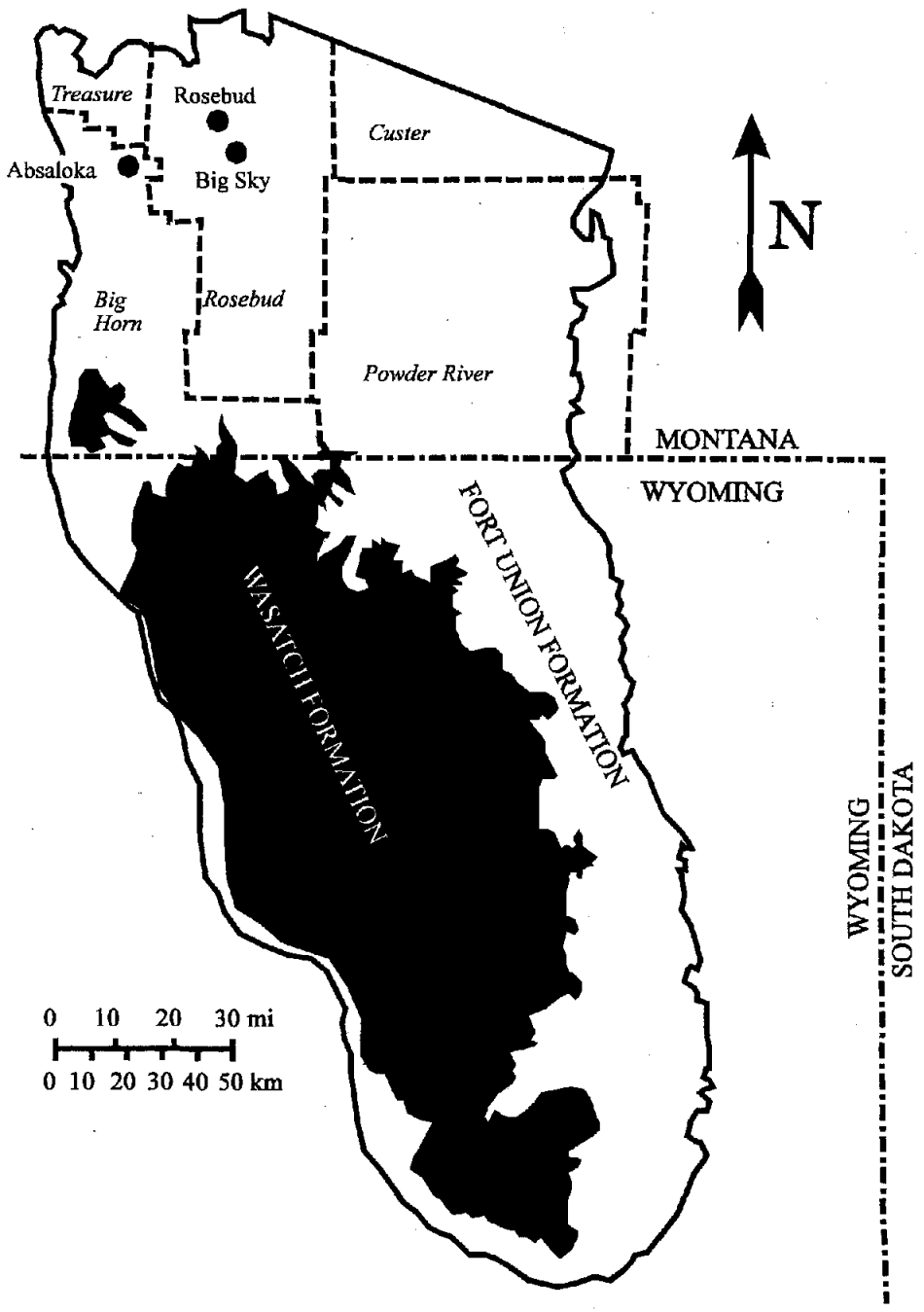

Figure 2. Geologic map of the Powder River Basin, Montana and Wyoming, showing the locations of the Absaloka, Big Sky and Rosebud mines, modified from Ayers and Kaiser (1984).

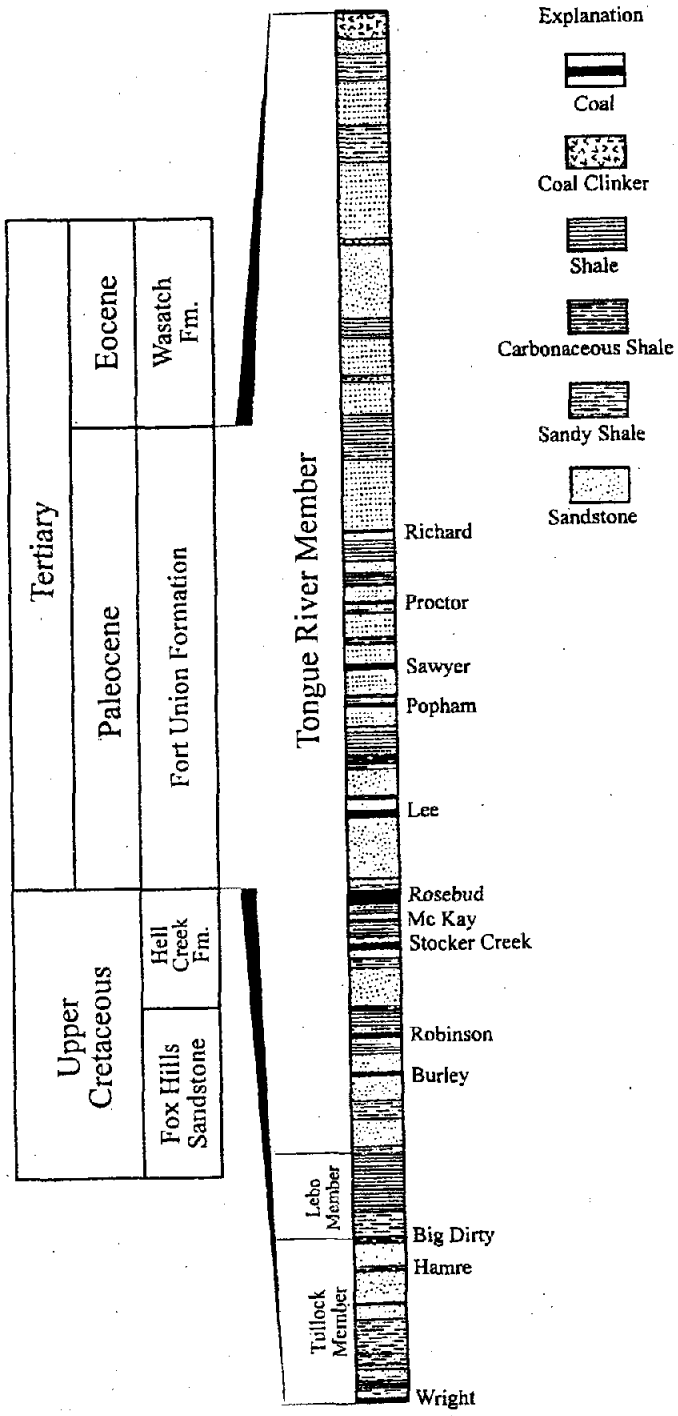

Figure 3. Stratigraphic column of the Fort Union Formation in the Big Sky and Rosebud mines area, showing the positions of coal beds (after Dobbin, 1930).

3.2 Stratigraphy of the Fort Union Formation

The Fort Union Formation is composed of three coal-bearing members which are, from older to younger, the Tullock, Lebo and Tongue River Members (Figure 3). The total thickness of the Fort Union Formation is 609 to 638 m in Rosebud and Big Sky mine areas (Dobbin, 1930). In the Montana portion of the basin, 11 coal beds are found in the Tullock Member and two in the Lebo. In places the Tongue River Member contains as many as 20 coal beds, some of which are as much as 12 m thick (Energy Resource Co. Inc., 1980). The Wyoming portion of the Powder River Basin contains the thickest coal seams in the United States, with some seams averaging 21 m in thickness (Noyes, 1978).

The Tullock Member of the Fort Union Formation consists of sequential beds of sandstone, sandy and carbonaceous shale and numerous thin impure coal beds. Its thickness is fairly uniform throughout the study area and ranges from 72 to 81 m (Dobbin, 1930). Although 10 lenticular coal beds are found in the Tullock Member, none is of adequate quantity and quality to be economically recoverable.

The Lebo Member of the Fort Union Formation is made up of dark-gray to black clay and shale, largely of volcanic origin (Dobbin, 1930). It contains beds of soft, gray cross-bedded sandstone, some of which may be as much as 3 m thick, but none is persistent for more than a hundred meters. Many ironstone concretions occur in the Lebo in great number. Some of the ferruginous concretionary layers are fairly persistent horizon markers. The top of the member is drawn at the point where there is a change from somber-colored clay to yellow sandstone and sandy shale. Except

for the basal coal bed, called the "Big Dirty", the Lebo is devoid of coal beds. The basal Big Dirty coal bed has been used as fuel by local ranchers, but in most places it contains so much carbonaceous shale that it produces too much ash to be of commercial value. The thickness of the Lebo Member at Rosebud and Big Sky mine area ranges from 32 to 51 m (Dobbin, 1930).

The Lebo Member shale grades upward through a transition zone of sandy shale into a group of beds of light-colored sandstone, sandy shale, carbonaceous shale, and coal, which constitute the Tongue River Member of the Fort Union formation. The Tongue River Member is 506 m thick in the study area (Dobbin, 1930). The lower 47 m contains no workable coal. The succeeding 180 m, however, contains 8 coal beds ranging in thickness from 1 to 9 m. Above is about 300 m of sandstone, sandy shale, and thin but persistent coal beds.

The Rosebud and McKay seams are part of the Tongue River Member. The Rosebud seam is about 108 m above the base of the member. Dobbin (1930) considered the McKay seam as a split of the Rosebud seam for many measurements showing the McKay seam was less than 2.3 m below the Rosebud seam. The maximum observed interval between the Rosebud and McKay seams is 9 m. At the Big Sky mine the Rosebud seam is 8 m thick, and the McKay seam, which is 6 m below, is 2.5 m thick. At the Absaloka mine the two are combined with a thickness of 9 m.

3.3 Stratigraphy of the Wasatch Formation

The Eocene Wasatch Formation overlies the Fort Union Formation along the basin axis in Wyoming. It is about 150 m thick along the Montana-Wyoming border, where it consists of multicolored claystone, sandstone and shale (Energy Resource Co. Inc., 1980). The Wasatch Formation also contains commercial grade coals in Wyoming.

4. SAMPLING

A sequence of stratigraphically controlled specimens was obtained by channel sampling at the Big Sky and Rosebud mines and by drill core at the Absaloka mine. Eight meters of the entire seam was collected at the Big Sky mine; 5.1 m of the 7.5 m thick seam at the Rosebud mine; and 9 m of the whole seam at the Absaloka mine. Sampling method and amount were determined by accessibility and safety considerations. The entire seam at Big Sky is accessible for channel sampling. At the Rosebud mine, however, the bottom 2.4 m of the seam is not accessible because it is not exposed at the sampling site. Channel sampling was not permitted at the Absaloka mine.

The channel sampling method described by Swanson and Huffman (1976) was used. A standard channel is 30 cm wide and 10 cm deep. In actual practice, however, it is difficult to sample in such a standard channel. A ladder was used to access the highwall sections at the Big Sky and Rosebud open pits. The profiles were measured, photographed and divided into intervals on the basis of observable characteristics before sampling. The criteria used to determine the sampling intervals were bedding, parting and relative luster. Samples were collected beginning at the top of the highwall by knocking off the coal with a geologic hammer along a channel. A plastic tarp was put on the bottom to catch the coal.

The sample drill at Absaloka mine penetrated the whole seam and went 0.5 m into the underclay. Samples of each were taken at 0.3 m intervals. All core and channel samples were sealed in heavy-duty plastic zipper storage bags and stored in plastic buckets for shipping. Upon arrival in Grand Forks, the samples were stored in a freezer before grinding and preparation of epoxy-coal pellets for petrographic and inorganic constituent analyses.

5. COAL PETROGRAPHY

5.1 Megascopic Description

5.11 Nomenclature

Two nomenclature systems for megascopic description of coal lithotypes in banded humic coal have been developed. Stopes (1919) presented four ingredients of banded bituminous coal, vitrain, clarain, durain and fusain. Thiessen (1929) suggested three main megascopic components of coal, anthraxylon, attritus and fusain. The characteristics of fusain are agreed upon by both Stopes and Thiessen. Stopes' vitrain, clarain and durain, however, are not exactly equivalent to Thiessen's anthraxylon and attritus. The disagreement comes from the manner of the development of each system. Stopes' system was developed by describing different layers of coal from their appearance, whereas Thiessen's terms were made to suggest the origin of the different types of materials that coal contains. The durain described by Stopes is hard, dull and granular material with flecks or hair-like streaks of bright coal. Clarain is different from durain by containing more vitreous bands or lenses. Thiessen's attritus is essentially synonymous with Stopes' clarain and durain, suggesting that they originated as an assortment of vegetable debris including small splinters of wood, cellular structures, spores, pollen grains, cuticles and bark. Stopes'

vitrain is described as being a black, vitreous, structureless band, that may split up to small cube-like segments, and has well-marked conchoidal fracture on curved irregular faces. Thiessen's anthraxylon is similar to vitrain except that anthraxylon has microscopic cellular structure. Thiessen suggested that anthraxylon originated from woody material. He agreed that vitrain is anthraxylon but did not agree that vitrain is structureless.

A modified nomenclature system was given by Schopf (1960). He adopted Stopes' vitrain and Thiessen's attritus and suggested vitrain, fusain, and attrital coal for banded humic coal of higher rank. For lignite, he suggested pre-vitrain instead of vitrain. He also suggested "impure coal" to describe mineral-rich lithotypes and "parting" to describe discrete bands of mineral sediments interbeded with coal.

The ICCP adopted Stopes' nomenclature. The descriptions of the four lithotypes were given by ICCP (ICCP, 1963, 1971), Stach and others (1975, 1982), and Bustin and others (1983). The following are the descriptions derived from Stach and others (1982).

Vitrain

Vitrain is black and of bright luster. Frequently it is brittle and crossed by fine cracks, and consequently it breaks cubically and tends to concentrate in the fines when a coal seam is mined. Thick vitrain layers show conchoidal fractures. In macroscopic description of seams, only the very bright layers with a thickness of at least several millimeters (3 - 10) are recorded as vitrain, whereas thinner layers are

counted as clarain. In humic coals, vitrain is widely distributed. It consists of vitrite and clarite V (see Table 4).

Clarain

The term clarain designates very finely stratified coal layers with a thickness of at least several millimeters (3 - 10), having a luster between that of vitrain and durain. Clarain is the most common macroscopic constituent of humic coals. It consists of alternating thin layers of vitrain, durain and sometimes also of fusain. Clarain can include vitrite, clarite, durite, trimacerite and fusite (Table 4).

Durain

Durain can be black or gray. It is always dull. Black durain can have a faintly greasy luster. Durain is very hard and consequently breaks into big lumps. Its fractured surfaces are rough. Only layers more than several millimeters (3 - 10) thick are recorded as durain; thinner dull bands are recorded as clarain. Durain is composed of the microlithotypes durite and trimacerite, and sometimes also of exinite-rich clarite (Table 4).

Fusain

Fusain closely resembles wood charcoal. It has silky luster, is black, frequently somewhat fibrous and usually soft and friable enough to rub off when handled. Less frequently, hard fusain consisting of hard fusite (Table 4) impregnated with mineral

matter can be recognized microscopically. Soft fusain consists of soft fusite with empty cell lumens. Usually, fusain is present in the form of lenses, some millimeter-thick and some centimeter-long.

The Stopes-ICCP nomenclature is used in this research. Schopf's terms "impure coal" and "parting" are also used.

5.12 Description of the Rosebud Seam

The megascopic description of the Rosebud coal seam is based on the samples from the Big Sky mine. Samples from the Rosebud mine have not been described because they do not represent the whole seam. Most of the Absaloka core samples are too friable to describe well. For the purpose of better observation of lithotypes, polished slabs of coal samples were prepared following the Pennsylvania State University procedure (The Penn. State Univ. Coal Research Section, 1983). Instead of paraplex P-43 cold setting plastic, epoxy resin was used to mount the slabs.

Descriptions of the Big Sky samples are given in Figure 4. Clarain is the most abundant lithotype of the coal. Although the thickest vitrain bands can be as thick as 3 to 5 cm, they are usually 1 to 2 mm, too thin to count. Fusain always appears as thin lenses and is often seen on surfaces of a hand specimens because it is soft and therefore tends to be the breaking site. Recognition of fusain is easier using hand specimens than polished surfaces because of its silky luster and fibrous, charcoal-like appearance. Impure coal occurs as hard, dull layers with a gray-brownish color.

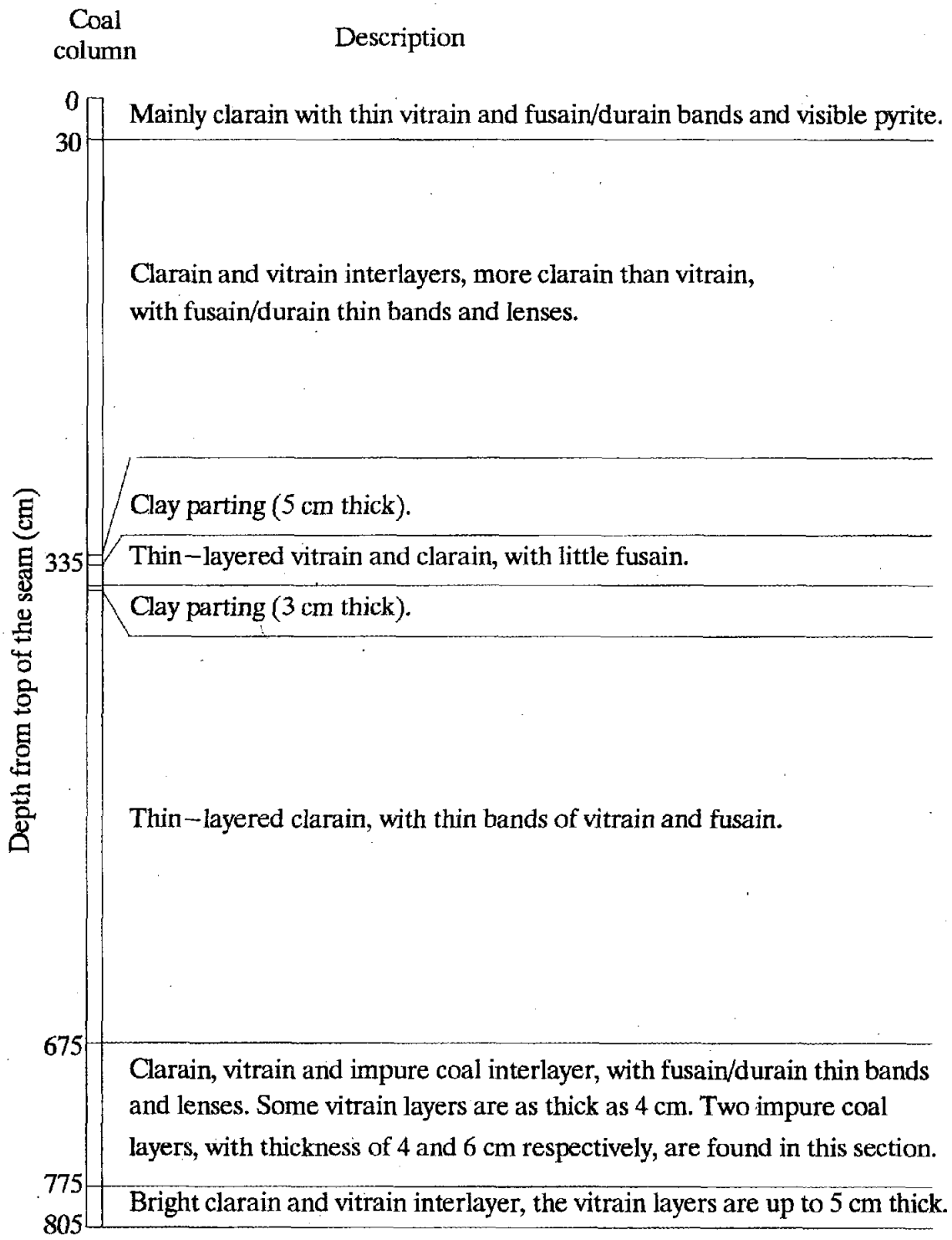

Figure 4. Megascopic description of the Rosebud seam at the Big Sky mine.

Microscopically, clay minerals are the main components of impure coal. Durain was not identified in hand specimens. Some thin "dull" bands and lenses which were found on polished slabs were confirmed by microscopic inspection to be fusinite with mineral cell-filling. Two clay partings separated by a 13 cm interval occur in the Rosebud seam at the Big Sky mine. The lower parting is 3 cm thick and located at 4.5 m above the base of the seam. The upper is 5 cm thick. At the Rosebud mine, the two partings may correspond to a single, 3.5 cm thick parting 5.1 m above the base. A 5 cm clay parting was also found at Absaloka mine 4 m above the base of the Rosebud-McKay seam. Comparison and correlation of the three profiles will be discussed in the section on microscopic petrography.

5.2 Microscopic Petrography

5.21 Terminology

Just as inorganic rocks are composed of minerals, coals are described as composed of macerals. Macerals are defined as the microscopically recognizable organic components of coal. Three different maceral groups for both high rank and low rank coals are described by ICCP (1963, 1971, 1975), Stach and others (1982) and Bustin and others (1983). Table 1 is the ICCP maceral classification for hard coals and Table 2 for brown coals and lignites. In addition to the macerals listed in Table 2, a few new macerals, such as exsudatinite and fluorinite, are introduced by Stach and others (1982).

Table 1. Maceral classification of hard coals (after International Committee for Coal Petrology, 1971, 1975)

Maceral Group	Maceral	Maceral Type
Vitrinite	Telinite	Telinite 1
		Telinite 2
	Collinite	Telocollinite
		Gelocollinite
		Desmocollinite
		Corpocollinite
	Vitrodetrinite	
Exinite	Sporinite	
	Cutinite	
	Resinite	
	Alginite	
	Liptodetrinite	
Inertinite	Micrinite	
	Macrinite	
	Semifusinite	
	Fusinite	Pyrofusinite
		Degradofusinite
	Sclerotinite	
	Inertodetrinite	

Table 2. Maceral classification of brown coals and lignites (after International Committee for Coal Petrology, 1971, 1975)

Maceral Group	Maceral Subgroup	Maceral	Maceral Type
Huminite	Humotelinite	Textinite	
		Ulminite	Texto–ulminite
			Eu–ulminite
	Humodetrinite	Attrinite	
		Densinite	
	Humocollinite	Gelinite	Porigelinite
			Levigelinite
		Corpohuminite	Phlobaphinite
			Pseudo–phlobaphinite
Liptinite	Sporinite		
	Cutinite		
	Resinite		
	Suberinite		
	Alginite		
	Liptodetrinite		
	Chlorophyllinite		
	Bituminite		
Inertinite	Fusinite		
	Semifusinite		
	Macrinite		
	Sclerotinite		
	Inertodetrinite		

Maceral groups differ in reflectance. Liptinite- (exinite-) group macerals have the lowest reflectance, vitrinite (huminite for low rank coals) macerals intermediate, and inertinite macerals the highest. The reflectance of a maceral may vary with chemical composition. For maceral groups of the same rank, liptinite contains more hydrogen, vitrinite more oxygen, and inertinite more carbon. Macerals of the same group are differentiated from one another by their morphology and structure, which reflect the type of original plant materials. Fluorescence is also used to distinguish the liptinite-group macerals.

Huminite-group macerals of low rank coals (brown coals and lignites) are the precursors of vitrinite macerals of high rank coals (bituminous coals and anthracite). The correlation of the macerals of these two groups is given in Table 3.

Nomenclature for subbituminous coals is not as well developed as for other coal types. The nomenclature for brown coals and lignites is employed in the study of subbituminous coals but is not completely suitable for them. An example is the maceral forming the groundmass of microlithotype clarite and some vitrinertite and trimacerite. If present in bituminous coals, this maceral would be called desmocollinite. Several similar terms were used for this maceral by different individuals studying low-rank coals, including densinite (Kalkreuth and others, 1991a), levigelinite (Kanza, 1983), and eu-gelinite (Moore and others, 1990). Referring to the definitions of the maceral types of the humocollinite subgroup in by Stach and others (1982), densinite is not the right term for describing this maceral since it is more gelified and has an appearance similar to desmocollinite. Eu-gelinite is defined as a

Table 3. Correlation of the huminite macerals of brown coals with the vitrinite macerals of hard coals (after International Committee fof Coal Petrology, 1971, 1975)

Brown Coal					Hard Coal		
Maceral Group	Maceral Subgroup	Maceral	Submaceral	Maceral Variety	Submaceral	Maceral	Maceral Group
Huminite	Humotelinite	Textinite		A (dark)	Telinite 1	Telinite	Vitrinite
				B (light)			
		Ulminite	Texto–ulminite	A (dark)			
				B (light)			
			Eu–ulminite	A (dark)			
				B (light)	Telinite 2		
	Humodetrinite	Attrinite				Vitrodetrinite	
		Densinite			Desmocollinite	Collinite	
	Humocollinite	Gelinite	Levi–gelinite Detrogelinite				
			Levi–gelinite Telogelinite		Telocollinite		
			Eugelinite		Gelocollinite		
			Porigelinite				
		Corpo–huminite	Phlobaphinite				
			Pseudo–Phlobaphinite				

maceral filling cavities such as shrinkage cracks, cleats and completely decomposed plant organs, and is a the suitable term for this maceral. Levigelinite is a sub-group name for maceral types detorgelinite, telogelinite and eu-gelinite, and therefore is not preferred for this maceral. Detrogelinite is the most suitable term, and preferred in this study.

Associations of macerals are termed microlithotypes (Stach and others, 1982). Microlithotypes are subdivided into three groups, i.e. monomaceral, bimaceral and trimaceral microlithotypes. The ICCP has agreed upon two conventions, the minimum band width of 50 microns and the so-called "5% rule". The minimum band width of 50 microns means that in analysis a microlithotype can only be recorded when it has a band width of at least 50 microns or covers a minimum surface of 50 X 50 microns. The "5%" rule is that a maceral has to be considered in naming or modifying a microlithotype when its abundance reaches 5% or more. Table 4 gives a classification of the microlithotypes of hard coal and their maceral composition. In addition to the microlithotypes defined in Table 4, a microlithotype group carbominerite is defined for coals with over 5 vol% pyrite or 20 vol% other mineral-matter.

5.22 Sample Preparation

Coal samples used for maceral and inorganic constituent analysis were prepared into epoxy pellets following standard ASTM (1988a) procedures. Half of each coal sample was split by the cone and quarter method, air dried for 24 hours,

Table 4. Summary of microlithotypes (after International Committee for Coal Petrology, 1971, 1975)

Maceral composition (mineral–free)		Microlithotype	Maceral–group composition (mineral–free)	Microlithotype group
Monomaceral				
Co	>95%	(Collite)*		
T	>95%	(Telite)*	V > 95%	Vitrite
VD	>95%			
S	>95%	Sporite		
Cu	>95%	(Cutite)*		
R	>95%	(Resite)*	E (L) > 95%	Liptite
A	>95%	Algite		
LD	>95%			
Sf	>95%	Semifusite		
F	>95%	Fusite		
Sc	>95%	(Sclerotite)*	I > 95%	Inertite
ID	>95%	Inertodetrite		
M	>95%	(Macroite)*		
Bimaceral				
V + S	>95%	Sporoclarite		
V + Cu	>95%	Cuticloclarite	V + E(L) > 95%	Clarite
V + R	>95%	(resinoclarite)*		V, E(L)
V + LD	>95%			
V + M	>95%			
V + Sf	>95%			
V + F	>95%		V + I > 95%	Vitrinertite
V + Sc	>95%			V, I
V + ID	>95%			
I + S	>95%	Sporodurite		
I + Cu	>95%	(Cuticlodurite)*		
I + R	>95%	(Resinodurite)*	I + E(L) > 95%	Durite
I + LD	>95%			I, E(L)
Trimaceral				
V, I, E	>5%	Duroclarite	V > I, E(L)	Trimacerite
		Vitrinertoliptite	E > I, V	V, I, E(L)
		Clarodurite	I > V, E(L)	

Co = Collinite; T=Telinite; VD = Vitrodetrinite; S = Sporinite; Cu = Cutinite; R = Resinite; A = Alginite; LD = Liptodetrinite; M = Macrinite; Sf = Semifusinite; F = Fusinite; Sc = Sclerotinite; Id = Inertodetrinite; V = Vitrinite; E = Exinite; L = Liptinite; I = Inertinite.

* The terms in parentheses are not presently in use.

and then crushed to pass a 20 mesh screen. Approximately 10-gram samples were split from each sample using a dual sample splitter. The 10-gram aliquots were vacuum dried for 24 hours at a pressure of 10 to 15 micrometers of mercury to remove moisture. Three grams were split and used to form a pellet with 4.5 grams of premixed epoxy resin and hardener. The coal and epoxy mixture was placed into a 1 inch diameter mold. After curing, the pellets were ground using a progression of 240, 320, 400, 600 and 800 grit diamond paper disks, and polished using 1-micron diamond paste and 0.3- and 0.05-micron gamma alumina polishing compound. Samples were cleaned in an ultrasonic bath for 5 minutes between each stage.

5.23 Analytical Methods

A Nikon optical microscope equipped with both white light and fluorescence blue light sources, a mechanical stage, and a P-1 photometer was used for maceral and microlithotype analysis and huminite reflectance measurement. The maceral and microlithotype analysis followed the combined maceral and microlithotype point count procedure in Stach and others (1982) and Bustin and others (1983).

A 20-point crossed-lined eye piece is recommended for combined maceral and microlithotype analysis. A 20-point graticule, with a designed edge length of 50 microns, is used for quantitative determination of maceral associations. The 50-micron edge length and the resulting 5 vol% represented by each of the 20 square areas correspond to the so-called 50 microns and 5% rules in microlithotype classification. Unfortunately, such an eye piece was not available in this research. A

50 X 50 micron area around the cross hairs and the volume percent of each maceral in the area had to be estimated. At least 500 points for both macerals and microlithotypes on each sample are required in order for the result to be representative.

Random huminite reflectance was measured on eu-ulminite B at a wavelength of 546 nm. Five Pennsylvania State University glass reflectance standards (Table 5) were used for calibration. The photometry system was calibrated before measurement of each sample. A coordination line of the reflectance values and corresponding photometer reading numbers of the standards (Figure 5) was used to calculate the reflectance of samples. An equation obtained from the coordination line was used to convert photometer readings to reflectance values. Since the coordination line is not perfectly straight, the equation for each segment is slightly different. Except for a very small number of low values, all measurements are between those of standards 1 and 2; therefore the equation for the line segment between these two standards was used to convert measured values to reflectance values as follows:

$$R = 0.138V - 0.1978$$

where V is the photometer reading, and R is the determined reflectance value.

Accuracy of reflectance measurements can be assumed to be given by the linearity of the standard reflectance values versus their corresponding photometer reading values. The closer the coordination line (Figure 5) to a straight line, the more accurate the measurements. The accuracy of the reflectance measurements is considered fairly high as the coordination line in Figure 5 is very close to a straight

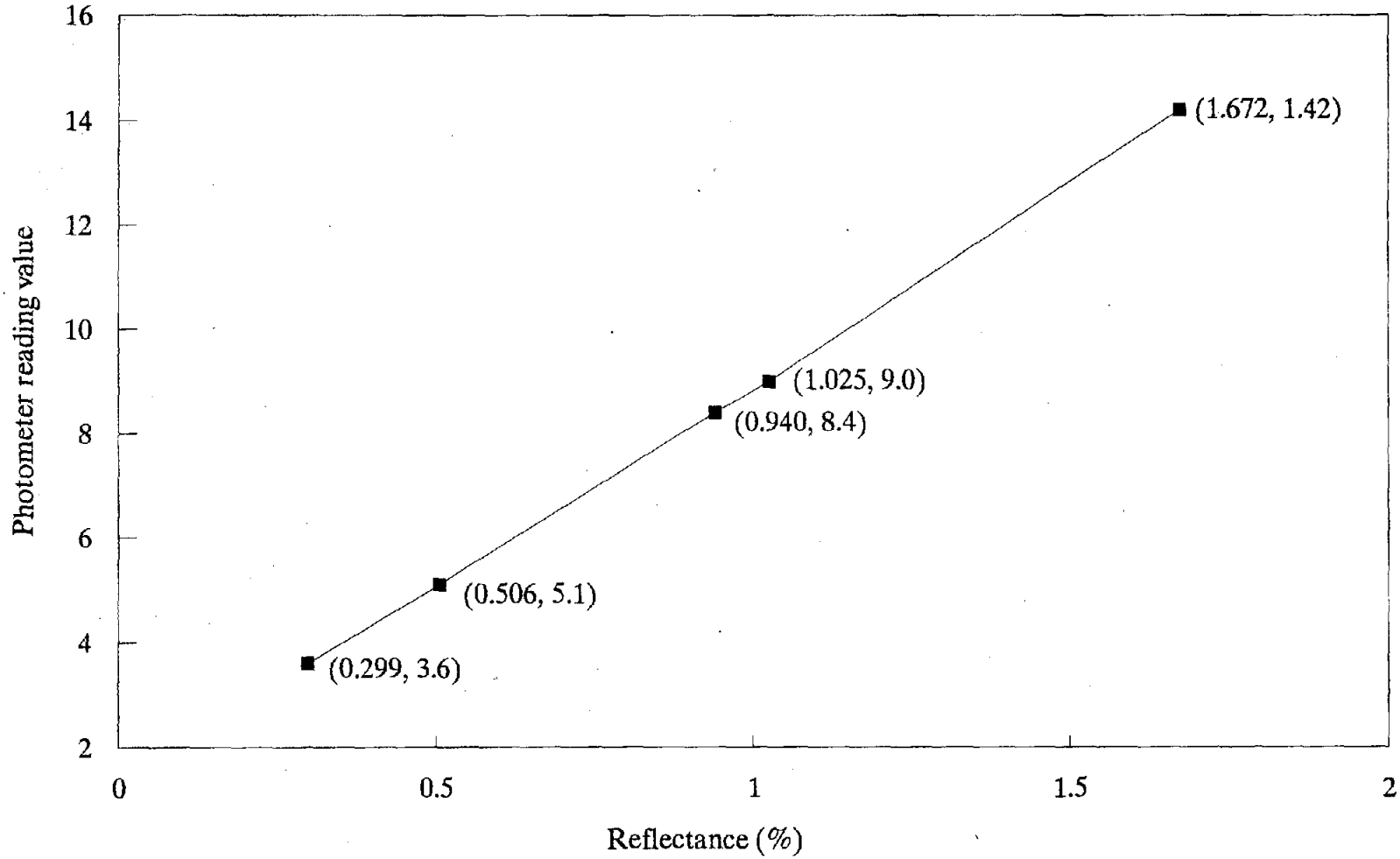

Figure 5. Correlation of photometer readings with the reflectances of standards.

line. The precision of the measurements was checked by repeated measurement on two selected samples (Table 6). The mean reflectance values and standard deviations of the repeated measurements for each sample are identical, indicating dependable precision.

Table 5. Refractive index and reflectance of the glass standards

Glass No.	Refractive Index	Reflectance Calculated	Reflectance Determined
1	1.6945	0.3026	0.299
2	1.7477	0.4958	0.506
3	1.8400	0.9207	0.940
4	1.8567	1.0085	1.025
5	1.9670	1.6618	1.762

Accuracy of maceral and microlithotype analysis was discussed in detail by Stach and others (1982). The accuracy of the analyses is described in terms of the reproducibility and the comparability of the results. The results of two analyses made by one operator on the same polished surface should not differ by more than 3 vol% for any maceral or maceral group. For analyses made on two different specimens of the same sample the results should not exceed 4 vol% for any maceral or maceral group. The results of two repeated or comparative analyses on microlithotypes should not differ by more than 6 vol% for any microlithotype.

Table 6. Results of repeated random huminite reflectance measurements for two Big Sky mine samples.

Sample No.	B09 FM	B09 RM	B10 FM	B10 RM
RRL(%)	0.34	0.36	0.47	0.41
	0.34	0.34	0.45	0.45
	0.40	0.34	0.44	0.43
	0.36	0.40	0.41	0.45
	0.37	0.36	0.41	0.45
	0.38	0.37	0.41	0.43
	0.38	0.38	0.41	0.47
	0.34	0.38	0.43	0.47
	0.37	0.34	0.43	0.47
	0.38	0.37	0.44	0.48
	0.38	0.38	0.41	0.44
	0.36	0.38	0.44	0.45
	0.38	0.36	0.43	0.40
	0.36	0.38	0.44	0.45
	0.37	0.36	0.43	0.41
	0.36	0.37	0.44	0.40
	0.37	0.36	0.38	
	0.36	0.37	0.44	
	0.40	0.36	0.41	
	0.38	0.40	0.37	
	0.40	0.38	0.48	
	0.38	0.40	0.48	
	0.40	0.38	0.41	
	0.36	0.40		
	0.34	0.36		
	0.38	0.34		
	0.37	0.38		
	0.37	0.37		
	0.38	0.37		
		0.38		
MRRL(%)	0.37	0.37	0.43	0.44
STD	0.018	0.018	0.026	0.026

RRL = randam reflectance; MRRL = mean randam reflectance; STD = Standard deviation; FM = first measurement; RM = repeated measurement.

Table 7. Results of repeated maceral and microlithotype analyses for two Big Sky mine samples

Sample No.	B01 FA	B01 RA	Diff.	B04 FA	B04 RA	Diff.
Textinite	1	0	1	2	1	1
Ulminite	26	31	5	30	35	5
Attrinite	1	1	0	0	0	0
Densinite	1	1	0	0	0	0
Detrogelinite	35	37	2	50	48	2
Phlobaphinite	0	0	0	0	0	0
Total Huminite	64	69	5	82	85	3
Sporinite	1	2	1	4	3	1
Cutinite	0	0	0	2	0	0
Resinite	0	1	1	0	0	0
Liptodetrinite	1	1	0	1	2	0
Total Liptinite	3	4	1	7	6	1
Fusinite	6	3	3	4	2	2
Semifusinite	7	7	0	1	2	1
Sclerotinite	0		0	1	0	1
Inertodetrinite	6	4	2	2	2	0
Total Inertinite	19	14	5	8	7	1
Pyrite	8	7	1	0	0	0
Other Minerals	5	6	1	2	2	0
Total Minerals	13	13	0	2	2	0
Vitrite	33	32	1	39	40	1
Inertite	7	7	0	4	3	1
Clarite	9	10	1	33	31	2
Huminertite	17	19	2	4	2	2
Durite	0	0	0	0	0	0
Trimcerite	21	17	4	18	20	2
Carbominerite	13	16	3	2	3	1

The results are given in vol%.
FA = first analysis; RA = Repeated analysis; Diff = difference between two analyses.

Table 7 lists the results of repeated analyses on two Big Sky samples. The differences of the two results for all macerals except ulminite are within 3 vol%, and the differences for all microlithotype within 4 vol%. One possible reason causing a difference for ulminite larger than 3 vol% is that ulminite, including eu-ulminite and texto-ulminite, is transitional with textinite, and the division between them is somewhat arbitrary. If these two macerals are combined, the difference of the total content between the two results is 3 vol% for sample B01 and 4 vol% for sample B04. Another possible reason is that 500 points counted in analysis cover only about half of the area of the pellet surface. If the repeated analyses were not done on same area, the results might be different. An independent test of accuracy was not made but the author's identification of macerals was verified by Hower (1992, personal communication).

5.24 Results

5.241 Coal Rank

The Rosebud seam at the Rosebud and Big Sky mines has been classified as a subbituminous B coal according to the Btu content calculated on a moist, mineral-free basis (Cole, 1980). However, the huminite reflectance measurements (Table 8 and Figures 6 and 7) indicate that its rank is transitional from lignite to subbituminous C (Kong and others, 1992, 1993). The Big Sky samples have the highest huminite reflectance values, ranging from 0.37% to 0.44% with an average

Table 8. Petrographic composition and huminite reflectance of the Rosebud seam samples

Sample No.	A01	A02	A03	A04	A05	A06	A07	A08	A09	A10	A11	A12	A13	A14	A15	A16	A17
Textinite	0	1	1	1	0	1	3	2	0	1	1	3	1	2	1	1	0
Ulminite	51	52	34	36	55	27	31	30	21	31	38	37	41	54	37	37	44
Attrinite	0	0	0	0	0	4	4	1	1	0	4	7	0	1	2	1	0
Densinite	0	1	0	0	0	0	0	0	0	1	1	1	0	0	0	0	0
Detrogelinite	32	26	44	47	33	20	31	42	43	51	24	27	42	23	42	38	43
Porigelinite	0	0	0	0	0	0	0	0	0	1	0	0	0	0	0	0	0
Phlobaphinite	0	0	0	0	1	0	0	0	0	0	0	0	0	1	1	0	1
Total huminite	83	81	78	84	89	53	69	75	67	85	68	76	84	81	83	76	88
Sporinite	2	4	4	2	2	2	1	4	2	2	1	0	1	0	1	1	0
Cutinite	0	0	1	0	1	2	0	1	1	1	0	0	0	0	1	0	0
Resinite	0	0	0	1	0	2	0	2	1	1	0	1	0	0	1	0	0
Fluorinite	0	0	1	1	1	0	0	0	0	0	0	0	0	0	0	0	0
Suberinite	0	0	0	0	0	0	0	0	0	0	0	0	0	0	0	0	0
Liptodetrinite	1	1	2	1	1	1	2	2	2	1	0	0	0	0	1	0	0
Total liptinite	3	5	7	4	4	7	4	9	6	5	1	1	2	1	4	1	1
Fusinite	6	3	1	7	2	24	8	6	11	3	11	8	7	10	4	9	1
Semifusinite	3	1	1	1	1	8	6	2	8	3	11	5	3	4	2	8	0
Sclerotinite	1	0	0	0	0	0	0	0	0	0	1	1	0	0	1	0	0
Micrinite	0	0	0	0	0	0	0	0	0	0	0	0	0	0	0	0	0
Inertodetrinite	1	2	1	2	1	5	7	5	8	2	8	9	3	5	1	5	0
Total inertinite	10	5	3	10	4	38	21	14	27	8	30	22	14	18	8	22	2
Pyrite	0	1	1	0	0	1	1	1	0	1	0	0	0	0	1	0	1
Other minerals	3	8	11	2	2	1	6	1	0	0	0	0	0	0	4	1	9
Vitrite	51	54	35	36	57	29	37	33	24	36	40	44	44	57	43	39	56
Liptite	0	0	0	0	0	0	0	0	0	0	0	0	0	0	0	0	0
Inertite	6	2	1	6	2	24	9	5	9	4	12	6	6	8	3	9	1
Clarite	10	6	37	28	16	7	3	7	9	15	1	2	12	1	22	2	28
Vitrinertite	3	0	0	1	1	12	17	6	17	2	38	37	5	23	0	37	0
Durite	0	0	0	0	0	1	0	0	0	0	0	0	0	0	0	0	0
Trimcerite	27	28	12	26	21	24	25	46	41	42	9	11	32	12	27	13	3
Carbominerite	4	10	14	2	3	2	9	3	0	2	0	1	1	0	4	0	13
Huminite reflectance	0.34	0.33	0.35	0.32	0.31	0.35	0.33	0.34	0.39	0.31	0.34	0.33	0.34	0.33	0.34	0.35	0.36

Table 8. (continued)

Sample No.	A18	A19	A20	A21	A22	A23	A24	A25	A26	A27	A28	A29	A30	Ameam	B01	B02
Textinite	2	1	2	0	0	0	1	1	0	2	1	0	4	1	1	2
Ulminite	36	16	33	31	32	20	33	23	44	23	25	24	48	35	26	32
Attrinite	3	3	1	0	0	0	0	1	0	0	0	0	0	1	1	1
Densinite	0	0	4	0	0	0	0	0	0	0	0	0	0	0	1	0
Detrogelinite	41	29	28	48	52	53	46	51	42	54	63	68	34	41	35	44
Porigelinite	0	0	0	0	0	0	0	0	0	0	0	0	0	0	0	0
Phlobaphinite	1	0	0	0	0	0	0	1	0	0	1	1	2	0	0	0
Total huminite	83	50	68	80	84	74	80	77	86	79	90	93	88	78	64	80
Sporinite	2	1	0	1	3	3	1	2	1	2	3	1	0	1	1	2
Cutinite	1	1	0	0	1	2	0	0	0	0	0	1	1	1	0	0
Resinite	0	0	0	1	0	1	0	1	1	1	0	0	0	1	0	0
Fluorinite	0	0	0	0	0	0	0	1	0	1	0	1	2	0	0	0
Suberinite	0	0	0	0	0	0	0	0	0	0	0	0	1	0	0	0
Liptodetrinite	4	4	1	1	3	4	1	3	0	1	0	1	1	1	1	1
Total liptinite	7	6	1	3	6	9	3	6	2	5	3	5	6	4	3	3
Fusinite	1	3	9	5	4	7	7	7	5	5	2	1	1	6	6	4
Semifusinite	2	2	10	5	2	4	4	4	3	3	1	0	0	4	7	2
Sclerotinite	0	0	0	0	0	1	0	0	0	1	0	0	0	0	0	0
Micrinite	0	0	0	0	0	0	0	0	0	0	0	0	0	0	0	0
Inertodetrinite	1	6	8	7	3	5	6	6	4	1	1	0	1	4	6	4
Total inertinite	5	11	27	17	9	17	18	17	12	11	5	1	3	14	19	11
Pyrite	0	0	1	0	0	0	0	0	0	0	1	1	1	0	8	0
Other minerals	6	33	3	0	0	1	0	0	0	5	1	0	3	3	5	6
Vitrite	38	18	39	38	39	28	42	28	54	35	39	44	65	41	33	42
Liptite	0	0	0	0	0	1	0	0	0	0	0	0	0	0	0	0
Inertite	2	4	11	7	4	7	9	8	6	6	3	0	1	6	7	3
Clarite	40	16	0	7	24	16	6	12	7	24	47	52	20	16	9	13
Vitrinertite	0	2	44	7	1	3	7	11	17	9	2	0	2	10	17	11
Durite	0	0	0	0	0	1	0	0	0	0	0	0	0	0	0	0
Trimcerite	14	23	3	40	32	45	37	40	16	20	7	2	6	23	21	23
Carbominerite	6	38	3	0	0	0	0	0	0	7	2	1	5	4	13	6
Huminite reflectance	0.32	0.37	0.33	0.33	0.37	0.34	0.35	0.36	0.35	0.35	0.35	0.34	0.35	0.34	0.37	0.38

Table 8. (continued)

Sample No.	B03	B04	B05	B07	B09	B10	B11	B12	B13	B14	Bmean	R01	R02	R04	R05	Rmean
Textinite	2	2	1	3	0	2	1	1	0	0	1	1	0	2	1	1
Ulminite	31	30	43	66	44	35	32	49	37	32	35	35	30	25	21	28
Attrinite	0	0	0	0	0	0	1	0	0	0	0	0	0	0	4	1
Densinite	1	0	0	0	0	2	3	0	0	0	1	0	1	0	4	1
Detrogelinite	48	50	45	19	42	44	42	27	48	58	43	42	48	53	36	46
Porigelinite	0	0	0	2	0	0	0	0	0	0	0	0	0	0	0	0
Phlobaphinite	0	0	0	1	0	1	0	0	0	0	0	0	0	0	0	0
Total huminite	83	82	88	90	86	83	78	77	86	90	81	78	78	79	66	76
Sporinite	2	4	3	1	3	4	4	3	3	1	3	3	7	4	1	4
Cutinite	0	2	0	0	0	0	0	0	1	2	1	0	0	0	0	0
Resinite	0	0	0	2	1	1	2	1	0	0	1	0	1	1	0	1
Fluorinite	0	0	0	0	0	0	0	0	0	3	0	0	1	0	0	0
Suberinite	0	0	0	0	0	0	0	0	0	0	0	0	0	0	0	0
Liptodetrinite	1	1	1	1	1	2	2	1	1	1	2	1	4	0	0	1
Total liptinite	3	7	4	3	4	8	8	5	5	8	6	5	12	6	2	5
Fusinite	6	4	1	0	5	4	9	6	1	1	5	5	1	5	7	5
Semifusinite	3	1	1	0	2	3	2	2	0	0	2	4	1	3	6	4
Sclerotinite	0	1	0	0	0	0	0	0	0	0	0	0	0	0	0	0
Micrinite	0	0	0	0	0	0	0	0	0	0	0	0	0	0	0	0
Inertodetrinite	5	2	2	0	1	1	2	0	1	1	2	4	4	5	16	6
Total inertinite	14	8	4	1	8	9	13	9	3	1	10	13	7	13	29	16
Pyrite	0	0	0	3	1	0	0	0	0	0	0	1	0	0	0	0
Other minerals	0	2	4	2	1	1	1	9	6	1	3	4	2	2	4	3
Vitrite	37	39	50	73	44	38	36	51	38	36	40	48	36	38	31	40
Liptite	0	0	0	0	0	0	0	0	0	0	0	0	0	0	0	0
Inertite	5	4	1	0	3	3	6	5	1	1	4	5	1	5	10	6
Clarite	14	33	27	18	18	18	9	10	42	59	20	21	38	30	8	23
Vitrinertite	10	4	3	0	1	4	12	2	1	0	7	7	1	6	40	12
Durite	0	0	0	0	0	0	0	0	0	0	0	0	0	0	1	0
Trimcerite	33	18	14	3	33	36	37	20	12	5	26	16	22	19	7	16
Carbominerite	0	2	4	6	1	1	1	11	6	0	3	4	2	3	3	3
Huminite reflectance	0.38	0.39	0.40	0.44	0.37	0.43	0.39	0.39	0.39	0.40	0.39	0.31	0.28	0.33	0.32	0.31

A = Absaloka mine samples; B = Big Sky samples; R = Rosebud samples;

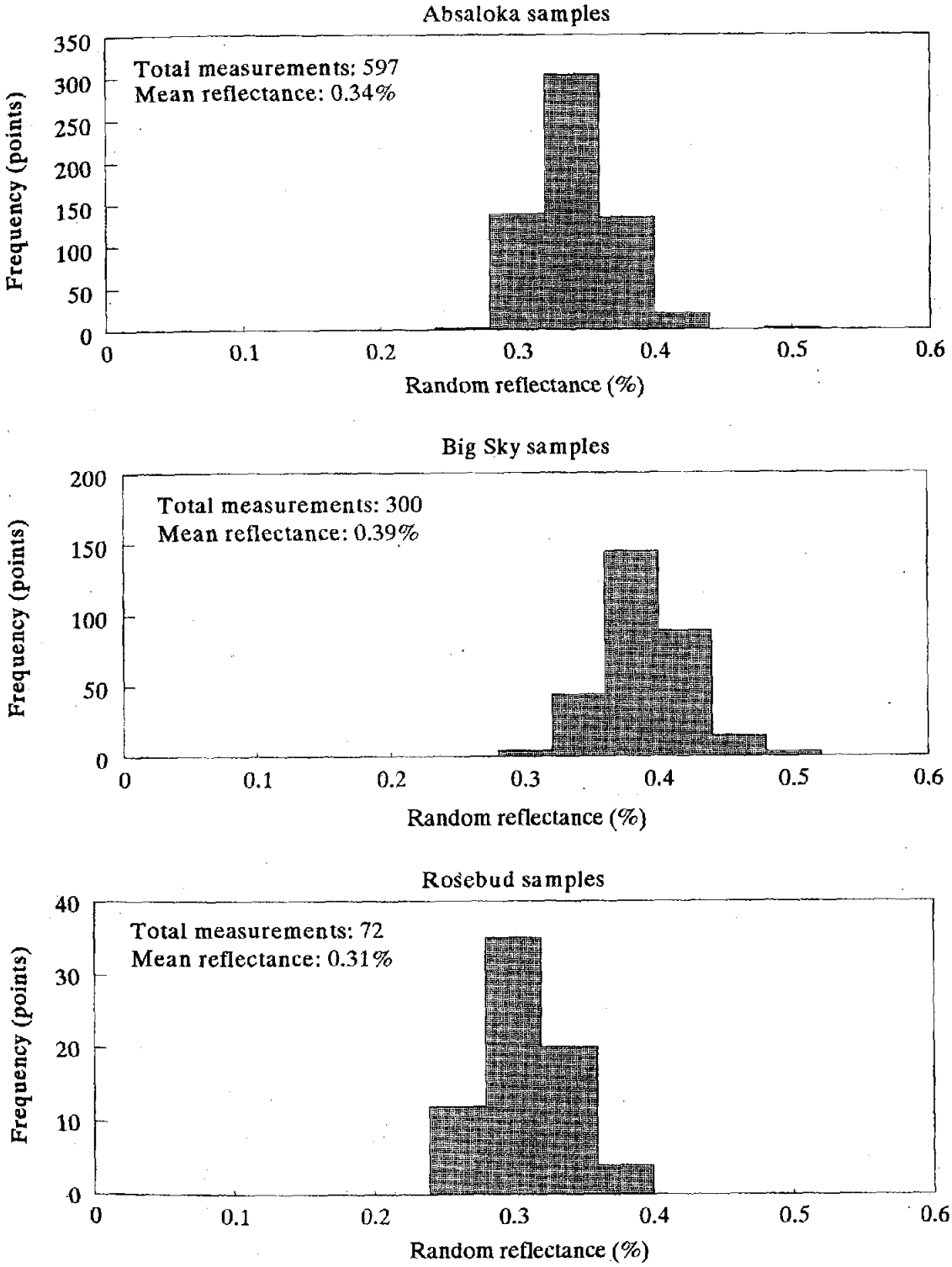

Figure 6. Frequency distribution of random huminite reflectance measurements of the Rosebud coal samples.

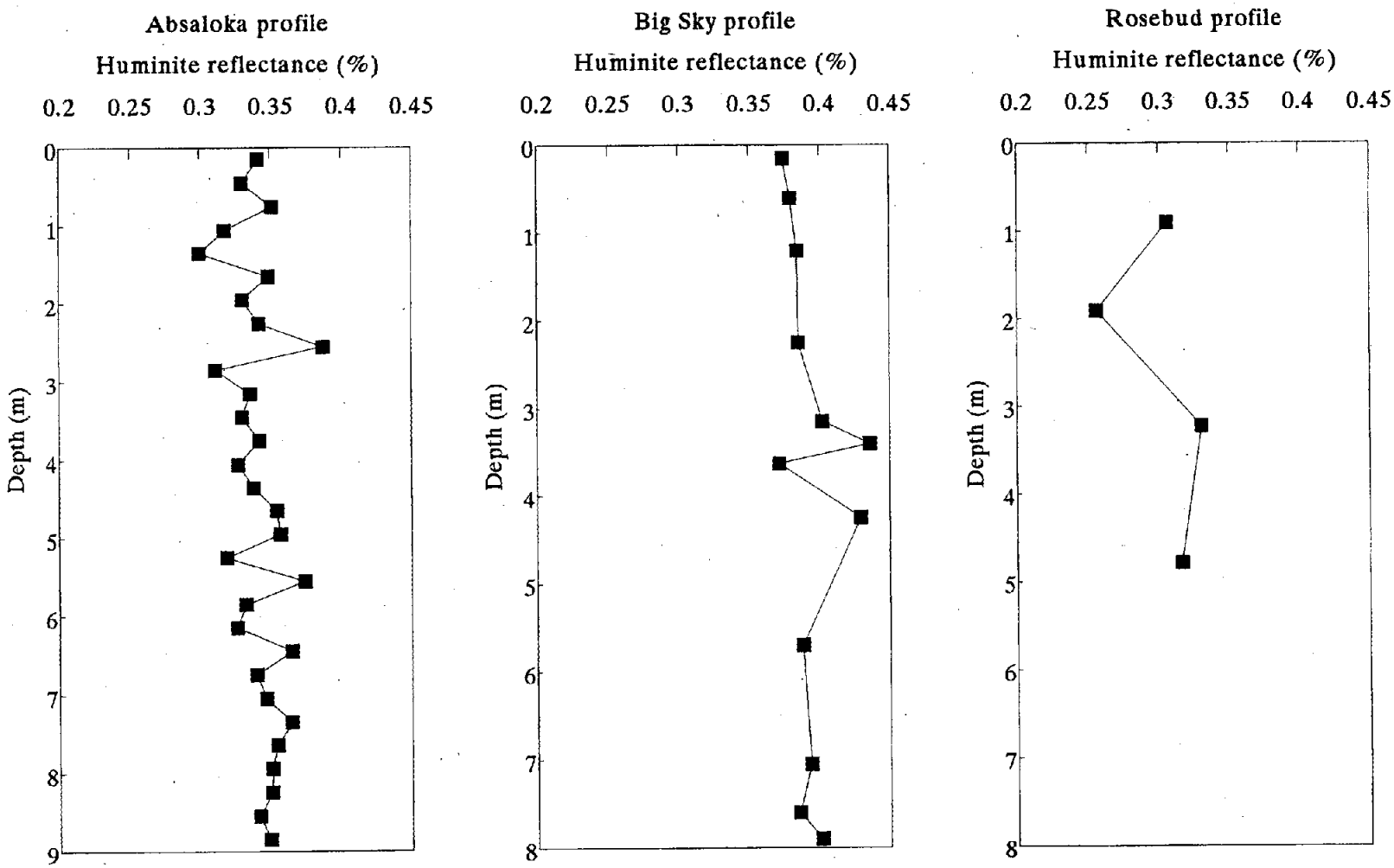

Figure 7. Huminite reflectance profiles for the Absaloka, Big Sky and Rosebud mine samples.

of 0.39%, ranking the coal as subbituminous C. The Absaloka samples have intermediate huminite reflectance, ranging from 0.32% to 0.37% with an average of 0.34%, and the Rosebud samples have the lowest, ranging from 0.28% to 0.33% with an average of 0.31%, both ranking as lignite. The difference in huminite reflectance and rank at different locations in the Rosebud coal indicates a corresponding difference in coalification, possibly caused by variation of original plant material or more likely by burial conditions and diagenic processes.

5.242 Petrographic Composition

Seven huminite group macerals, six liptinite macerals, and 5 inertinite macerals were identified and recorded in point counting. Usually, the mineral substances associated with coal are recorded as a total in maceral analysis, without subdivision into individual minerals (Stach and others, 1982). Since pyrite is the most important mineral determining coal quality and the most easily recognizable mineral on polished surfaces, it was recorded separately in this research. Eight microlithotype groups were recorded according to maceral and mineral association. The results listed in Table 8 are given in volume percent. The location of each sample is given in Figures 8 and 9.

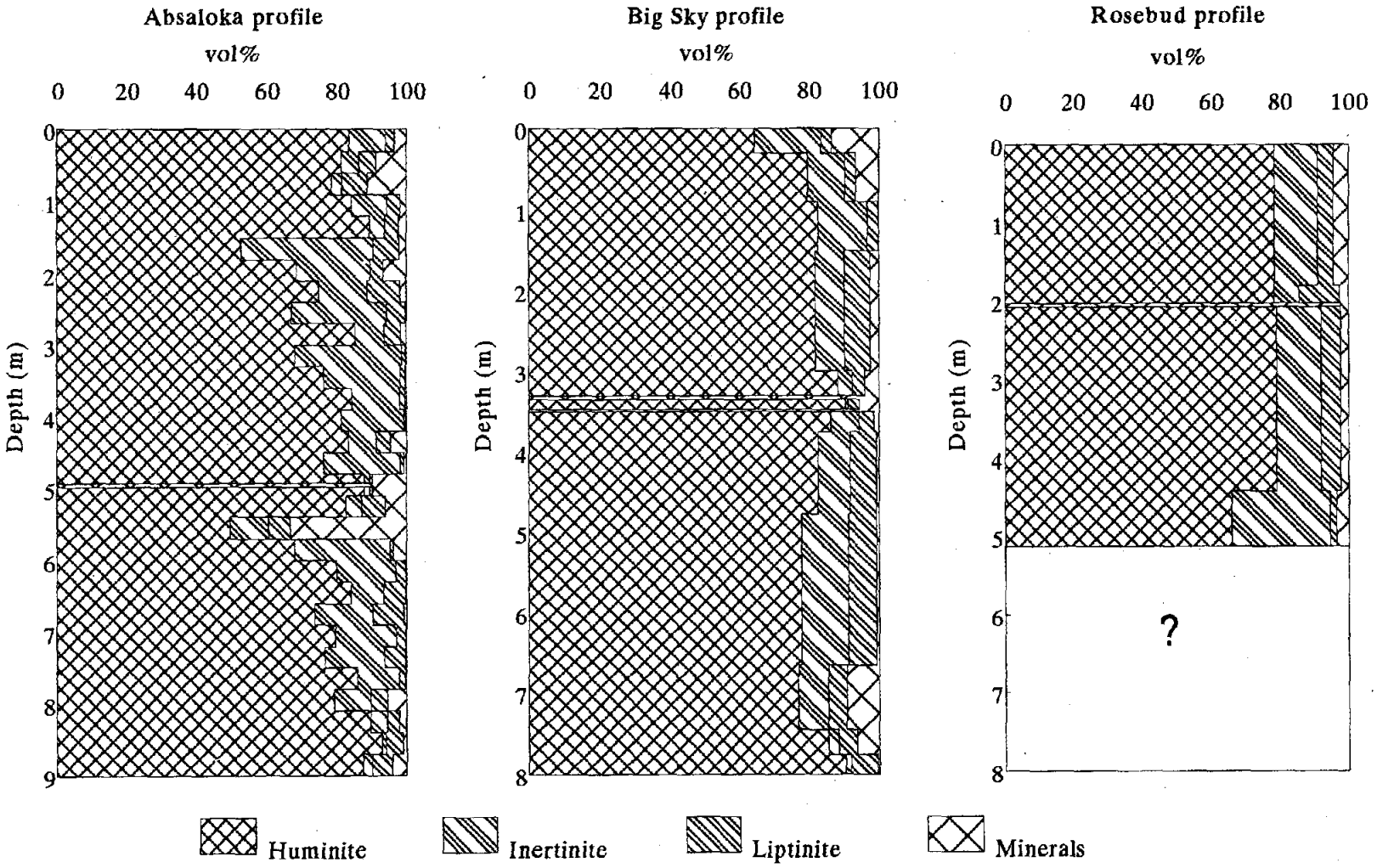

Figure 8. Maceral group profiles for the Absaloka, Big Sky and Rosebud mine samples.

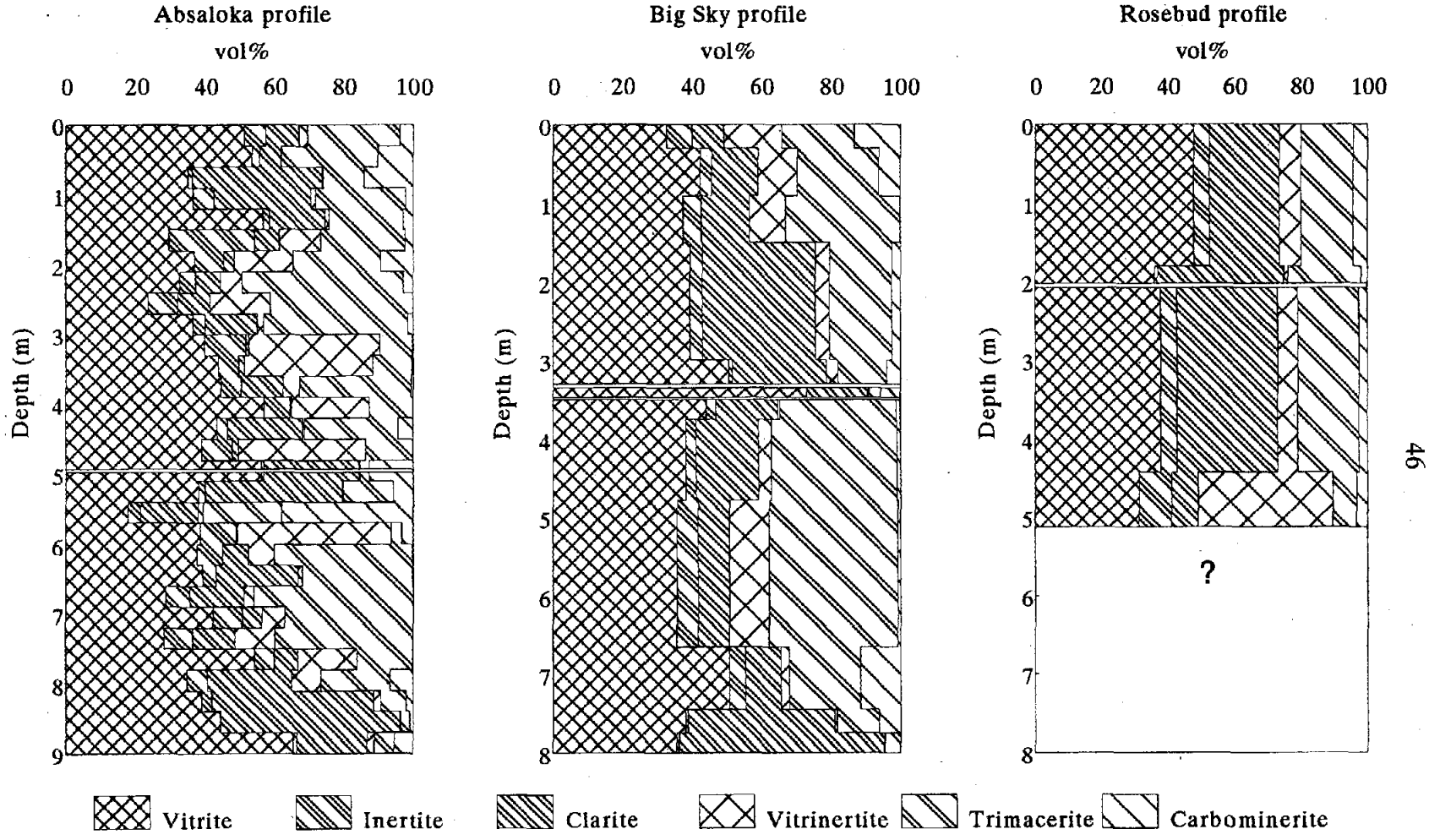

Figure 9. Microlithotype group profiles for the Absaloka, Big Sky and Rosebud mine samples.

5.242.1 Macerals

Major observations of maceral occurrence in the Rosebud coal include:

1) Huminite-group macerals are the dominant components of all samples (Table 8), ranging from 50 to 93% with an average of 81% for Big Sky samples, 78% for Absaloka samples and 76% for Rosebud samples. Representative photomicrographs of huminite group macerals are shown in Plates I and II. Ulminite and detrogelinite are the two most abundant macerals of this group. Ulminite content ranges from 16 to 66% with an average of 35% for Absaloka and Big Sky samples, and 28% for Rosebud samples. Detrogelinite content ranges from 19 to 68% with an average of 41% for Absaloka samples, 43% for Big Sky samples and 46% for Rosebud samples. Other huminite macerals include textinite, attrinite, densinite, porigelinite and phlobaphinite.

2) Liptinite is the least abundant of the three maceral groups (Table 8). Examples of the liptinite group macerals are shown in Plates IV and V. The total of liptinite group macerals ranges from 1 to 12% with an average of 4% for Absaloka samples, 6% for Big Sky samples and 5% for Rosebud samples. Sporinite and liptodetrinite are the two most abundant macerals of this group. Sporinite ranges from 0 to 7% with an average of 1% for Absaloka samples, 3% for Big Sky, and 4% for Rosebud. Liptodetrinite ranges from 0 to 4% with an average of 1% for Absaloka samples, 2% for Big Sky, and 1% for Rosebud. Other recorded liptinite macerals include resinite, cutinite, fluorinite and suberinite.

3) Content of the inertinite group macerals varies significantly from sample to sample, ranging from 1 to 38% with an average of 14% for Absaloka samples, 10% for Big Sky samples and 16% for Rosebud samples (Table 8). Examples of the inertinite group macerals are shown in Plates II and III. Fusinite, semifusinite and inertodetrinite are the major components of this group. Sclerotinite and micrinite total less than one percent.

5.242.2 Minerals

Although the content of recognizable minerals in individual samples is variable, samples from each mine have similar mean mineral contents of 4, 3, and 3% for Absaloka, Big Sky and Rosebud samples respectively (Table 8). The mineral content is very low except in certain layers including the top and bottom of the seam and partings. In most samples, pyrite content is less than 1%. Two Big Sky samples have very high pyrite content. The sample from the top 30 cm of the seam (B01) has pyrite as high as 8%. The other pyrite-rich sample (B07) is from the 25-cm-thick layer between the two partings, which has 3% pyrite. Other minerals are difficult to identify accurately using reflected light. The results of mineral analysis using SEM/EPMA is described in the following chapter.

5.242.3 Microlithotypes

Since microlithotypes are associations of macerals, their proportions are closely related to maceral composition in coal. Major observations on microlithotype group abundances include:

1) Vitrite, the group of microlithotypes composed of single maceral group huminite, is the most abundant for all samples, ranging from 18 to 73% with an average of 41% for Absaloka samples, 40% for Big Sky, and 31% for Rosebud.

2) Other abundant groups of microlithotypes include clarite, vitrinertite and trimacerite, which consist of different combinations of huminite, liptinite and inertinite group macerals (Table 4). Clarite ranges from 0 to 59% with an average of 16% for Absaloka samples, 20% for Big Sky, and 23% for Rosebud. Vitrinertite ranges from 0 to 44% with an average of 10% for Absaloka samples, 7% for Big Sky, and 12% for Rosebud. Trimacerite ranges from 2 to 46% with an average of 23% for Absaloka samples, 26% for Big Sky, and 16% for Rosebud.

3) Inertite and carbominerite are abundant in some inertinite- or mineral-rich samples (Table 8). Inertite ranges from 0 to 24% with an average of 6% for Absaloka samples, 4% for Big Sky, and 6% for Rosebud. Carbominerite ranges from 0 to 38% with an average of 4% for Absaloka samples, and 3% Big Sky and Rosebud.

4) Liptite, the microlithotype group composed by the single maceral group liptinite, and durite, the association of liptinite and inertinite, are rarely encountered.

5.243 Petrographic Variation

The petrographic analysis results (Table 8) show that coals from the three mines are similar in mean contents of huminite macerals (76 to 81%), liptinite macerals (4 to 6%), and minerals (3 to 4%). Inertinite macerals are somewhat more variable, ranging from 10 to 16%. In terms of microlithotype content, the coal from the three mines is also similar, especially in the monomaceral microlithotype groups vitrite (40 to 41%) and inertite (4 to 6%), and the mineral-rich microlithotype group carbominerite (3 to 4%). The other major microlithotypes clarite, vitrinertite and trimacerite are more variable, ranging from 16 to 23%, 7 to 12% and 17 to 26% respectively, because they are sensitive to the variation of liptinite and inertinite. The mean random huminite reflectance varies greatly from 0.31% at the Rosebud mine to 0.34% at the Absaloka mine and 0.39% at the Big Sky mine. The vertical variation of coal petrography and huminite reflectance at the Absaloka and Big Sky mines is shown in detail in Figures 7, 8 and 9. Data are limited for the coal of the Rosebud mine, which will not be discussed. The following petrographic features and correlations are observed:

1) The base of the seam at each mine is a 1 to 1.5 m mineral-rich zone with relatively high huminite and low inertinite. This zone is characterized by relatively high carbominerite, vitrite and clarite microlithotype groups.

2) The seam at each mine has a 5.5 to 6.5 m thick central zone with relatively low huminite and high inertinite, and contains a prominent parting zone which at each mine is 1 to 2 m thick and contains one or two partings, or mineral-rich layers

with relatively variable maceral content but typically high huminite. The microlithotype content in this zone is relatively low in vitrite and carbominerite, high in trimacerite and vitrinertite, and variable in other microlithotype groups.

3) At Absaloka, the central zone is overlain by a 0.5 m zone of relatively high huminite and low inertinite, and relatively high contents of microlithotype groups vitrite and clarite.

4) The upper part of the seam at each mine is a 0.5 to 1 m zone with high mineral content or a high proportion of carbominerite. At both mines inertinite increases upward in this zone. At Absaloka, both minerals and liptinite decrease upward. At Big Sky, minerals increase upward, particularly pyrite which is 7.9% in the top sample.

5) Vertical huminite reflectance profiles are quite variable but appear to be somewhat correlated to maceral composition. For example, the central thick zone at the Absaloka and Big Sky mines is characterized by highly irregular reflectance patterns compared to the zones above and below (Figures 7 and 8). There is also a direct correlation of mean huminite reflectance with mean huminite content (Figure 10) and an inverse correlation with mean inertinite content (Figure 11) even though the range of the reflectance values and the maceral contents for each mine are quite high. The correlation of mean huminite reflectance with maceral abundance may suggest a possible relationship of coalification with depositional environment (see Chapter 6).

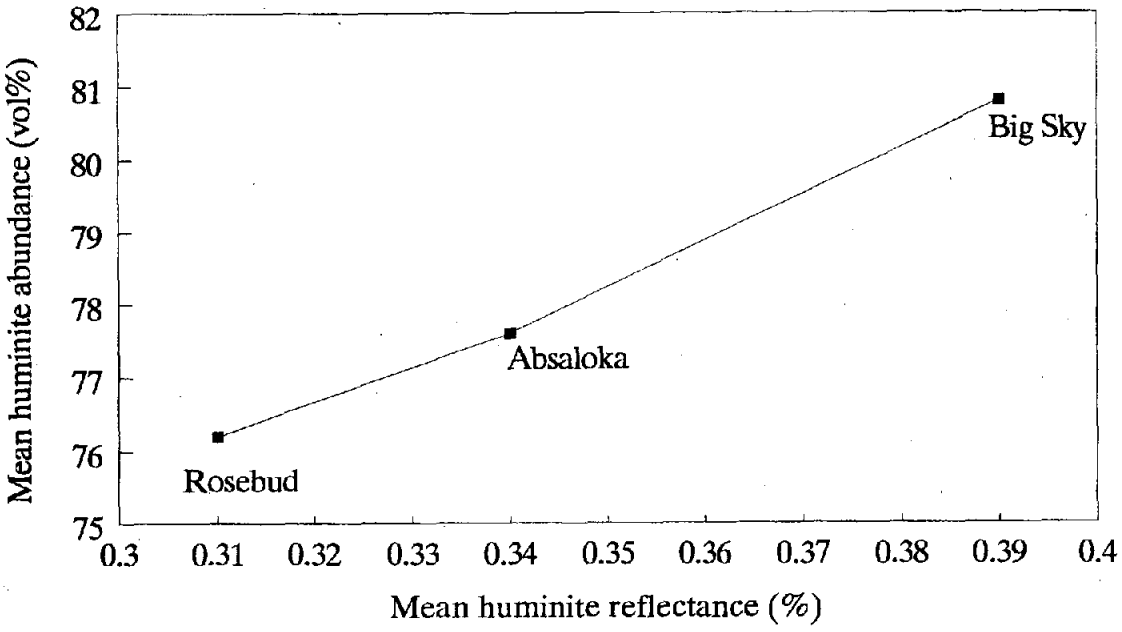

Figure 10. Correlation between mean huminite reflectance and mean huminite abundance for the Absaloka, Big Sky and Rosebud mine samples.

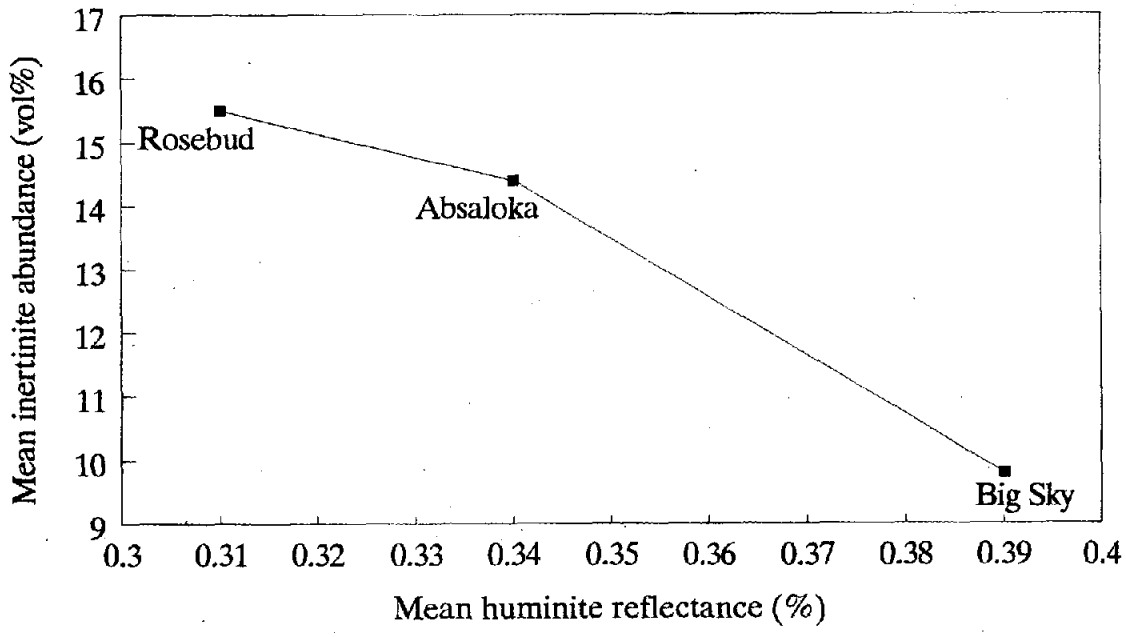

Figure 11. Correlation between mean huminite reflectance and mean inertinite abundance for the Absaloka, Big Sky and Rosebud mine samples.

In summary, within-seam variations of petrographic composition and huminite reflectance are high. At Absaloka and Big Sky, petrographic variation delineates lithologic layering. It may be possible to correlate petrographic units between the Absaloka and Big Sky profiles because of similar lithologic sequence and thickness, but this would be risky because of the over 30 km distance between these two mines the frequent occurrence of other coal beds. Correlation of mean huminite reflectance and mean maceral abundance may suggest a possible relationship of coalification with depositional environment.

6. DEPOSITIONAL ENVIRONMENT

The relationship between coal petrography and depositional environments has been the subject of numerous studies. In coal petrology, coal depositional environments are considered from the perspective of the factors controlling the formation and preservation of ancient peat. Although there is general agreement that the main factors include type of peat-forming flora, climate, geomorphology and tectonic setting, there is much dispute over their precise role in development of ancient mires (Kalkreuth and others, 1991a).

Interpretation of coal depositional environment is based on interpretation of the genesis of macerals, microlithotypes, and lithotypes. Since lithotypes are layers of coal beds which are primarily described qualitatively, controversy on their classification and description still remains. Maceral and microlithotype analysis is necessary in the genetic interpretation of lithotypes. Genetic models using simple diagrams have been developed to interpret the relationship between petrography and depositional environment on the basis of either microlithotype proportion (Hacquebard and Donaldson, 1969; Smyth, 1979, 1984; Marchioni, 1980; Hunt, 1982; Hunt and Hobday, 1984; Hunt and Smyth, 1989), or maceral content (Diessel, 1982, 1986; Mukhopadhyay, 1986; Gentzis and Goodarzi, 1990; Kalkreuth and others, 1991a, 1991b).

6.1 Interpretation of Depositional Environment Based on Microlithotypes

The first diagram relating coal microlithotypes to depositional environment was developed by Hacquebard and Donaldson (1969). Incorporating the results of studies by Teichmuller (1950, 1952) and Teichmuller and Thomson (1958) of Tertiary brown coals and those by Spackman and others (1966) on recent Florida Everglades sediments, Hacquebard and Donaldson (1969) derived the microlithotypes characteristic of the various moor environments in which peat developed.

1) Forest terrestrial moor: fusito-clarite.

2) Forest moor: clarite rich in vitrinite and with little exinite.

3) Reed moor: cuticle-clarite and duroclarite.

4) Open moor: clarodurite, durite and carboargillite.

On the basis of these assumptions, two triangular diagrams identifying peat facies were constructed to illustrate the relationship of microlithotype composition with depositional environments.

Detailed microlithotype analysis is required in using Hacquebard and Donaldson's facies diagrams. One microlithotype used in these diagrams, fusito-clarite, was not defined in the International Handbook of Coal Petrography. Later, two similar ternary diagrams were developed by Smyth (1979, 1984) and Hunt (1982) from their studies of Permian bituminous coal of Australia. Both Smyth's and Hunt's diagrams use microlithotype groups instead of individual microlithotypes as petrographic components. The following five depositional environments (Figure 12a)

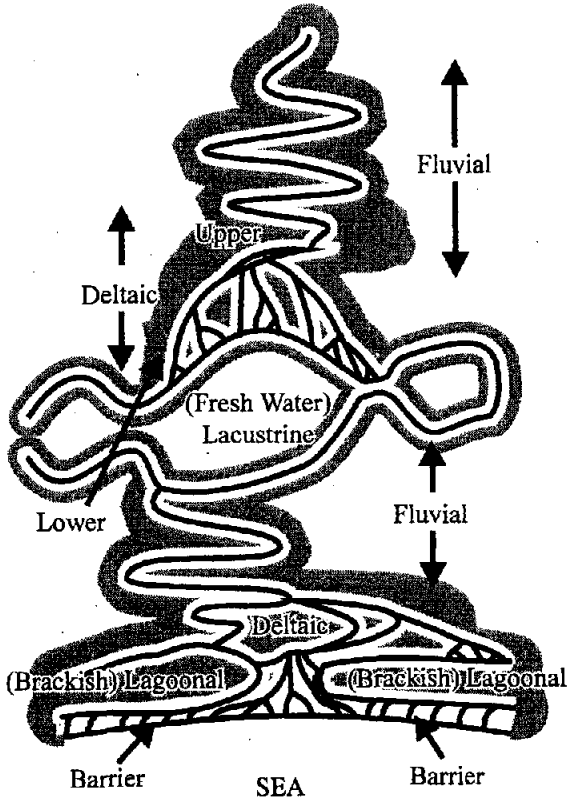

(a)

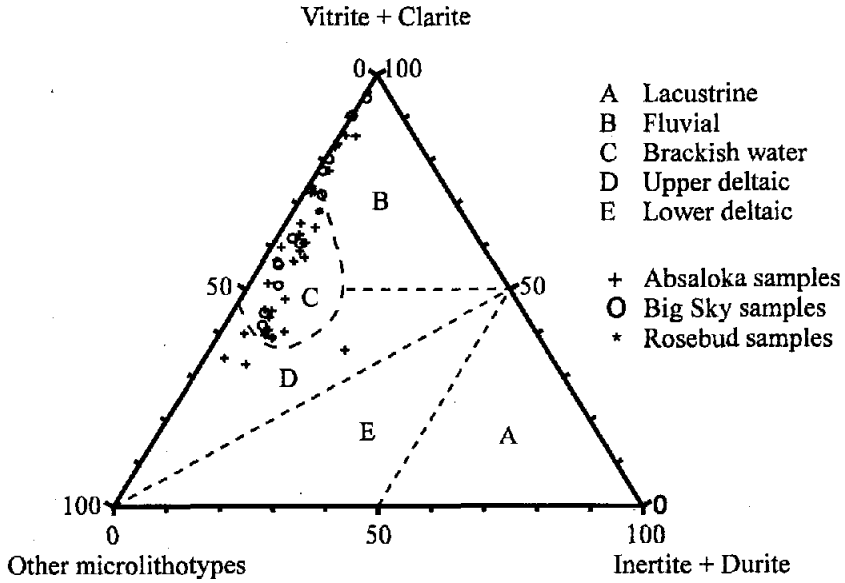

(b)

Figure 12. Depositional environments of peat formation (a) and related microlithotypes (b) (Smyth, 1979, 1984) for the Rosebud coal.

can be distinguished from Smyth's (1979, 1984) diagram (Figure 12b) on the basis of microlithotype composition.

1) Lacustrine: lower coastal plain, plus area dominated by coal swamps;

2) Fluvial;

3) Brackish water (lagoonal): channel belt plus large lake;

4) Upper deltaic: upper coastal plain;

5) Lower deltaic: area dominated by channel deposits, plus minor upper coastal plain deposits.

With few exceptions, microlithotype data points for the Rosebud seam plot in the fluvial and brackish water lagoonal environments of Smyth's (1979, 1984) diagram (Figure 12b). This is in agreement with the interpretation of the lacustrine and fluvial-deltaic depositional environment of the Fort Union Formation (Ayers, 1986; Flores, 1986; and Flores and Ethridge, 1985).

6.2 Interpretation of Depositional Environment Based on Macerals

Diessel (1982) interpreted coal depositional environments based on the occurrence of certain macerals which he considered to be diagnostic of facies. The depositional significance of other macerals was considered ambiguous and they are not included in the interpretive scheme. The "diagnostic" macerals include telinite, telocollinite, semifusinite, fusinite, inertodetrinite, alginite and sporinite.

Telinite (textinite) and telocollinite (ulminite) are derived from partly gelified woody tissue and are indicative of both the abundance of wood-producing plants and

the degree of biochemical gelification, which in turn is related to the availability of relatively high levels of moisture (Kalkreuth and others, 1991a). Semifusinite and fusinite also indicate input from woody vegetation, but under relatively dry conditions conducive to the formation of charcoal from fire (pyrofusinite) or under oxidizing conditions conducive to fungal and bacterial attack (degradofusinite). Inertodetrinite forms from disintegration of fusinite and semifusinite and has the same origin as these macerals. Most inertodetrinite is transported from its site of formation and deposited in a sub-aqueous environment. Sporinite is derived from several regions of a swamp-land, but most is transported to the limno-telmatic of limnic zones. Alginite precursors require a sub-aqueous environment to develop.

Based on the composition of diagnostic and non-diagnostic macerals, Diessel (1982) designed a maceral approach to coal facies analysis using the following petrographic indices.

T(elinite) = Telinite + Telocollinite

F(usinite) = Fusinite + Semifusinite

W(oody) = T + F

D(ispersed) = Alginite + Sporinite + Inertodetrinite

R(emainder) = Non-diagnostic Macerals (principally desmocollinite)

Coals with less than 50% diagnostic macerals (W + D) are assigned to a mixed facies. Coals with around 50% or more of the diagnostic macerals are plotted in a facies ternary diagram (Figure 13) with normalized T, F, D indices. In this diagram the ratio (T+F)/D (or W/D) is called wood ratio and is indicative of the degree to

which plant materials rich in woody tissue have contributed to the peat versus the dispersed materials representing transported detritus. $(T+F)/D < 1$ is assigned to the open moor facies and > 1 to the forest moor. The T/F ratio indicates the degree of gelification of the woody tissue and also the "dryness" of the environment.

To apply this scheme to low-rank coals, these petrographic indices must be modified to the corresponding low rank coal macerals. The following equations are used to calculate those indices in this research.

T = Textinite + Ulminite + Suberinite

F = Fusinite + Semifusinite

W = T+F

D = Inertodetrinite + Attrinite + Sporinite + Alginite + Sclerotinite

R = Remainder

Twenty of the 30 Absaloka samples, 8 of the 12 Big Sky samples, and 2 of the 4 Rosebud samples have diagnostic macerals (W+D) more than 50%. With one exception, all these samples plot in the wet forest moor facies (Figure 13). The Big Sky samples plot in the region with $(T+F)/D > 4$, whereas one Rosebud sample and some of the Absaloka samples plot in the $(T+F)/D < 4$ region. The Rosebud and some Absaloka samples also have lower T/F ratio, indicating the Rosebud and Absaloka coals formed in moors having more input of dispersed materials and under drier conditions.

Seeking to determine the influence of larger scale depositional processes on the petrography of coals, Diessel (1986) modified his earlier approach and developed

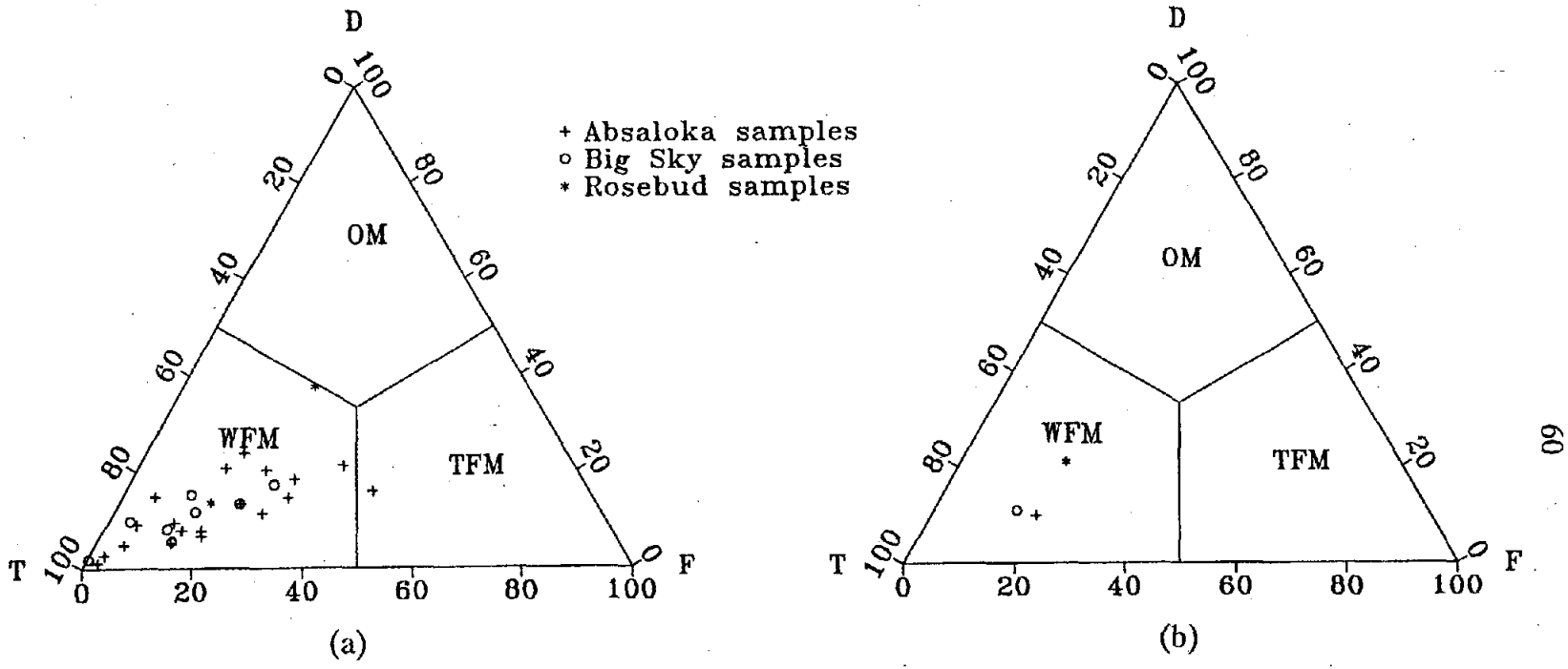

T = Textinite + Ulminite + Suberinite F = Fusinite + Semifusinite
D = Inertodetrinite + Attrinite + Sporinite + Alginite + Sclerotinite
OM = Open moor WFM = Wet forest moor TFM = Terrestrial forest moor

Figure 13. Facies diagram based on "diagnostic" macerals (modified from Diessel, 1982; Kalkreuth and others, 1991) for the Rosebud coal. (a) plots of samples with D + T + F > 50%; (b) plots of the mean composition of samples from each mine.

a new facies diagram by introducing two new petrographic indices, gelification index (GI) and tissue preservation index (TPI) which are calculated from the following equations (Kalkreuth and others, 1991a):

$$TPI = \frac{Telinite + Telocollinite + Fusinite + Semifusinite}{Desmocollinite + Macrinite + Inertodetrinite}$$

$$GI = \frac{Vitrinite + Macrinite}{Fusinite + Semifusinite + Inertodetrinite}$$

GI contrasts the partially and completely gelified macerals with the ungelified macerals, reflecting the moisture level during the formation of peat and soft brown coals (Diessel, 1986; Kalkreuth and others, 1991a). TPI compares the proportions of the structure-preserved macerals with those in which tissue structure is destroyed biochemically or mechanically, reflecting in part the input of woody vegetation. This scheme does not include the liptinite group macerals, but includes desmocollinite (densinite and detrogelinite for low rank coals), a major component which is not included in his earlier ternary diagram. In his new facies diagram, seams from the upper delta plain, lower delta plain, piedmont plain, transgressive and regressive back barriers and abandoned lower delta plain, each plot in fairly well-defined areas with little overlap.

In applying Diessel's approach to low-rank coal, Kalkreuth and others (1991b) modified these two indices and suggested the following equations:

$$TPI = \frac{Humotelinite + Corpohuminite(in-situ) + Fusinite + Semifusinite}{Gelinite + Macrinite + Humodetrinite}$$

$$GI = \frac{All\ Huminite\ (Except\ Texto-ulminite\ and\ Detrohuminite) + Macrinite}{Semifusinite + Fusinite + Inertodetrinite + Texto-ulminite + Detrohuminite}$$

The maceral names used by Kalkreuth and others are not exactly same as those used in this study. Their texto-ulminite, for example, is equivalent to the textinite in this study, and detrohuminite is equivalent to attrinite and densinite. The following equations, which are modified from the Kalkreuth and others, are used in this study.

$$TPI = \frac{Textinite + Ulminite + Porigelinite + Phlobaphinite + Fusinite + Semifusinite}{Detrogelinite + Attrinite + Densinite + Inertodetrinite}$$

$$GI = \frac{Ulminite + Porigelinite + Phlobaphinite + Detrogelinite}{Textinite + Attrinite + Densinite + Fusinite + Semifusinite + Inertodetrinite}$$

Samples of the Rosebud seam plot in a wide area of the diagram, but most plot in the fen facies region (Figure 14). The Absaloka samples are more dispersed than the Big Sky and Rosebud samples because of their smaller size. Each Absaloka sample represents a shorter period of depositional history than the Rosebud and most Big Sky samples do. The dispersion of the points indicates that the area of the moor in which the seam developed was changing during depositional history. In spite of the variation in moor facies illustrated by individual samples, the three mean compositions plot in or near the fen facies area. In terms of the large scale environment, the Absaloka and Big Sky mines are in the lower and upper delta plain

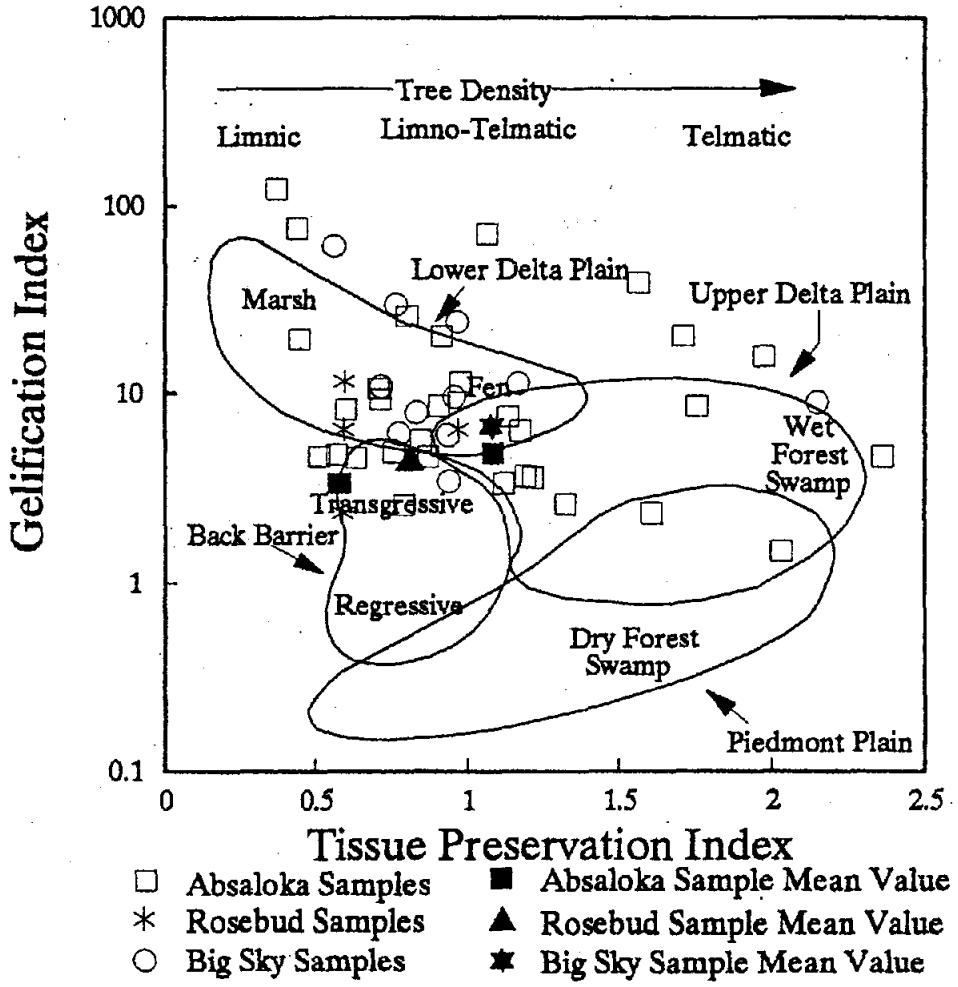

Figure 14. Depositional environment of the Rosebud seam illustrated by Diessel's (1986) facies diagram modified by Kalkreuth and others (1991).

overlap region and the Rosebud mine in a transitional zone between lower delta plain and transgressive back barrier. Figure 14 also shows that the Rosebud coal has the lowest GI and TPI values, the Absaloka and Big Sky coals have about same TPI but the Big Sky has higher GI value. In addition to indicating depositional environment, the GI also aids in interpreting the difference in huminite reflectance of the coals from the three mines.

Diessel's model does not take into consideration the liptinite and mineral content of the coal. Liptinite may influence the final outcome of the coal depositional model (Gentzis and Goodarzi, 1990). From the study of Texas Tertiary lignite, Mukhopadhyay (1986) developed a different ternary facies diagram (Figure 15). He suggested that the macerals which are non-diagnostic according to Diessel (1982) may also reflect depositional setting. Humodetrinite and humocollinite indicate input of herbaceous vegetation typical of a reed-marsh complex rather than an arboreal swamp suggested by homotelinite. The liptinite macerals also provide clues for recognition of the depositional environment. High content of terrestrial liptinite (sporinite, cutinite, and suberinite) and resinite indicate deposition in a forested swamp environment, whereas high liptodetrinite and sporinite (either less than or equal to amount of liptodetrinite) indicate reed-marsh vegetation.

Apexes of Mukhopadhyay's ternary diagram are A: humotelinite + terrestrial liptinite + resinite, B: humodetrinite + humocollinite (excluding corpohuminite) + liptodetrinite + sapropelinite + alginite, and C: inertinite. In this research, the term sapropelinite is not used because it is not recommended by ICCP. Phlobaphinite and

sporinite are added to apex A since it is usually found in cells of woody tissue. The B/A ratio indicates the proportion of arboreal and herbaceous vegetation. As in Diessel's facies diagram, samples plot in a wide area but most in the transitional zone between reed marsh and forest swamp facies (Figure 15), agreeing with the location in the fen facies of Diessel's (1986) diagram. Most of the samples have the B/A ratio around 1. Some have the ratio greater and some smaller than 1, indicating a variation of vegetation accumulated during depositional history.

In summary, the Rosebud seam was developed in one or several adjacent mires in a lagoonal and fluvial-deltaic depositional system with vegetation mixed or alternating from arboreal to herbaceous.

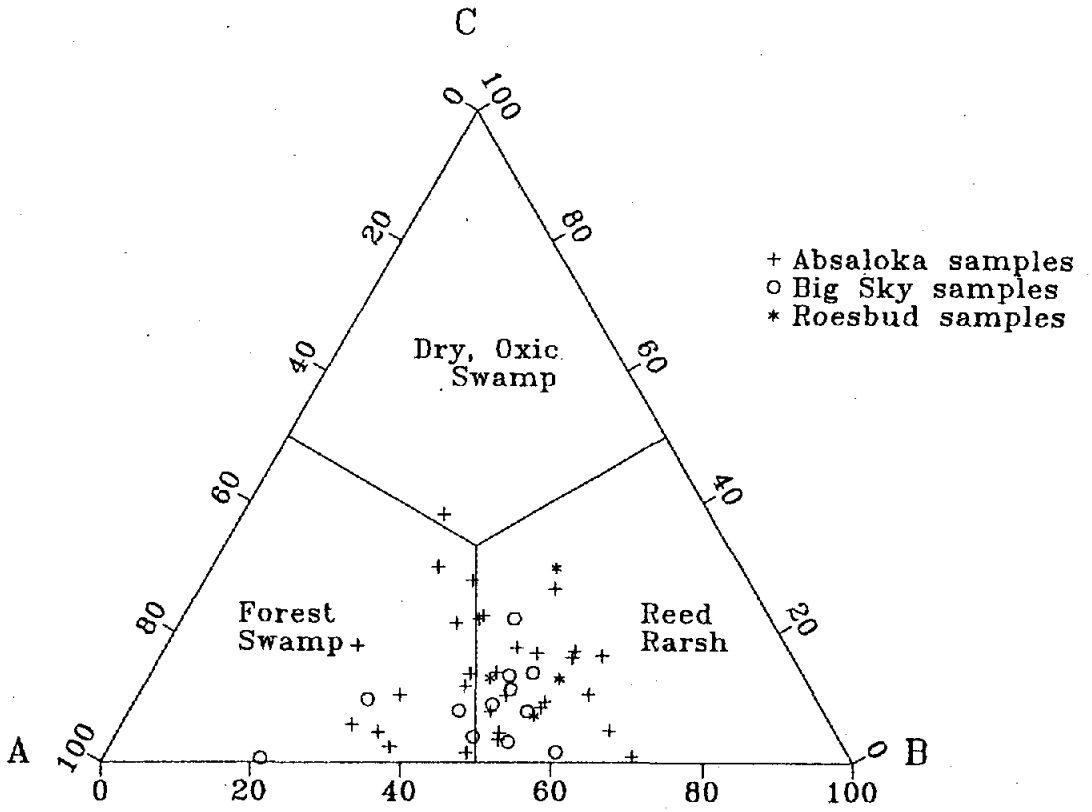

A Textinite, Ulminite, Porigelinite, Phlobaphinite, Cutinite, Fluorinite, Resinite, Suberinite
B Attrinite, Densinite, Detrogelinite, Liptodetrinite
C Inertinite

Figure 15. Maceral composition of the Rosebud coal plotting in ternary diagram (modified from Mukhopahyay, 1986) according to the combination of different maceral types at three apexes, which are related to peat forming environments.

7. INORGANIC GEOCHEMISTRY

7.1 Analytical Methods

Analysis of minerals and organically associated inorganic elements is performed with a combined optical microscope and scanning electron microscope and electron probe microanalysis system (SEM/EPMA). The SEM/EPMA system consists of a JEOL JX35 scanning electron microscope/microprobe, a TN 5600 EDS analyzer and a TN 8500CX image analyzer. The system is interfaced to two personal computers for data manipulation and storage. The TN 5600 EDS analyzer can be programmed for stage automation.

Computer-controlled scanning electron microscopy (CCSEM) and image analysis are used for quantitative mineral analysis. These methods can determine the size, morphology, composition and association of minerals in coal (Galbreath, 1993; Zygarlicke and Steadman, 1990). A total of 33 mineral phases (Table 9) are identified automatically in CCSEM analysis based on their elemental compositions. The disadvantage of this method is that CCSEM cannot provide any information on crystal structure. This is adequate for coal utilization purposes, such as the prediction of ash formation during combustion, but not for mineralogical interpretation. Some "minerals" noted in CCSEM analysis, such as 11 to 19 and 30 to 32 in Table 9,

Table 9. CCSEM mineral phase classification on the basis of atom ratio (after Galbreath, 1993)

Mineral	Definition
1) Quartz	$Al \leq 5$, $Si \geq 80$
2) Iron Oxide	$Si < 10$, $S \leq 5$, $Mg \leq 5$, $Al \leq 5$, $Fe \geq 80$
3) Periclase	$Mg \geq 80$, $Ca \leq 5$
4) Rutile	$S \leq 5$, $(Ti+Ba) \geq 80$
5) Alumina	$Al \geq 80$
6) Calcite	$S < 10$, $Mg \leq 5$, $Si \leq 5$, $P \leq 5$, $Ti \leq 5$, $Ba \leq 5$, $Ca \geq 80$
7) Dolomite	$Mg \geq 5$, $Ca > 10$, $(Ca+Mg) \geq 80$
8) Ankerite	$S < 15$, $Mg < Fe$, $Fe > 20$, $Ca > 20$, $(Ca+Mg+Fe) \geq 80$
9) Kaolinite	$(Al+Si) \geq 80$, $0.8 < Si/Al < 1.5$, $Fe \leq 5$, $K \leq 5$, $Ca \leq 5$
10) Montmorillonite	$(Al+Si) \geq 80$, $0.8 < Si/Al < 2.5$, $Fe \leq 5$, $K \leq 5$, $Ca \leq 5$
11) K-Al-Silicate	$Na \leq 5$, $Ca \leq 5$, $Fe \leq 5$, $K \leq 5$, $Si > 20$, $Al \geq 15$, $(K+Al+Si) \geq 80$
12) Fe-Al-Silicate	$Fe \geq 5$, $Al \geq 15$, $Si > 20$, $S \leq 5$, $Ca \leq 5$, $K \leq 5$, $Na \leq 5$, $(Fe+Al+Si) \geq 80$
13) Ca-Al-Silicate	$S \leq 5$, $K \leq 5$, $Na \leq 5$, $Fe \leq 5$, $Ca \geq 5$, $Al \geq 15$, $Si > 20$, $(Ca+Al+Si) \geq 80$
14) Na-Al-Silicate	$S \leq 5$, $K \leq 5$, $Ca \leq 5$, $Fe \leq 5$, $Na \geq 5$, $Al \geq 15$, $Si > 20$, $(Na+Al+Si) \geq 80$
15) Aluminosilicate	$K \leq 5$, $Ca \leq 5$, $Fe \leq 5$, $Na \leq 5$, $Al \geq 20$, $Si > 20$, $(Al+Si) \geq 80$

Table 9. (continued)

16) Mixed Silicates	$S \leq 5$, $K < 10$, $Ca < 10$, $Fe < 10$, $Na < 10$, $Al > 20$, $Si > 20$, $(Al+Si+Fe+Ca+Na+K) \geq 80$
17) Fe-Silicate	$Fe > 10$, $S \leq 5$, $Ca \leq 5$, $K \leq 5$, $Na \leq 5$, $Al \leq 5$, $Si > 20$, $(Fe+Si) \geq 80$
18) Ca-Silicate	$S \leq 5$, $K \leq 5$, $Na \leq 5$, $Fe \leq 5$, $Ca > 10$, $Si > 20$, $(Ca+Si) \geq 80$
19) Ca-Aluminate	$P \leq 5$, $S \leq 5$, $Si \leq 5$, $Al \geq 15$, $Ca \geq 20$, $(Ca+Al) \geq 80$
20) Pyrite	$Ca < 10$, $10 \leq Fe \leq 40$, $S > 40$, $(Fe+S) \geq 80$
21) Pyrrhotite	$10 \leq S < 40$, $Fe > 40$, $(Fe+S) > 80$
22) Oxidized Pyrrhotite	$Ba < 5$, $Ca < 10$, $Fe > 40$, $S > 5$, $Fe/S > 1.5$, $(Fe+S) > 80$
23) Gypsum	$Ti < 10$, $Ba < 10$, $Si < 10$, $S > 20$, $Ca > 20$, $(S+Ca) \geq 80$
24) Barite	$Fe < 10$, $Ca \leq 5$, $S > 20$, $(Ba+Ti) > 20$, $(Ba+Ti+S) \geq 80$
25) Apatite	$P \geq 20$, $Ca \geq 20$, $Al \leq 5$, $S \leq 5$, $(Ca+P) \geq 80$
26) Ca-Al-P	$Ca > 10$, $Al > 10$, $P > 10$, $S \leq 5$, $Si \leq 5$, $(Ca+Al+P) \geq 80$
27) KCl	$K \geq 30$, $Cl \geq 30$, $(K+Cl) \geq 80$
28) Gypsum/Barite	$Fe \leq 5$, $Ca \geq 5$, $Ba \geq 5$, $Ti \geq 5$, $S > 20$, $(Ca+Ba+S+Ti) \geq 80$
29) Gypsum/Al-Silicate	$Al \geq 5$, $Si \geq 5$, $S \geq 5$, $Ca \geq 5$, $(Al+Si+S+Ca) \geq 80$
30) Si-Rich	$65 \leq Si < 80$
31) Ca-Rich	$65 \geq Ca < 80$, $Al < 15$
32) Ca-Si-Rich	$(Si+Ca) > 80$, $Ca > 20$, $Si > 20$
33) Unknown	All other compositions

cannot be identified without crystal and structural information such as might be obtained by X-ray diffraction and optical methods.

Five representative Big Sky samples and one Absaloka sample were selected for CCSEM analysis. They were ground to minus 60 mesh and prepared into polished pellets using the same procedure described in the previous chapter except the polishing step. Instead of alumina compound, 0.25 micron diamond compound was used in final polishing to reduce the possibility of alumina contamination. The polished pellets were carbon coated before performing CCSEM analysis.

The analysis of organically associated inorganic elements using SEM/EPMA was performed manually. Because SEM/EPMA cannot be used to identify macerals, the maceral particles need to be labeled (Folkedahl and others, 1992). The primary method was to inscribe a grid into the polished surface, assign grid numbers, and optically map selected areas by locating all the coal particles and labeling the maceral types. After mapping, the sample was ultrasonically cleaned and carbon coated. The pre-identified particles were easily located under SEM by comparison of the map and backscattered electron images (BEI). Considering that inorganic elements might not be uniformly distributed in macerals, a few small mineral-free rectangles in each particle were scanned rather than "point analyzed" to ensure representative results. The SEM/EPMA was operated at 15 kev and EDS spectra were acquired for 180 seconds. Because of limited SEM/EPMA hours, only one sample was analyzed. An inertinite-rich sample (A06) was selected to ensure adequate numbers of inertinite and huminite particles for analysis.

The evaluation of the accuracy and precision of the CCSEM analysis of coal minerals has been impeded because there are no certified coal or coal-ash mineral standards available, and there are only a limited number of laboratories employing CCSEM available to perform collaborative testing (Galbreath, 1993). Casuccio and others (1990) conducted an inter-laboratory testing study and evaluated the data from four participating laboratories. The repeatability relative standard deviation (ASTM, 1988b) for major minerals (>5 wt% on mineral basis) was <20%. The reproducibility relative standard deviation (ASTM, 1988b) for major minerals was <35% (Galbreath, 1993). Galbreath (1993, and personal communication) evaluated the precision of the CCSEM analysis at UNDEERC Natural Materials Analytical Research Laboratory. The Pittsburgh No. 8 and Illinois No. 6 coals from the Argonne Premium Coal Samples Program (Vorres, 1989) were analyzed periodically ten and four times, respectively, over an eight-month period. The repeatability relative standard deviation was <20% for major minerals, <40% for minor minerals (1 - 5 wt% on mineral basis), and 50% for trace minerals (<1 wt% on mineral basis).

The evaluation of the accuracy and precision of the analysis of maceral-associated elements has not been made because the analytical procedure is still under development. Improving the analytical procedure and conducting collaborative testing are necessary for future work. Therefore the reported results in Table 14 and Figure 17 should be considered provisional values.

7.2 Results

7.21 Mineral Composition

A total of 25 mineral phases were identified by CCSEM from the Big Sky samples. These phases include oxide minerals (quartz, iron oxide, rutile), carbonate minerals (calcite, dolomite), clay minerals (kaolinite, montmorillonite, K-Al-silicate, Fe-Al-silicate, Ca-Al-silicate, Na-Al-silicate, aluminosilicate, mixed silicate), sulfide minerals (pyrite, pyrrhotite), sulfate minerals (gypsum, barite), phosphate minerals (apatite), and some hypothetical mineral phases (alumina, Fe-silicate, Ca-silicate, gypsum/Al-silicate, Si-rich, Ca-rich) and unknown phases.

Tables 10 and 11 list all the "identified" phases and their quantity in the five Big Sky samples and one Absaloka sample. The data are given in weight percent on mineral basis in Table 10 and on a whole coal basis in Table 11. Sample B-I represents the top 30 cm of the seam, sample B-II the layer between the top layer and the upper parting, sample B-III the layer between the two partings, sample B-IV the layer between the lower parting and the 60 cm layer at the bottom, and sample B-V the 60 cm bottom layer. The mineral content of each sample counted using optical methods is also listed in the table for comparison. Although the microscopically counted mineral content is higher than that quantified by CCSEM for all samples, the two results are comparable except for sample B-I. The reason for the large difference on sample B-I is not clear; perhaps the high content of pyrite on

Table 10. Mineral composition of the Rosebud seam samples determined by computer–controlled scanning electron microscopy (CCSEM)

Sample No.	B–I	B–II	B–III	B–IV	B–V	A06
Total vol%	6.3	2.54	4.27	2.47	2.82	2.5
Total wt%	14.91	4.98	8.88	4.76	5.33	5.23
wt% on mineral basis						
Quartz	9.0	26.5	6.6	30.4	5.4	15.9
Iron Oxide	0.4	0.3	0.1	0.3	0.1	0.3
Rutile		0.3	0.3	0.1	0.2	0.3
Alumina		0.2	0.2			0.2
Calcite	0.2	15.9	1.1	2.9	0.6	0.8
Dolomite	0.1	0.1	0.2		0.2	
Kaolinite	7.2	35.4	41.5	44.0	73.3	44.6
Montmorillonite	1.5	1.4	1.9	1.4	4.1	0.1
K–Al–silicate	8.4	1.9	8.8	0.6	1.0	
Fe–Al–silicate	0.3		0.3			
Ca–Al–silicate		0.3	0.3	0.6	1.0	0.8
Na–Al–silicate					0.2	
Aluminosilicate	0.9	3.2	2.0	5.6	2.1	6.6
Mixed Al–silicate	0.5	0.4	0.3	0.7	1.3	
Fe–Silicate	0.1					
Ca–Silicste		0.1				
Pyrite	56.7	9.3	28.1	7.2	2.9	24.6
Pyrrhotite	0.4					
Oxidized pyrrhotite	0.1	0.2	0.2			
Gypsum	2.4	0.1	0.1	0.1	0.4	0.1
Barite	1.0	0.8		0.7	2.9	
Apatite	0.2	0.2		0.9		0.1
Ca–Al–P (Crandallite?)						2.3
Gypsum/Al–silicate	0.7	0.1	0.3	0.1	0.2	0.2
Si–rich	3.4	0.5	1.8	0.5	0.4	
Ca–rich		0.3	0.2	0.1	0.1	0.2
Unknown	6.4	2.5	5.7	3.7	3.5	2.8
Total petrographically counted vol%	13.3	3.0	5.6	2.5	3.4	2.1

B = Big Sky mine sample; A = Absaloka mine sample.

Table 11. Mineral composition of the Rosebud coal samples on coal basis (wt%) calculated from the data in Table 10.

Sample No.	B–I	B–II	B–III	B–IV	B–V	A06
Quartz	1.34	1.32	0.59	1.45	0.29	0.83
Iron Oxide	0.06	0.01	0.01	0.01	0.01	0.02
Rutile		0.01	0.03	0.00	0.01	0.02
Alumina		0.01	0.02			0.01
Calcite	0.03	0.79	0.10	0.14	0.03	0.04
Dolomite	0.01	0.00	0.02		0.01	
Kaolinite	1.07	1.76	3.69	2.09	3.91	2.33
Montmorillonite	0.22	0.07	0.17	0.07	0.22	0.01
K–Al–silicate	1.25	0.09	0.78	0.03	0.05	
Fe–Al–silicate	0.04		0.03			
Ca–Al–silicate		0.01	0.03	0.03	0.05	0.04
Na–Al–silicate					0.01	
Aluminosilicate	0.13	0.16	0.18	0.27	0.11	0.35
Mixed Al–silicate	0.07	0.02	0.03	0.03	0.07	
Fe–Silicate	0.01					
Ca–Silicste		0.00				
Pyrite	8.45	0.46	2.50	0.34	0.15	1.29
Pyrrhotite	0.06					
Oxidized pyrrhotite	0.01	0.01	0.02			
Gypsum	0.36	0.00	0.01	0.00	0.02	0.01
Barite	0.15	0.04		0.03	0.15	
Apatite	0.03	0.01		0.04		0.01
Ca, Al–P						0.12
Gypsum/Al–silicate	0.10	0.00	0.03	0.00	0.01	0.01
Si–rich	0.51	0.02	0.16	0.02	0.02	
Ca–rich		0.01	0.02	0.00	0.01	0.01
Unknown	0.95	0.12	0.51	0.18	0.19	0.15

B = Big Sky mine sample; A = Absalok mine sample.

the polished surface is an artifact resulting from settling caused by gravity during setting of the epoxy in sample preparation.

Quartz

Quartz is one of the major minerals in all samples. The lowest concentration of quartz is 0.3 wt% on coal basis (5.4 wt% on mineral basis) in sample B-V. The next lowest concentration is 0.6 wt% (6.6 wt% on mineral basis) in sample B-III. The rest of the samples have similar quartz contents of 1.3 to 1.4 wt% on coal basis. Quartz was always found in association with clarite and trimacerite as angular fragments in a detrogelinite groundmass (Plate VI-1), suggesting that it is allochthonous and brought into the sedimentary basin by surface water or wind.

Clay Minerals

Clay minerals are the most abundant minerals for the whole seam at Big Sky, ranging from 2.13 to 4.98 wt% in the five samples on coal basis. Kaolinite is the most abundant clay mineral ranging from 1.07 to 3.91 wt% on coal basis (7.2 to 73.3 wt% on mineral basis), followed by K-Al-silicate and aluminosilicate identified by CCSEM as possible clay minerals. Two samples (B-III, B-V) which are particularly rich in identified clay minerals coincide with those poor in quartz. The reason for this coincidence is not understood. Clay minerals can be associated with any major macerals as either aggregates of micron-sized authigenic crystals or fragmental grains ranging from sub-micron size to over 100 microns. Authigenic kaolinite often fills the

cell lumens of the structured macerals textinite, ulminite, fusinite and semifusinite as euhedral to anhedral crystals, sometimes associated with the phosphate mineral crandallite(?) (Plates V-4, VII-1, VII-2). Fragmental kaolinite particles were found in association with maceral detrogelinite and fragments of quartz (Plate VI-1), zircon (Plate VII-3), and rutile (Plate VII-4). They might originate from kaolinized mineral or rock fragments, or more possibly, volcanic glass.

Carbonate Minerals

Although two carbonate minerals, calcite and dolomite, were identified, only calcite is common. Calcite in sample B-II amounts to 0.8 wt% on coal basis (15.9 wt% on mineral basis). In sample B-III and B-IV, its concentration is as low as 0.1 wt% on coal basis, and in the other two samples close to zero. Calcite occurs in cracks as an epigenetic mineral.

Sulfide Minerals

Pyrite is the only important sulfide mineral identified by CCSEM. It is extremely abundant in the top 30 cm (sample B-I) of the seam, with 8.5 wt% on coal basis (56.7 wt% on mineral basis). The other pyrite-rich sample is B-III, in which pyrite counts 2.5 wt% on coal basis (28.1 wt% on mineral basis). In the remaining samples, pyrite is less than 0.5 wt% on coal basis. Pyrrhotite was encountered as a trace mineral only in sample B-I, and oxidized pyrrhotite in sample B-I, B-II and B-III. Two generations of pyrite were recognized optically according to their habits.

Diagenic pyrite occurs as framboids (Plate III-3), whereas epigenic pyrite occurs as anhedral to euhedral crystals in coal cracks (Plates III-4).

Sulfate Minerals

The sulfate minerals are minor authigenic phases gypsum and barite in all of the samples. Their total concentration is greater than 0.1 wt% on coal basis only in sample B-I and B-V.

Phosphate Minerals

Only one phosphate mineral, apatite, was recognized by CCSEM as a trace mineral in the Big Sky samples. It occurs either as anhedral crystals in association with kaolinite (Plate Vi-3) or as fragments in tonstein (Plate VI-4). However, another phosphate mineral, crandallite(?) was identified by optical microscope and manual SEM inspection. CCSEM analysis on one Absaloka sample (A06) indicated that the concentration of this phase (reported as Ca Al-P by CCSEM) was as high as 2.3 wt% on mineral basis (0.1 wt% on coal basis).

Crandallite(?) was found in cell lumens of woody structures, either in textinite, ulminite, fusinite, or semifusinite (Plates V-4, VII-1 and VII-2). Most crandallite(?) crystals are spherical with diameters of a few to 10 microns. Microscopically, they can be easily recognized by their unique orange-yellow fluorescence when illuminated with blue fluorescent incident light (Plate V-4). Larger crandallite(?) crystals are variable from core to shell in fluorescence and in brightness of backscattered electron

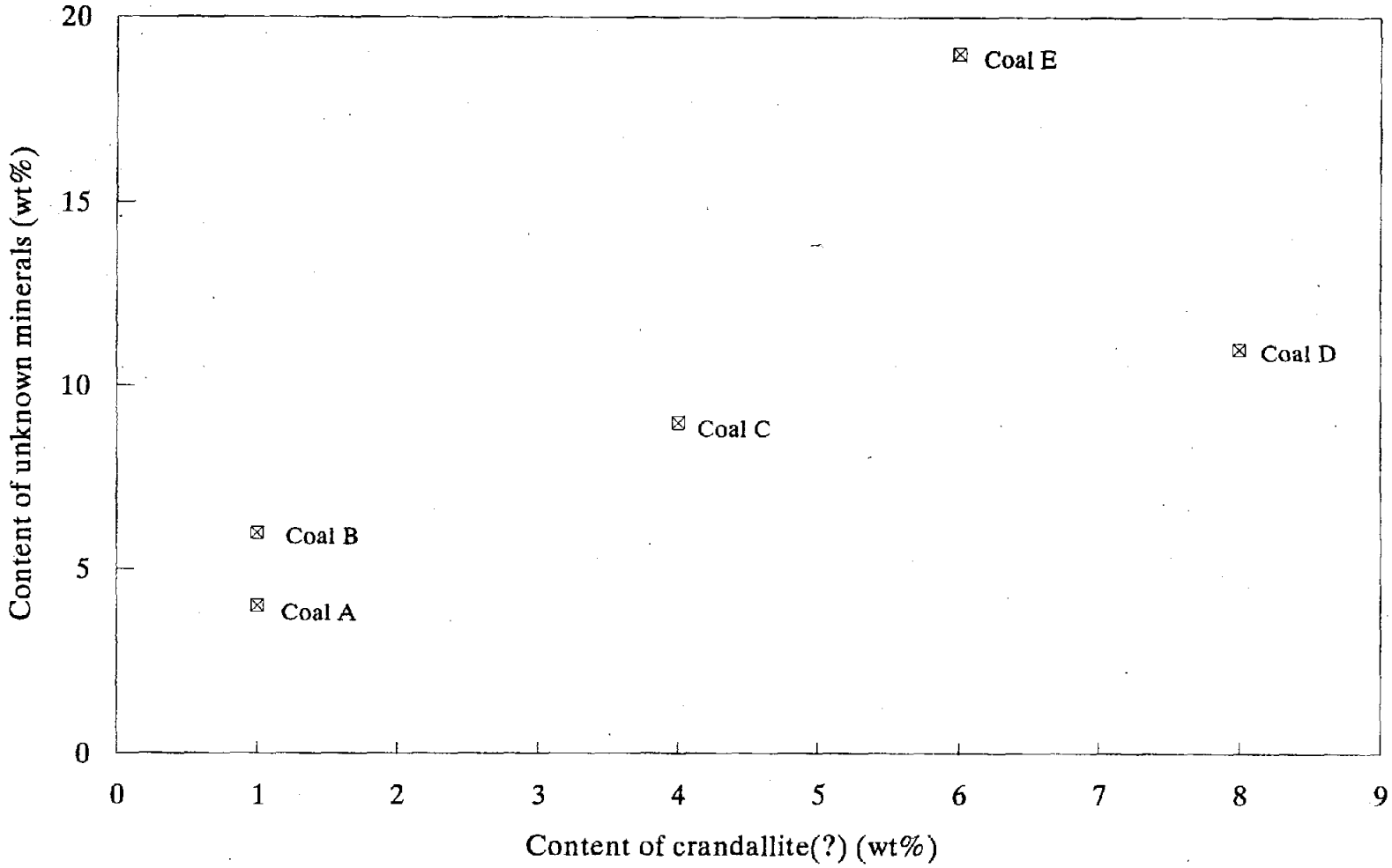

Figure 16. Correlation of CCSEM identified crandallite(?) content and that of unknown minerals in five Powder River Basin coals (wt% on mineral basis). From Weisbecker and others (1992).

image (BEI), suggesting possible variability in chemical composition. Crandallite(?) particles in the Big Sky samples are very fine (less than 2 micron) and associated with clays. The failure to recognize them by CCSEM is perhaps because they are too fine to be identified. Possibly the crandallite(?)-clay mixtures are classified by CCSEM as unknown phases. Previous analysis of five other Powder River Basin coals (Weisbecker and others, 1992) indicated that the content of unknown mineral phases in CCSEM results is positively related to the content of crandallite(?) (Figure 16). This means that the actual crandallite(?) content in those coals might be higher than that reported by CCSEM analysis. In fact, crandallite(?) may be a major mineral phases in some Powder River Basin coals.

Chemically, crandallite is one of the crandallite-group minerals, which are trigonal phosphates and arsenates of general formulas $AB_3(XO_4)_2(OH)_5H_2O$ or $AB_3(XO_4)_2(OH)_6$ (X = Ba, Bi, Ca, Ce, Nd, Pb, Sr, Th; B = Al, Fe^{+3}; X = As, P, Si) (Fleischer, 1980). End members of this group are listed in Table 12. In crandallite, Ca^{+2} can be replaced by Sr^{+2} or Ba^{+2}. Microprobe analysis reveals that Ba/Ca ratio in this mineral ranges from 0.03 to 0.32 (Table 13). Pure minerals of this group should have an element ratio of A/B/X = 1/3/2, but none of the A/B/X ratios calculated from the electron microprobe analysis data is close this number. It is not understood whether this indicates the inaccuracy of the analysis or suggests other similar minerals. Further mineralogical work needs to be done on this mineral phase.

Table 12. Chemical composition of crandallite group minerals (after Fleischer, 1980; Gary and others, 1972)

Crandallite	$CaAl_3(PO_4)_2(OH)_5H_2O$
Gorceixite	$BaAl_3(PO_4)_2(OH)_5H_2O$
Goyazite	$SrAl_3(PO_4)_2(OH)_5H_2O$
Plumbogummite	$PbAl_3(PO_4)_2(OH)_5H_2O$
Dussertite	$BaFe^{+3}{}_3(AsO_4)_2(OH)_5$
Eylettersite	$(Th, Pb)_{1-x}Al_3(PO_4, SiO_4)_2(OH)_6$
Florencite	$CeAl_3(PO_4)_2(OH)_6$
Florencite(Nd)	$(Nd, Ce)Al_3(PO_4)_2(OH)_6$
Waylandite	$(Bi, Ca)Al_3(PO_4, SiO_4)_2(OH)_6$
Zairite	$Bi(Fe^{+3}, Al)_3(PO_4)_2(OH)_6$

Other Mineral Phases

Other identified phases include rutile, iron oxides, alumina, Fe-silicate, Ca-silicate, gypsum/Al-silicate, Si-rich phase and Ca-rich phase. Rutile contents ranged from 0.1 to 0.3 wt% (mineral basis) in all samples except B-I. Alumina is a trace phase encountered only in sample B-II and B-III with concentration 0.2 wt% on mineral basis (0.0 wt% on coal basis). Fe-silicate and Ca-silicate phases are even rarer and it is not clear what specific minerals they are. Unknown mineral phases count for 2.5 to 6.4 wt% on mineral basis; they might represent mixtures of two or

Table 13. Chemical composition (atom%) of crandallite(?) in samples A06, A18 and R05, determined by electron microprobe analysis at the EERC Natural Materials Analytical Research Laboratory

Analysis No.	1	2	3	4	5	6	7	8	9	10	11
Na	0.28	0.31	0.18	0.008	0.004	0.001	0.65	0.55	0.004	0.38	0.002
Mg	0.002	0	0.005	0.002	0	0.008	0.49	0.001	0.82	0.008	0.43
Al	17.89	20.91	21.98	19.74	19.41	19.09	19.19	19.11	18.82	18.87	19.05
Si	0.79	0.22	0.006	0	0	0	0.009	0	0	3.63	0
P	8.93	9.77	9.09	7.2	9.44	10.45	9.24	9.9	9.16	7.42	9.97
S	0.34	0.008	0.008	0.27	0.37	0.007	0.007	0.006	0.6	0.007	0.29
Cl	0.29	0.004	0.004	0.14	0.86	0.35	0.38	0.003	0.59	0.83	0.35
K	0.21	0.001	0.09	0.008	0.002	0.002	0.001	0	0.001	0.002	0.21
Ca	8.58	5.25	4.64	11.5	5.95	6.44	6.95	7.81	6.39	5.16	6.41
Ti	0.009	0.0085	0.18	0.001	0.009	0.18	0.21	0.009	0.009	0.009	0.009
Cr	0.007	0.0068	0.006	0.008	0.007	0.007	0.007	0.007	0.007	0.27	0.007
Fe	0.006	0.21	0.0053	0.006	0.0064	0.0065	0.27	0.006	0.34	0.006	0.006
Ba	0.56	0.68	1.49	0.36	0.58	0.34	0.41	0.56	0.27	0.32	0.37
O(by difference)	62.14	62.64	62.34	60.78	63.38	63.14	62.21	62.07	63	63.11	62.91
Ba/Ca	0.07	0.13	0.32	0.03	0.10	0.05	0.06	0.07	0.04	0.06	0.06
(Ca+Ba)	9.14	5.93	6.13	11.86	6.53	6.78	7.36	8.37	6.66	5.48	6.78
(Al+Fe)	17.90	21.12	21.99	19.75	19.42	19.10	19.46	19.12	19.16	18.88	19.06
(P+Si)	9.72	9.99	9.10	7.20	9.44	10.45	9.25	9.90	9.16	11.05	9.97
(Al+Fe)/(Ca+Ba)	1.96	3.56	3.59	1.66	2.97	2.82	2.64	2.28	2.88	3.44	2.81
(P+Si)/(Ca+Ba)	1.06	1.68	1.48	0.61	1.45	1.54	1.26	1.18	1.38	2.02	1.47
(Al+Fe)/(P+Si)	1.84	2.11	2.42	2.74	2.06	1.83	2.10	1.93	2.09	1.71	1.91

more minerals. Zircon (Plate VII-3), though not identified by CCSEM, was found by manual SEM inspection. Along with fragmental quartz, kaolinite and rutile (Plate VII-40), zircon was found as sub-angular fragments associated with detrogelinite.

A similar mineral association was found in the Wyodak-Anderson seam of the basin in a previous study, and was interpreted to originate from volcanic ash (Triplehorn and others, 1991). The fragmental quartz, zircon, rutile and apatite grains in the Rosebud coal might have been derived from volcanic ash, the fragmental kaolinite from kaolinized volcanic glass fragments, and the authigenic kaolinite and crandallite in cells of structured macerals from reprecipitation of dissolved components of original ash material.

7.22 Organically Associated Inorganic Elements in Major Macerals

Thirteen elements, Na, Mg, Al, Si, P, S, Cl, K, Ca, Ti, Mn, Fe and Ba were analyzed in the macerals ulminite, detrogelinite and fusinite in one Absaloka sample (A06) (Table 14 and Figure 17). The total content of the 13 elements is 1.31 to 5.39 wt% (on element basis) in fusinite, 2.21 to 3.50 wt% in ulminite, and 2.44 to 2.84 in detrogelinite. Seven elements, Na, Mg, Al, Si, S, Cl and Ca, make up over 95% of the total element concentration. Ca is the richest in all the three macerals, followed by Al, Mg, S, Na, Cl and Si.

Table 14. Reported concentrations (wt%) of elements in fusinite, ulminite and detrogelinite of sample A06

	Na	Mg	Al	Si	P	S	Cl	K	Ca	Ti	Mn	Fe	Ba	Total
F−1	0.15	0.33	0.71	0.09	0.00	0.19	0.15	0.04	1.40	0.00	0.00	0.00	0.00	3.06
F−2	0.24	0.38	0.55	0.20	0.00	0.22	0.19	0.00	1.48	0.00	0.00	0.09	0.00	3.35
F−3	0.14	0.46	0.34	0.11	0.00	0.29	0.10	0.00	1.36	0.00	0.00	0.00	0.00	2.80
F−4	0.18	0.39	0.34	0.11	0.00	0.18	0.17	0.00	0.76	0.00	0.00	0.00	0.00	2.13
F−5	0.14	0.44	1.40	0.98	0.00	0.23	0.12	0.00	1.94	0.06	0.08	0.00	0.00	5.39
F−6	0.15	0.48	1.04	0.66	0.00	0.20	0.12	0.04	1.71	0.00	0.00	0.00	0.00	4.40
F−7	0.00	0.22	0.08	0.07	0.00	0.17	0.17	0.02	0.45	0.00	0.00	0.00	0.13	1.31
F−8	0.17	0.45	0.09	0.09	0.00	0.19	0.04	0.04	1.09	0.00	0.00	0.00	0.00	2.16
F−9	0.11	0.44	0.07	0.07	0.00	0.20	0.07	0.04	1.01	0.00	0.00	0.00	0.00	2.01
F−10	0.29	0.57	1.13	0.17	0.00	0.17	0.09	0.00	0.96	0.00	0.00	0.00	0.00	3.38
F−11	0.19	0.40	0.22	0.07	0.00	0.20	0.05	0.00	1.21	0.00	0.00	0.00	0.00	2.34
F−12	0.10	0.33	0.54	0.25	0.00	0.10	0.26	0.00	0.42	0.06	0.00	0.00	0.00	2.06
F−13	0.20	0.20	0.07	0.00	0.00	0.19	0.06	0.00	0.62	0.00	0.00	0.00	0.00	1.34
F−14	0.09	0.08	0.59	0.07	0.00	0.23	0.06	0.02	0.74	0.00	0.00	0.00	0.00	1.88
Mean	0.15	0.37	0.51	0.21	0.00	0.20	0.12	0.01	1.08	0.01	0.01	0.01	0.01	2.69
U−1	0.19	0.37	0.60	0.10	0.00	0.44	0.12	0.00	1.02	0.00	0.00	0.00	0.00	2.84
U−2	0.15	0.34	0.44	0.02	0.00	0.46	0.12	0.00	0.79	0.00	0.14	0.08	0.09	2.63
U−3	0.15	0.34	0.56	0.06	0.00	0.42	0.10	0.00	0.96	0.04	0.06	0.00	0.00	2.69
U−4	0.14	0.30	0.24	0.07	0.00	0.34	0.13	0.00	0.91	0.08	0.00	0.00	0.00	2.21
U−5	0.12	0.27	0.63	0.07	0.00	0.32	0.03	0.00	0.94	0.12	0.08	0.00	0.00	2.58
U−6	0.10	0.30	0.42	0.07	0.00	0.30	0.07	0.03	0.92	0.05	0.00	0.00	0.00	2.26
U−7	0.27	0.33	0.47	0.06	0.00	0.39	0.03	0.00	0.90	0.00	0.00	0.06	0.08	2.59
U−8	0.20	0.36	0.60	0.06	0.00	0.42	0.05	0.04	1.04	0.00	0.00	0.00	0.00	2.77
U−9	0.09	0.26	0.81	0.07	0.11	0.43	0.05	0.05	1.32	0.09	0.00	0.07	0.15	3.50
U−10	0.22	0.34	0.39	0.08	0.00	0.46	0.07	0.04	1.23	0.15	0.00	0.00	0.00	2.98
U−11	0.14	0.33	0.45	0.12	0.00	0.43	0.06	0.05	1.06	0.07	0.00	0.00	0.00	2.71
U−12	0.23	0.41	0.49	0.06	0.00	0.44	0.08	0.04	1.26	0.00	0.00	0.00	0.00	3.01
U−13	0.16	0.41	0.50	0.04	0.00	0.46	0.09	0.03	1.11	0.00	0.00	0.00	0.00	2.80
Mean	0.17	0.34	0.51	0.07	0.01	0.41	0.08	0.02	1.04	0.05	0.02	0.02	0.02	2.74
D−1	0.06	0.22	0.30	0.16	0.00	0.48	0.17	0.00	1.05	0.00	0.00	0.00	0.00	2.44
D−2	0.07	0.24	0.40	0.10	0.00	0.48	0.24	0.00	1.16	0.06	0.00	0.00	0.09	2.84
D−3	0.15	0.29	0.38	0.12	0.00	0.42	0.43	0.00	0.95	0.00	0.00	0.00	0.00	2.74
D−4	0.18	0.45	0.43	0.22	0.00	0.28	0.10	0.00	1.18	0.00	0.00	0.00	0.00	2.84
Mean	0.12	0.30	0.38	0.15	0.00	0.42	0.24	0.00	1.09	0.02	0.00	0.00	0.02	2.72

F = fusinite; U = ulminite; D = detrogelinite.

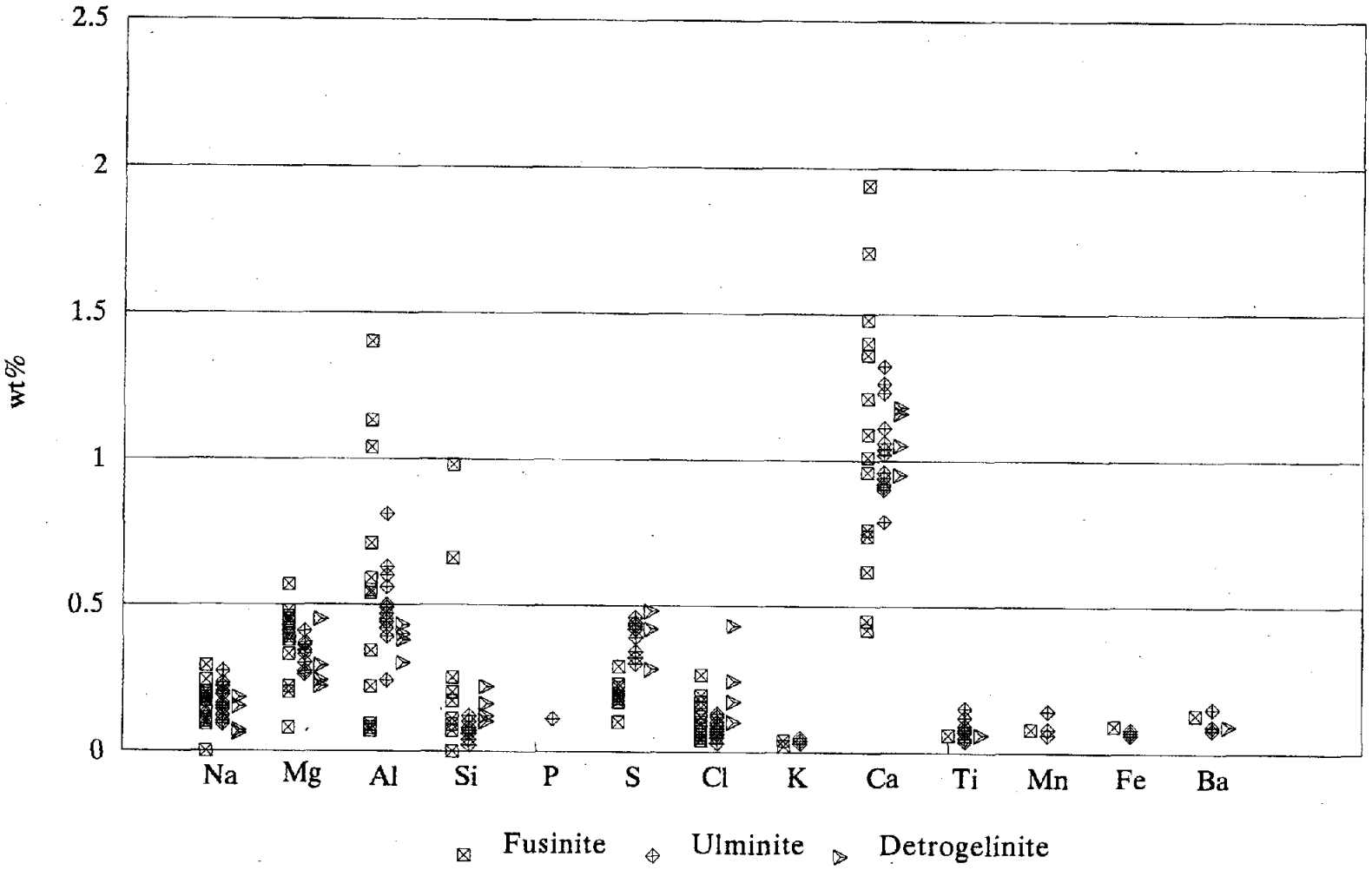

Figure 17. Inorganic elements associated with fusinite, ulminite and detrogelinite in sample A06 from the Absaloka mine.

Na

Although the concentration of Na in detrogelinite is a little lower than in fusinite and ulminite, it is similar in the three major macerals. Although one analysis on fusinite did not detect Na, the other 13 analyses on this maceral reported Na concentrations ranging from 0.09 to 0.29 wt% with an average of 0.15 wt%. In ulminite, its concentration ranges from 0.09 to 0.27 wt% with an average of 0.17 wt%, and in detrogelinite from 0.06 to 0.18 wt% with an average of 0.12 wt%.

Mg

Like Na, Mg has comparable concentrations in the three macerals. Except for one lower value (0.08 wt%), fusinite has Mg content from 0.20 to 0.57 wt% with an average of 0.37 wt%, ulminite from 0.26 to 0.41 wt% with an average of 0.34 wt%, and detrogelinite from 0.22 to 0.45 wt% with an average of 0.30 wt%.

Al

Aluminum is the second richest element in the macerals after Ca. Although it has the same average concentration (0.51 wt%) in fusinite and ulminite, its concentration range in fusinite is much wider than in ulminite (Figure 17). Its concentration is lower in detrogelinite, ranging from 0.30 to 0.43 wt% with an average of 0.38 wt%.

Si

Two analyses of fusinite reported Si concentration unusually higher than the rest. These two analyses also have much higher Al, Ca and total-element concentrations (Table 14 and Figure 17). It is possible that the electron beam penetrated through the maceral and detected some mineral underneath. Minerals are commonly present in the cell lumens of fusinite. Discarding the two highest and the one lowest (0.00 wt%) number, Si has about the same concentration in fusinite (0.07 to 0.25 wt% with an average of 0.12 wt%) and detrogelinite (0.10 to 0.22 wt% with an average of 0.15 wt%), but has a lower concentration in ulminite (0.02 to 0.12 wt% with an average of 0.07 wt%).

S

Sulfur has about same concentration in ulminite and detrogelinite, ranging 0.30 to 0.46 wt% with an average of 0.41 wt%, and 0.28 to 0.48 wt% with an average of 0.42 wt%, respectively. Fusinite has significantly lower sulfur concentration, ranging 0.10 to 0.29 wt% with an average of 0.20 wt%.

Cl

Detrogelinite has the highest Cl content, ranging 0.10 to 0.43 wt% with an average of 0.24 wt%, followed by fusinite, ranging 0.04 to 0.26 wt% with an average of 0.12 wt%. Ulminite has the lowest Cl content, ranging 0.3 to 0.12 wt% with an average of 0.08 wt%.

extractable elements may be present as coordination complexes. In what form Si and Cl are present in macerals is not well understood. Neither ammonium acetate nor hydrochloric acid can extract Si from coal.

The exchangeable ions could have been precipitated by groundwater during the periods of peat development and diagenesis. Ground water normally contains various ions such as Na^{+}, Mg^{++}, K^{+} and Ca^{++}. The capacity of a maceral to exchange those ions depends upon the fraction of total oxygen functional groups in its molecular structure. The macerals of the Rosebud coal may have molecular structures similar to those of the Wyodak coal, as they are in the same basin and are of the same rank. A similar fraction of oxygen functional groups in inertinite and huminite may be the explanation of similar concentrations of exchangeable ions (Na, Mg, Ca) in the three macerals.

Factors governing the concentration of elements incorporated as coordination complexes in macerals are not well understood. Macerals may inherit those elements from original plant materials. The fraction of elements of this origin depends upon their concentration in original plant materials. Huminite macerals could incorporate some elements in their molecular structures during gelification. Fusinite and semifusinite may lose some inherited elements when woody tissue is burnt, especially the volatile elements like S, O and H. As a result, the distribution of the organic elements and inorganic elements incorporated as coordination complexes is complicated.

7.3 Application to Combustion

Development of a detailed understand of ash formation and deposition during combustion can be ascertained through a study of the petrography and inorganic geochemistry of coals. Accurate prediction of the role of inorganic constituents during combustion requires a quantitative data of coal composition and combustion conditions. Extensive discussion of combustion conditions is beyond the scope of this study. However, the dependence of ash formation and deposition on the distribution of coal macerals and inorganic components is discussed n this section.

Minerals and organically associated inorganic elements are distributed in several forms in pulverized coal used for combustion. Organically associated inorganic elements are more evenly distributed within coal particles. Mineral grains are included in the coal or excluded, depending upon the fineness of the ground coal particles and the size of mineral grains. For example, the coarse calcite in the Rosebud coal will more likely occur as excluded particles when the coal is pulverized, while the fine (<10 micron) crandallite(?) grains will remain included in the coal. The fine, diagenic framboidal pyrite is more likely included, while the coarse, epigenic pyrite is more likely excluded. Quantitative data for included and excluded mineral grains can be determined by CCSEM and automated image analysis (AIA) (Steadman and others, 199).

During combustion, the inorganic components of coal undergo complex physical and chemical transformations to produce intermediate ash species which include inorganic gases, liquids and solids (Benson and others, 1992). Fireside ash

deposition, fouling and slagging occur when intermediate ash species accumulate on heat-transfer surfaces. The accumulation of ash particles depends upon their ability to arrive at the heat-transfer surfaces and to form strong bonds with the surfaces. The formation of strong bonds depends upon the temperature, physical and chemical characteristics of the heat transfer surfaces, melting behavior of ash particles, and thermal and chemical compatibility of the ash species and the material (steel) of which the heat-transfer surface is made (Abbott and Austin, 1986; Benson and Austin, 1990). Once a strongly bonded ash layer has accumulated, the temperature of the surface increases, leading to more efficient capture of impacting ash particles.

The partitioning of the inorganic components to form ash intermediates during combustion depends upon the association and physical and chemical characteristics of the inorganic components and combustion conditions (Benson and others, 1992). There are three possible associations of organic and inorganic components in pulverized coal: 1) excluded mineral particles; 2) included mineral grains and organically bound inorganic elements in maceral; and 3) organically bound inorganic elements in maceral. The transformations of excluded minerals are dependent upon their physical and chemical characteristics. Excluded quartz can be pass through the combustion system without minimal changes in morphology and chemistry. Excluded clay minerals may fragment during dehydration, melt, and form cenospheres (Benson and others, 1992). Excluded carbonate minerals, such as calcite, will fragment because of their cleavage and will change into oxides with loss of CO_2. The behavior of excluded pyrite is dependent upon morphology. Framboidal pyrite fragments more

easily than massive pyrite. Both framboidal and massive pyrite transform to pyrrhotite and oxidize to FeO, Fe_3O_4 and Fe_2O_3 during combustion (Benson and others, 1992).

The transformation of included mineral grains is dependent upon the combustion characteristics of char (Benson and others, 1992). Coal combustion may be considered as a two-stage process consisting of devolatilization and char combustion. The first stage involves the heating and pyrolysis of coal particles and includes the release, ignition and combustion of the volatiles. The second stage is the combustion of the char. In the first stage, most nonvolatile inorganic species remain with char. During the second stage, each mineral grain may form one ash particle without fragmentation and coalescence, or break into several fragments as a result of char fragmentation, or coalesce into large ash particle when the reducing char surface brings the mineral grains together. Chemical decomposition and reaction of mineral grain with organically associated cations may also occur in this stage. The influence of macerals on char fragmentation is a subject to be further studied.

Organically bound inorganic elements transform into fine particles through vaporization and condensation during combustion (Benson and others, 1992). The condensation occurs on heat transfer surfaces or surfaces of entrained ash particles and ash deposits, producing low melting-point phases. The development of liquid phase materials results in the formation of fouling deposits. Oxides such as K_2O, Na_2O, CaO are known as strong fluxing agents which can cause liquids to form at relatively low temperature when added to the Al_2O_3 - SiO_2 system. In addition, reactions occur between the organically associated cations and mineral grains

associated in coal particles and between the cations and organic sulfur during combustion. The reaction of cations and sulfur produces a sulfate phase which is very important in the formation of low-temperature fouling deposits, both in terms of providing liquid for sintering and fly ash capture and in dissolution of aluminosilicates.

8. SUMMARY AND CONCLUSIONS

1) Macroscopically, the dominant lithotypes in Rosebud coal are clarain layers and thin vitrain layers, and less abundant fusain and durain layers or lenses. Most of the vitrain layers are too thin to be counted, although a few as thick as 3 to 5 cm were found. Microscopically, the most abundant maceral group is huminite, followed by inertinite, liptinite, along with a few percent of minerals. The samples from each mine have similar mean petrographic compositions except somewhat variable inertinite. Within-seam petrographic variation is high and delineates lithologic layering similar in sequence and thickness at the Absaloka and Big Sky mines.

2) Despite the similarity in petrographic composition, samples from the three mines are variable in mean huminite reflectance from 0.31% at the Rosebud to 0.34% at the Absaloka and 0.39% at the Big Sky mine, indicating that the coal is transitional from lignite at Absaloka and Rosebud to subbituminous C at Big Sky. A direct relation of mean huminite reflectance with mean huminite abundance and an inverse relation with mean inertinite abundance were recognized, suggesting a possible correlation between coalification and depositional environment.

3) Maceral and microlithotype abundances indicated that the Rosebud seam was developed in a mire or several adjacent mires in a lagoonal and fluvial-deltaic

depositional system with mixed vegetation or alternating from arboreal to herbaceous vegetation.

4) Mineral content in the Rosebud seam is dominated by clay minerals, quartz and calcite. Pyrite content is low except in the top 30 cm of the Big Sky profile. The samples from the Big Sky mine, excluding that of the top layer, have mean pyrite abundance of 0.4 wt%. A phosphate mineral, crandallite(?), was found as an authigenic mineral in some layers. This mineral, along with kaolinite, quartz, zircon, rutile and apatite, might originate from volcanic ash.

5) Organically associated inorganic elements have significant concentration in macerals. Calcium is the richest inorganic element in ulminite, detrogelinite and fusinite, followed by Al, S, Mg, Cl and Na. These elements are present in macerals either in the form of ions associated with oxygen functional groups or as coordination complexes in the coal molecular structure.

6) Both minerals and organically associated inorganic elements contribute to ash deposition during combustion. Organically bound cations and sulfur may react during combustion to produce low melting-point sulfate phases which are important in the formation of low-temperature fouling deposits.

7) Several subjects are suggested for future studies including: a) investigation of the correlation of the huminite reflectance with macerals; b) investigation of the correlation of inorganic components (mineral and maceral-associated elements) of the Rosebud coal with its depositional environment and coalification history; c) investigation of the distribution and association of trace metals As, Se, Co, Ni, Cd,

Hg and Pb in the Rosebud coal as well as other western low-rank coals; d) improvement of the analytical procedure for maceral-associated elements; and e) combustion testing of the Rosebud coal to determine the effect of the inorganic components on ash formation and deposition and the behavior of the trace metals during combustion.

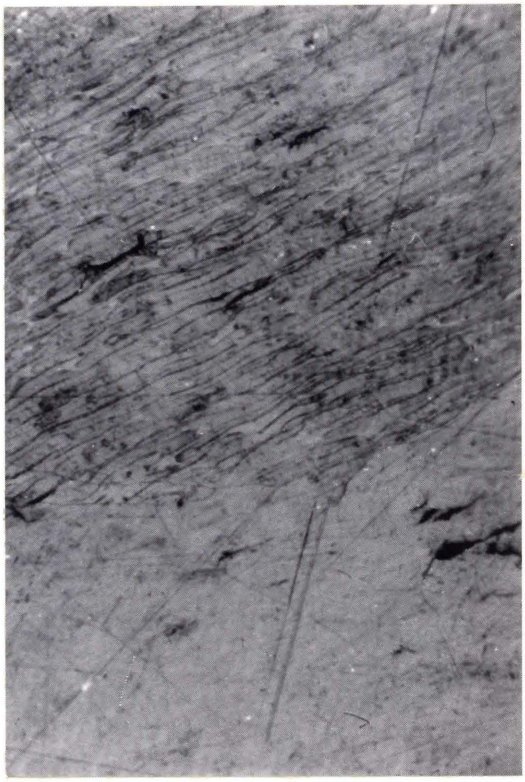

I-2

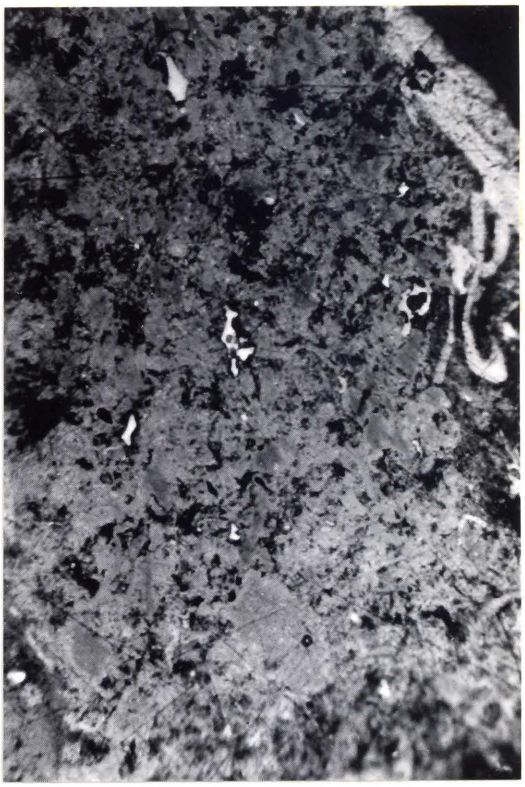

I-4

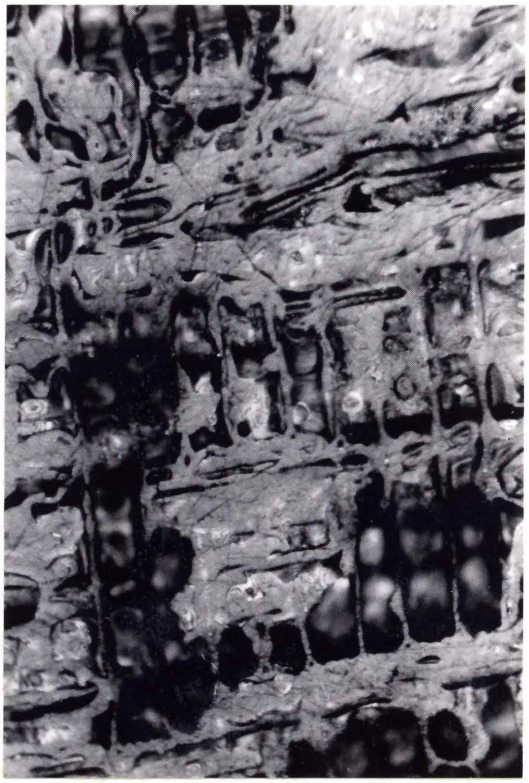

I-1

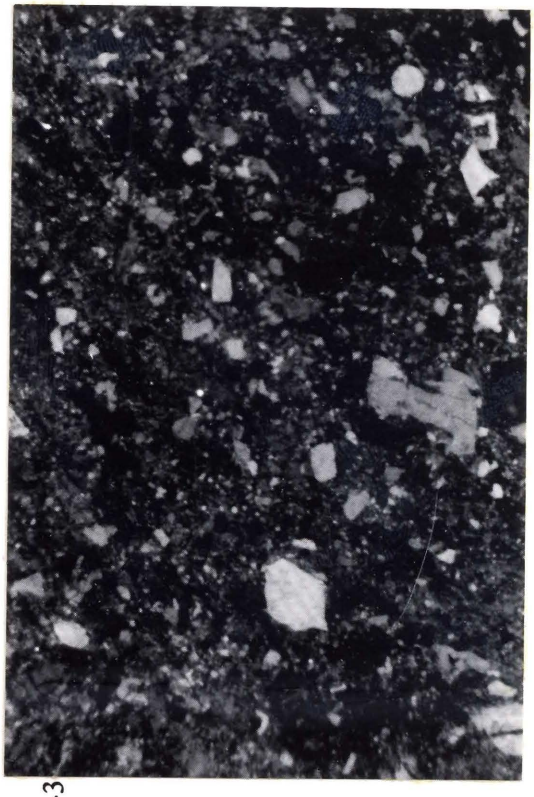

I-3

II-2

II-4

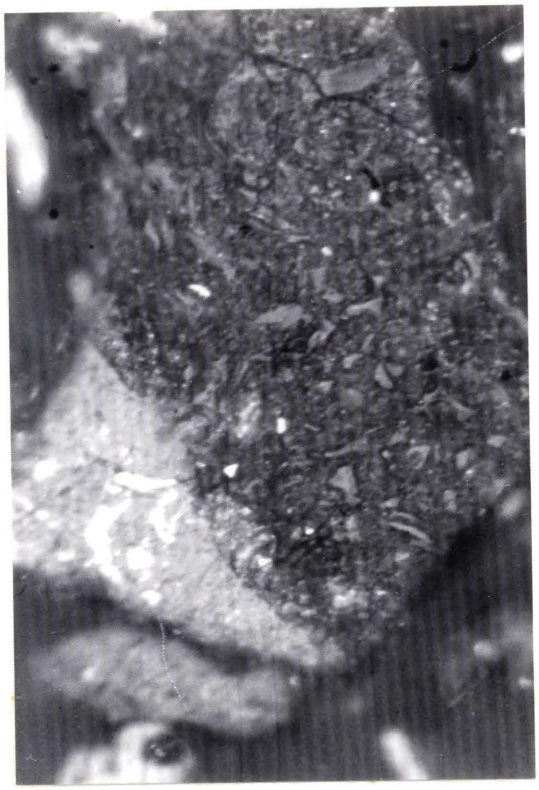

II-1

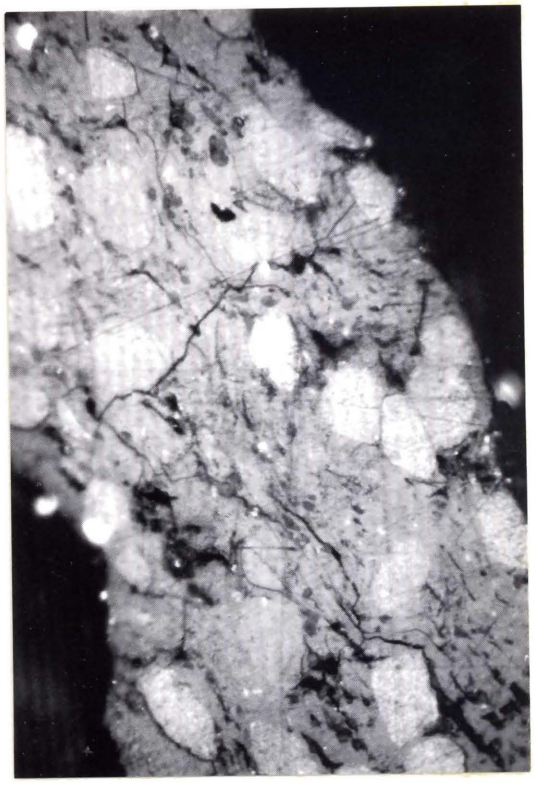

II-3

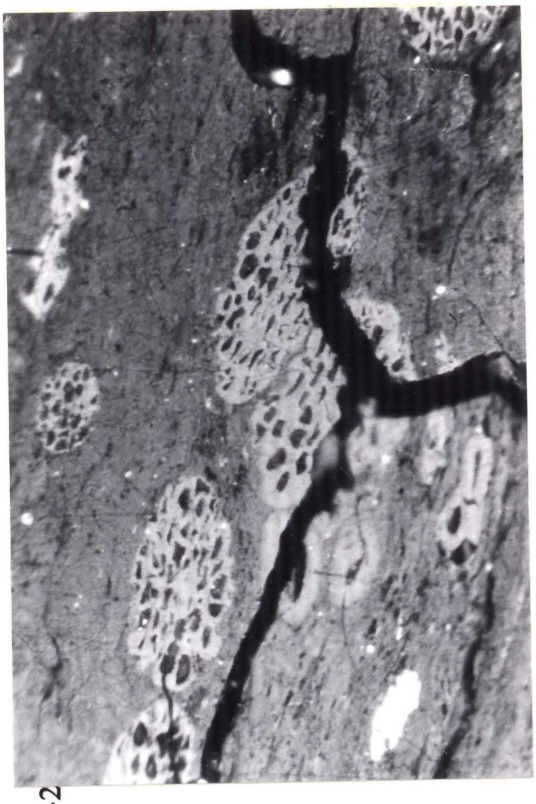

III-2

III-4

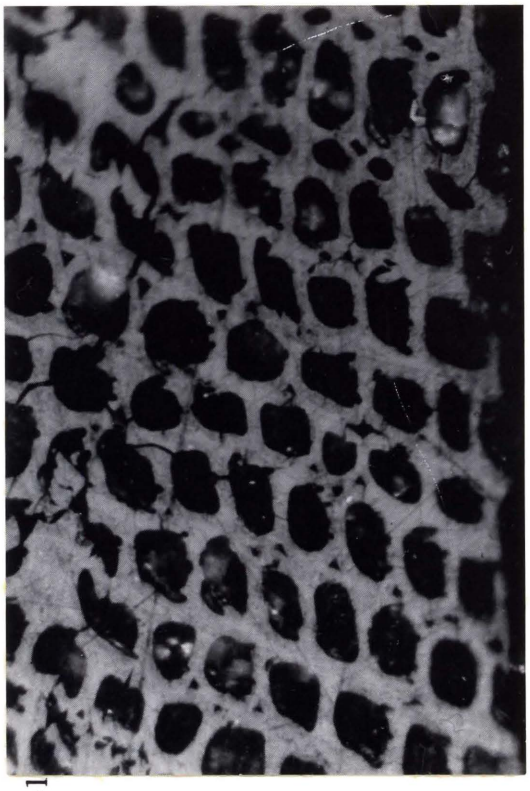

III-1

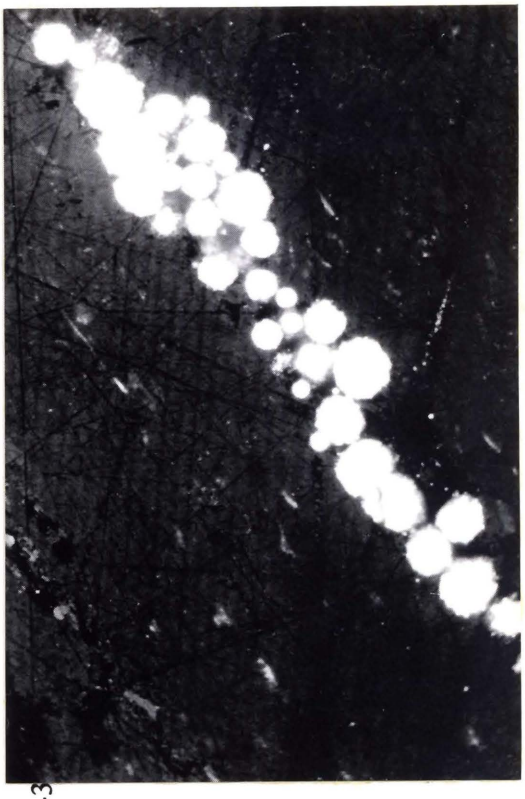

III-3

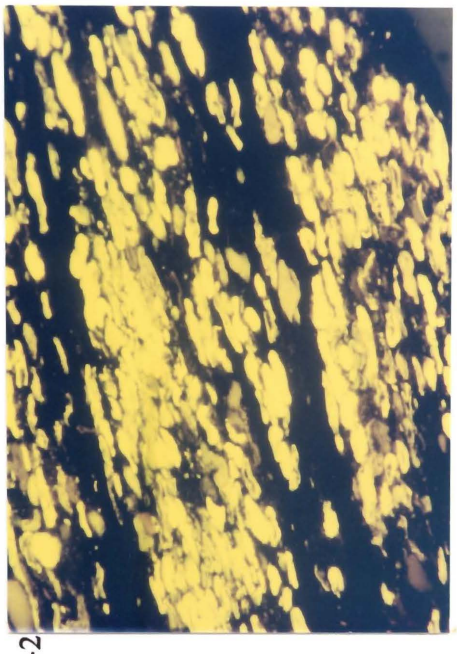

IV-2

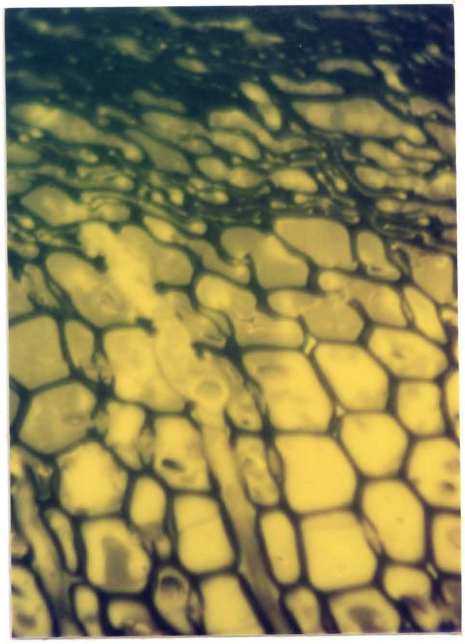

IV-4

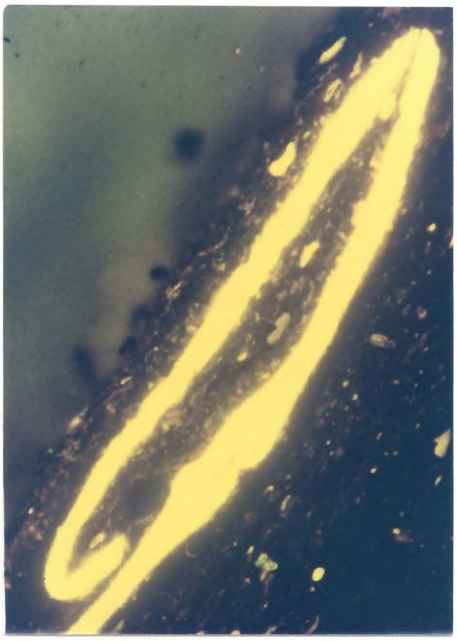

IV-1

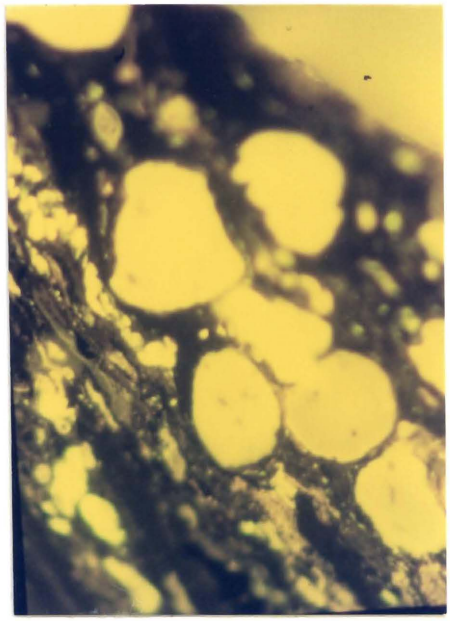

IV-3

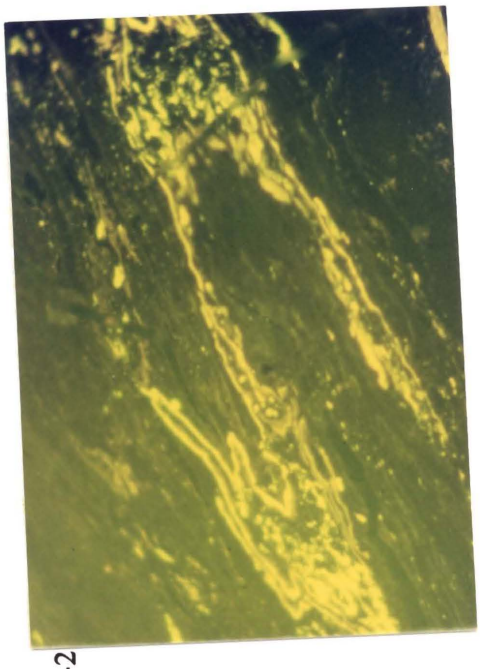

V-2

V-4

V-1

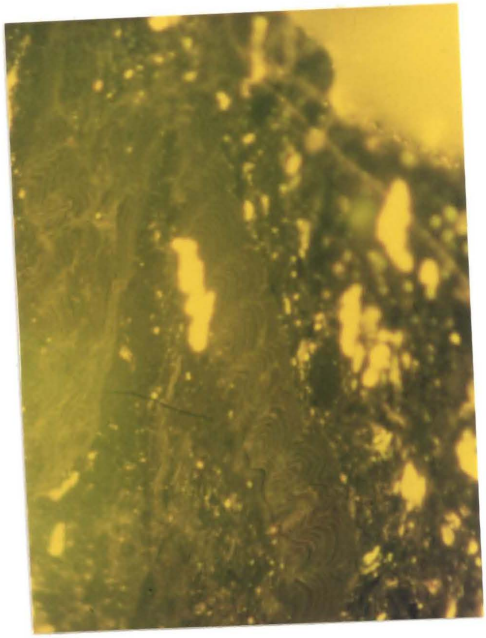

V-3

VI-1

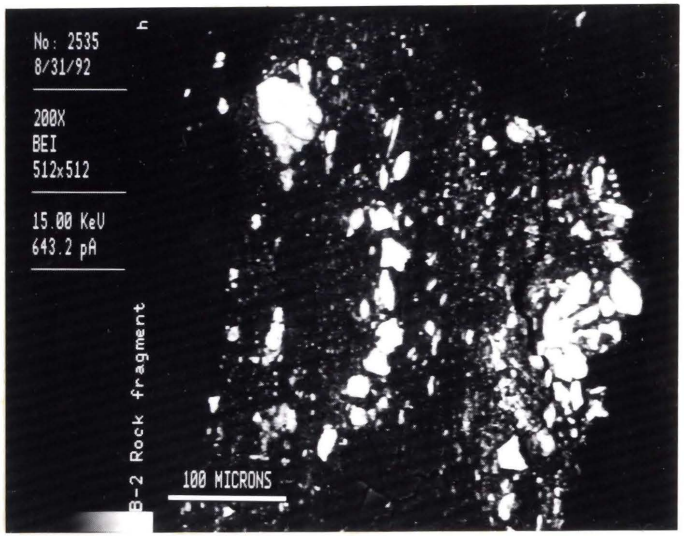

VI-2

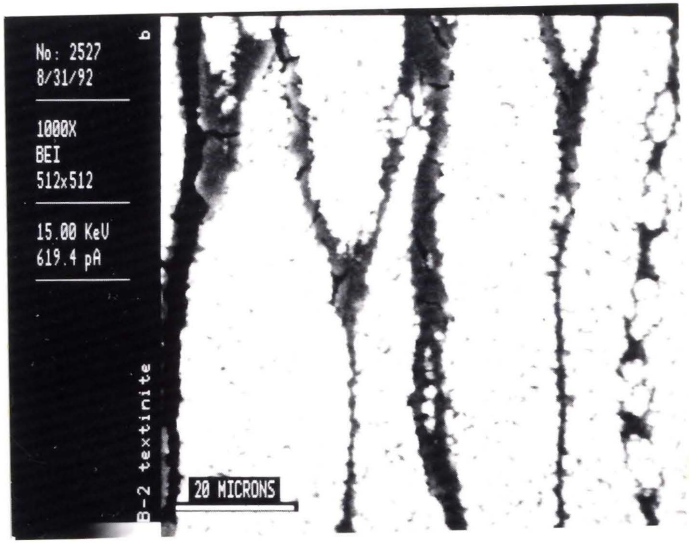

VI-3

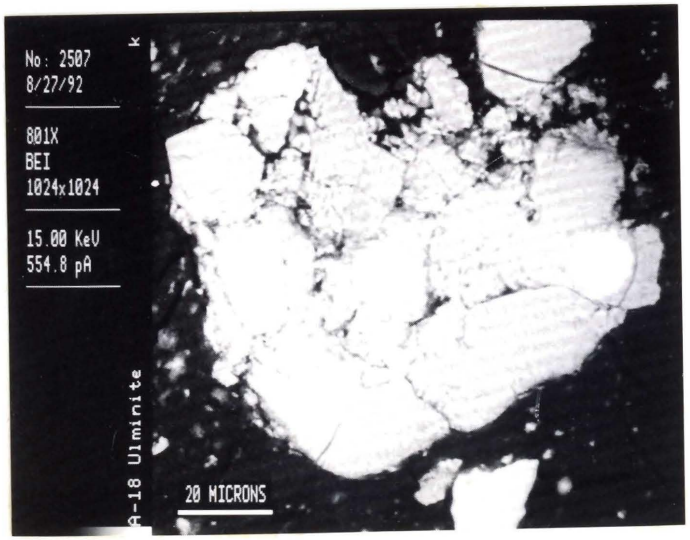

VI-4

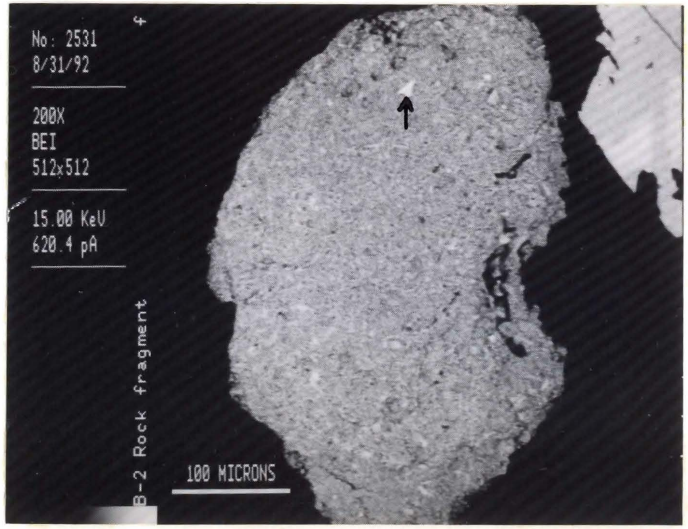

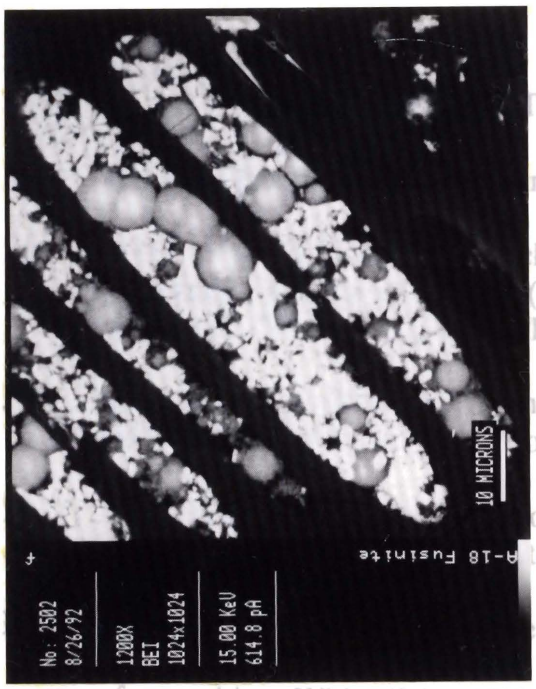

VII-2

VII-4

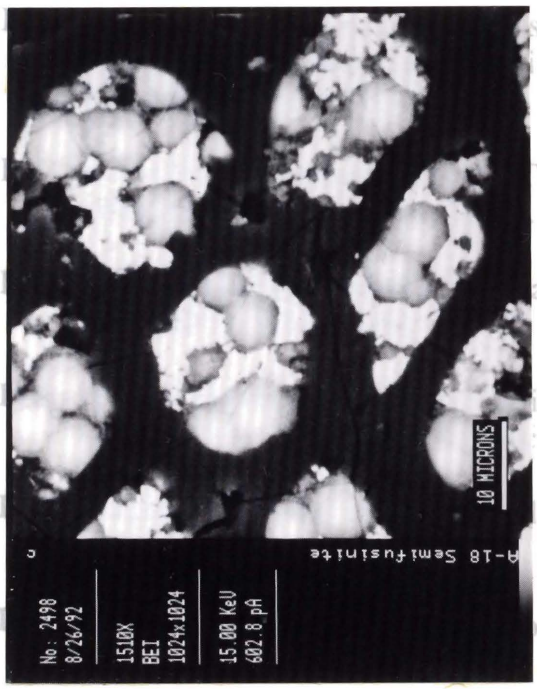

VII-1

VII-3

DESCRIPTION OF PLATES

I-1. Textinite B with open cell lumens. White light, 40X oil objective, chrome film.

I-2. Eu-ulminite B, left half: un-etched; right half: etched. It already has an appearance similar to vitrinite (telocollinite). Its woody structure is revealed by etching. White light, 40X oil objective, chrome film.

I-3. Attrinite (gray) mixed with some inertodetrinite (bright) and mineral (dark) particles. White light, 40X oil objective, tungsten film.

I-4. Densinite, the individual components are cemented tightly together in comparison with attrinite. White light, 40X oil objective, chrome film.

II-1. Detrogelinite including a few inertodetrinite particles. Un-etched detrogelinite (up-left) has similar appearance with eu-ulminite, but shows detritus structure after etching. White light, 40X oil objective, chrome film.

II-2. Tabular phlobaphinite and suberinite (dark cell walls). White light, 40X oil objective, chrome film.

II-3. Porigelinite and phlobaphinite as cell filling of ulminite. Porigelinite particles have high reflectance, already similar to micrinite. White light, 40X oil objective, chrome film.

II-4. Fusinite with high reflectance. The cell lumens are filled with kaolinite and crandallite (see also Plate III-8). White light, 40X oil objective, chrome film.

III-1. Semifusinite with cell-filling of crandallite(?) and kaolinite (see also Plates V-4 and VII-1). White light, 40X oil objective, chrome film.

III-2. Sclerotinite in detrogelinite matrix. Most of the sclerotinite particles are multi-celled. white light, 40X oil objective, chrome film.

III-3. Framboidal pyrite distributing along coal banding. White light, 40X oil objective, chrome film.

III-4. Post-diagenic pyrite in fractures of coal. White light, 40X oil objective, chrome film.

IV-1. A megaspore. Blue fluorescent light, 20X dry objective, chrome film.

IV-2. Microspores. Blue fluorescent light, 20X dry objective, chrome film.

IV-3. Isolated resin bodies. Blue fluorescent light, 40X oil objective, chrome film.

IV-4. Resinite as cell-filling in woody structure. Blue fluorescent light, 40X oil objective, chrome film.

V-1. Liptodetrinite. Blue fluorescent light, 40X oil objective, chrome film.

V-2. Amorphous, strong fluorescing fluorinite in association with band-like cutinite. Blue fluorescent light, 40X oil objective, chrome film.

V-3. The same picture as Plate II-2, but under blue fluorescent light, showing suberinite with weak fluorescence. 40X oil objective, chrome film.

V-4. The same picture as Plate III-1, but under blue fluorescent light. The cell-filled crandallite(?) shows strong fluorescence. 40X oil objective, chrome film.

VI-1. Fragmental quartz and kaolinite in detrogelinite matrix. Backscattered electron image, 15 Kev, 643.2 pA.

VI-2. Aggregates of fine kaolinite crystals (white) filling in the cell lumens of textinite (dark gray). Backscattered electron image, 15 Kev, 619.4 pA.

IV-3. Apatite (white) in association with kaolinite (light gray). The dark gray background is maceral detrogelinite, Backscattered electron image, 15 Kev, 554.8 pA.

VI-4. A fragmental apatite particle (angular and white) in tonstein fragment composed mainly of clay minerals. The other mineral on upper-right corner is calcite. Backscattered electron image, 15 Kev, 620.4 pA.

VII-1. Crandallite(?) (light gray ball-shaped particles) and kaolinite (white, amorphous particles) association as cell-filling of semifusinite (dark background). This is part of the area in Plates III-1 and V-4. Backscattered electron image, 15 Kev, 602.8 pA.

VII-2. Crandallite(?) (light grey ball-shaped particles) and fine kaolinite crystal (white) association as cell-filling of fusinite (Plate II-4). Some cell lumens are empty. Backscattered electron image, 15 Kev, 614.8 pA.

VII-3. A zircon particle (white particle in the center) in association with kaolinite (light gray), the dark grey matrix is maceral detrogelinite. Backscattered electron image, 15 Kev, 566.0 pA.

VII-4. A rutile particle (the white particle in the center) in detrogelinite matrix (dark gray). The light gray particles are kaolinite. Backscattered electron image, 15 Kev, 586.0 pA.

REFERENCES

Abbott, M. F. and Austin, L. G., 1986, Slag deposit initiation using a drop tube furnace: in Vorres, K. S., ed. Mineral Matter and Ash in Coal, ACS Symposium Series 301, Washington D. C..

American Society for Testing and Materials (ASTM), 1988a, Standard method for preparing coal samples for analysis (D2013), in Annual 1988 Book of ASTM Standards: p. 221-232.

American Society for Testing and Materials (ASTM), 1988b, Standard terminology relating to statistics (E456-88), in Annual 1988 Book of ASTM Standards: p. 300-308.

Ayers, W. B., Jr., 1986, Lacustrine and Fluvial-Deltaic Depositional System, Fort Union Formation (Paleocene), Powder River Basin, Wyoming and Montana: The American Association of Petroleum Geologists, v. 70, no. 11, p.1651-1673.

Ayers, W. B. and Kaiser, W. R., 1984, Lacustrine-interdeltaic coal in Fort Union Formation (Paleocene), Powder River Basin, Wyoming and Montana, in Rahmani, R. and Flores, R. M., eds., Sedimentology of coal and coal-bearing sequences: International Association of Sedimentologists Special Publication 7, p. 61-84.

Baker, A. A., 1928, The northward extension of the Sheridan coal field, Big Horn and Rosebud Counties, Montana: U. S. Geological Survey Bulletin, no. 806(b), p. 15-67.

Ball, C. G., 1935, Mineral matter of No. 6 bed coal at West Frankfort, Franklin County, Illinois: Illinois Geological Survey, Report of Investigation, no. 33, 106 p.

Bass, N. W., 1931-1932, The Ashland coal field, Rosebud, Powder River and Custer Counties, Montana: U. S. Geological Survey Bulletin, no. 831(b), p. 19-105.

Benson, S. A., Zygarlicke, C. J. and Karner, F. R., 1984, Occurrence of Detrital, Authigenic and Adsorbed inorganic Constituents in Lignite from the Beulah Mine, North Dakota: Proceedings: Symposium on the Geology of Rocky Mountain Coal: North Dakota Geological Society Publication 84-1, p. 12-27.

Benson, S. A. and Holm, P. L., 1985, Comparison of Inorganic Constituents in Three Low-Rank Coals: Ind. Eng. Chem. Res. Dev. 1985, 24, p. 145-149.

Benson, S. A. and Austin, L. G., 1990, Study of slag deposit initiation using a laboratory-scale furnace: in Bryers, R. W. and Vorres, K. S., eds., Mineral Matter and Ash Deposition, Engineering Foundation, New York, N.Y., p. 261-278.

Benson, S. A., Jones, M. L. and Harb, J. N., 1992, Ash formation and deposition: in Smoot, L. D., ed., Fundamentals of Coal Combustion for Clean and Efficent Use. Elsvier, p. 299-373.

Bustin, R. M., Cameron, A. R., Grieve, D. A. and Kalkreuth, W. D., 1983, Coal Petrology, Its Principles, Methods and Applications: Geological Association of Canada, Short Course Notes, Volume 3.

Casuccio, G. S., Gruelich, F. A., Hamburg, G., Huggins, F. E., Nissen, D. A. and Vleeskens, J. M., 1990, Coal mineral analysis: a check on interlaboratory agreement: Scanning Electron Microscopy, v. 4, no. 2, p. 227-236.

Cecil, C. B., Stanton, R. W., Allshouse, S. D. and Finkelman, R. B., 1978, Geologic controls on mineral matter in the Upper Freeport coal bed: proceedings: Symposium on coal cleaning to achieve energy and environmental goals, p. 110-125.

Chao, E. C. T., Minkin, J. A. and Thompson, C. L., 1983, Recommended Procedures of Coal Description: Geological Survey Circular 894, 31 p.

Chao, E. C. T., Minkin, J. A. and Back, J. M., 1984, Petrographic Characteristics and Depositional Environment of the Paleocene 61-m-thick Big George Coal Bed, Powder River Basin, Wyoming: in Houghton, R. L. and Clausen, E. N., eds., 1984 Symposium on the Geology of Rocky Mountain Coal, p. 41-60.

Cole, G., 1980, A guide to coal geology, resources and production: Montana Bureau of Mines and Geology, Special publication 83.

Crowley, S. S., Ruppert, L. F., Belkin, H. E. and Moore, T. A., 1992, The geochemistry of the Anderson-Dietz coal bed of the Powder River Basin, Montana, in relation to detrital and volcanic ash components: Abstracts and program, Ninth annual meeting of The Society of Organic Petrology, 1992.

Davis, A., Russel, S. J., Rimmer, S. M. and Yeakel,J. D., 1984, Some genetic implications of silica and aluminosilicates in peat and coal: Int. J. Coal Geol., v. 3, p. 293-314.

Demir. I. and Harvey R. D., 1991, Variation of organic sulfur in macerals of selected Illinois Basin coals: Org. Geochem. v. 17, no. 4, p. 525-533.

Diessel, K., 1982, An appraisal of coal facies based on maceral characteristics: Aust. Coal Geol., v. 4, no. 2, p. 474-484.

Diessel, K., 1986. The correlation between coal facies and depositional environments, In: Advances in the Study of the Sydney Basin; Proceedings of 20th Symposium, The University of Newcastle, p. 19-22.

Dobbin, C. E., 1929, The Forsyth coal field, Rosebud, Treasure and Big Horn Counties, Montana: U. S. Geological Survey Bulletin, no. 812(a), P. 1-55.

Energy Resources Co. Inc., 1980, Low Rank Coal Study, v. 2, Resource Characterization, Walnut Creek, Calif., p. 46-68.

Fleischer, M., 1980, Glossary of Mineral Species: Mineral Record, P.O. Box 35565, Tuscson, Arizona 85740, 192 p..

Flores, R. M., 1981, Coal deposition in fluvial Paleoenvironments of the Paleocene Tongue River Member of the Fort Union Formation, Powder River area, Powder River Basin, Wyoming and Montana, in Ethridge, F. G. and Flores, R. M., eds., Recent and Ancient Nonmarine Depositional Environments: Models for Exploration. Spec. Publs. Soc. Econ. Paleot. Miner., Tulsa, v. 31, p. 169-190.

Flores, R. M., 1982, Basin facies analysis of coal rich Tertiary fluvial deposits, northern Powder River Basin, Montana and Wyoming: Spec. Publs. Int. Assoc. Sediment. v. 6, p. 501-515.

Flores, R. M. and Ethridge, F. G., 1985, Evolution of Intermedin fluvial system of Tertiary Powder River Basin, Montana and Wyoming, in Flores, R. M. and Kaplan, S. S., eds., Cenozoic Paleogeography of west-central United States: Society of Economic Paleotonlogists and Mineralogists, Rocky Mountain Section, p. 107-126.

Flores, R. M., 1986, Styles of coal deposition in Tertiary alluvial deposits, Powder River Basin, Montana and Wyoming, in Lyons, P. C. and Rice, C. L., eds., Paleoenvironmental and Tectonic Controls in Coal-Forming Basins in the United States: The Geological Society of America Special Paper No. 210, p. 79-104.

Folkedahl, B. C., Kong, L. and Steadman, E. N., 1992. The analysis of coal macerals and their associated inorganics. Abstract and program, 9th International Pittsburgh coal conference, October 12-16, 1992

Fowkes, W. W., 1978, Separation and identification of minerals from lignites, in Karr, C., Jr., ed., Analytical methods for coal and coal products, v. II: Academic Press, Inc., p. 293-314.

Galbreath, K., 1993, Standard operating procedure for coal/ash mineral analysis by computer-controlled scanning electron microscopy: University of North Dakota Energy and Environmental Research Center unpublished report, Grand Forks, 14p..
Gary, M., McAfee, R., Jr. and Wolf, C. L., eds., 1972, Glossary of Geology: American Geological Institute, Washington, D. C., 805 p..

Gentzis, T. and Goodarzi, F., 1990. Petrology, depositional environment and utilization potential of Late Paleocene coals from the Obed-Marsh deposit, West-Central Alberta, Canada: Int. J. Coal Geol., v. 16, p. 287-308.

Given, P. H., 1984, An essay on the organic geochemistry of coal, in M. L. Gorbaty, J. W. Larsen, and I. Wender, ed., Coal Science, v. 3, 137.

Given, P. H. and Miller, R. N., 1987, The association of major, minor and trace inorganic elements with lignites. III. Trace elements in four lignites and general discussion of all data from this study: Geochimica et Cosmochimica Acta, v. 51, p. 1843-1853.

Hacquebard, P. A. and Donaldson, J. R., 1969, Carboniferous coal deposition associated with floodplain and limnic environments in Nova Scotia, in E. C. Dapples and M. E. Hopkins (Editors), Environments of Coal Deposition. Geo. Soc. Am. Spec. Pap., no. 114, p. 143-191.

Harris, L. A., Yust, C. S. and Crouse, R. S., 1977, Direct determination of pyritic and organic sulfur by combined coal petrography and microprobe analysis (CPMA) - a feasibility study: Fuel, v. 56, p. 393-396.

Harrison, C. H., 1991, Electron microprobe analysis of coal macerals: Org. Geochem. v. 17, v. 4, p. 439-449.

Harvey, R. D. and Ruch, R. R., 1984, Overview of mineral matter in U. S. coals: ACS, Div. Fuel Chem., Preprints, v. 29, no. 4, p. 76-83.

Hippo, E. J., Crelling, J. C. and Malhotra, V. M., 1991, Molecular Structure of Coal and Coal macerals: EPRI EAR/GS-7437, Project 8003-21 Final Report.

Hunt, J. W., 1982, Relationship between microlithotype and maceral composition of coals and geological setting of coal measures in the Permian basins of eastern Australia: Aust. Coal Geol., v. 4, no. 2, p. 484-502.

Hunt, J. W. and Hobday, D., 1984, Petrographic composition and sulfur content of coals associated with alluvial fans in Permian Sydney Basin and Gunnedah Basins, eastern Australia: Int. Assoc. Sedimentol. Spec. Pupl., v. 7, p. 43-60.

Hunt, J. W. and Smyth, M., 1989, Origin of inertinite rich coals of Australia Cratonic basins: Int. J. Coal Geol., v. 12, p. 381-424.

International Committee for Coal Petrology (ICCP), 1963, Handbook of Coal Petrography (2nd edition): Centre National de la Recherche Scientifique, Paris, France.

International Committee for Coal Petrology (ICCP), 1971, International Handbook of Coal Petrography (Supplement 1): Centre National de la Recherche Scientifique, Paris, France.

International Committee for Coal Petrology (ICCP), 1975, International Handbook of Coal Petrography (Supplement 2): Centre National de la Recherche Scientifique, Paris, France.

Jones, M. L. and Benson, S. A., 1987, An overview of fouling/slagging with western coals: Conference on effects of coal quality on power plants, Atlanta, Georgia, October 13-15, 1987.

Kalkreuth, W. D., Marchioni, D. L. Calder, J. H., Lamberson, M. N., Naylor, R. D. and Paul, J., 1991a, The relationship between coal petrography and depositional environments from selected coal basins in Canada: Int. J. Coal Geol. v. 19, p. 21-76.

Kalkreuth, W., Kotis, T., Papanicolaou, C. and Kokkinakis, P., 1991b, The geology and coal petrology of Miocene lignite profile at Meliadi Mine, Katerini, Greece: Int. J. Coal Geol., v. 17, p. 51-67.

Kanza, E. G. J., 1983, Comparative petrography of selected Montana coals: Montana College of Mineral Science and Technology Master's thesis, Butte, Montana, 65 p..

Karner, F. R., Kleesattel, D. R., Schobert, H. H. and Huber, T. P., 1982, Inorganic chemistry of huminite group macerals in four low-rank coals of the Western United States: Geol. Soc. Am. Abstracts with programs, v. 17, P. 623.

Karner, F. R., Benson, S. A., Schobert, H. H. and Roaldson, R. G., 1984, Geochemical variation of inorganic constituents in a North Dakota lignite, in Schobert, H. H., ed., The Chemistry of Low Rank Coals: ACS symposium series 264, 175.

Karner, F. R., Schobert, H. H. and Benson, S. A., 1986a, Elemental distribution and association with inorganic and organic components in North Dakota lignites, in Vorres, Karl S., ed., Mineral Matter And Ash in Coal: American Chemical Society, p. 71-89.

Karner, F. R., Hoff, J. L. and Schobert, H. H., 1986b, Electron microprobe technique for quantitative analysis of coal and coal macerals: Work performed under cooperative agreement No. DE-FC2183FE60181 for U.S. Department of Fossil Energy, Morgantown Energy Technology Center, Grand Forks Project Office, Grand Forks, N. D., Presented at the National Meeting of the American Chemistry Society, New York.

Karner, F. R., Schobert, H. H., Zygarlicke, C. J., Hoff, J. L. and Huber, T. P., 1987, Quantitative analysis of coal and coal components by scanning electron microscopy and electron microprobe analysis: American Chemical Society Preprints of Paper, v. p. 49-57.

Kleesattel, D. R., 1985, Petrology of the Beulah-Zap lignite bed, Sentinel Butte formation (Paleocene), Mercer County, North Dakota: Unpublished M. S. Thesis, University of North Dakota, Grand Forks, N. D., 187p..

Knappen, R. S. and Moulton, G. F., 1930, Geology and mineral resources of parts of carbon, Big Horn, Yellowstone and Stillwater Counties, Montana: U. S. Geological Survey Bulletin, no. 822(a), p. 1-70.

Kong, L., Karner, F. R., Steadman, E. N. and Benson S. A., 1992. Petrographic variation in the Rosebud coal, Powder River Basin, Montana. Abstract and program, 9th annual meeting of the Society for Organic Petrology, July 23-24, University Park, Pennsylvania.

Kong, L., Karner, F. R., Benson, S. A. and Steadman, E. N., 1993 (in press). Petrologic analysis of the Rosebud seam at the Absaloka, Big Sky and Rosebud mines, Powder River Basin, Montana: Organic Geochemistry.

Mackowsky, M-Th., 1968, Mineral matter in coal, in Murchison, D. G. and Westall, T. S., eds., Coal and coal-bearing strata: American Elsevier, New York, p. 309-321.

Marchioni, D. 1980, Petrography and depositional environment of the Liddell Seam, Upper Hunter Valley, New South Wales: Int. J. Coal Geol. v. 1, p. 35-62.

Moore, T. A., 1986, Characteristics of coal bed splitting in the Anderson-Dietz coal seam (Paleocene), Powder River Basin, Montana: Unpublished M. S. Thesis, University of Kentucky, Lexington, KY, 109 p.

Moore, T. A., 1990, The effects of clastic sedimentation on organic facies development within a Tertiary subbituminous coal bed, Powder River Basin, Montana, U. S. A.: Int. J. Coal Geol., v. 18, p. 187-209.

Moore, T. A., Stanton, R. W., Pocknall, D. T. and Flores R. M., 1990, Maceral and palynomorph facies from two Tertiary peat-forming environments in the Powder River Basin, U. S. A.: Int. J. Coal Geol., v. 15, p. 293-316.

Mukhopadhyay, P., 1986, Petrography of selected Wilcox and Jackson Group lignites from the Tertiary of Texas, in R. Finkelman and D. Casagrande, eds., Geology of Gulf Coast Lignites: The 1986 Annual meeting of the Geological Society of America, Coal Geology Division, Field Trip, p. 126-145.

Noyes, R., ed., 1978, Coal Resources, Characteristics and Ownership in the U.S.A., Noyes Data Corp., N. J., 1978.

Parr, S. W., 1932, The analysis of fuel, gas, water, and lubricants: McGraw-Hill, New York, 49 p.

The Pennsylvania State University Coal Research Section, 1983, Preparation of coal sample for megascopic inspection: Short Course in the Theory and Practice of Coal Petrology, June 6-9, 1983, University Park, Pennsylvania.

Pierce, W. G., 1936, The Rosebud coal field, Rosebud and Custer Counties, Montana: U. S. Geological Survey Bulletin, no. 847(b), p. 43-120.

Raymond, R., Jr. and Gooley, R., 1978, A review of organic sulfur analysis in coal and a new procedure: Scanning Electron Microscopy, I, SEM Inc. AMF O'Hare (Chicago), p. 93-106.

Rich, F. J., Dorsett, R. K. and Chapman, C. R., 1988, Petrography, sedimentology and geochemistry the Wyodak coal, Wyodak, Wyoming: Wyoming geological association Guidebook, Thirty-ninth field conference, p.237-247.

Rogers, G. S. and Lee, W., 1923, Geology of the Tullock Creek coal field, Rosebud and Big Horn Counties, Montana: U. S. Geological Survey Bulletin, no.749. 180 p..

Sarofim, Adel F., Howard, Jack B. and Padia, Ashok S., 1977, The physical transformation of the mineral matter in pulverized coal under simulated combustion conditions: Combustion Science and Technology, v. 16, p. 187-204.

Schopf, J. M., 1960, Field description and sampling of coal beds: Geol. Surv. Bull. 1111-B. 67 p.

Smyth, M., 1979. Hydrocarbon generation in the Fly Lake-Brolga area of the Cooper Basin: J. Aust. Petrol. Explor. Ass. v. 19, p. 108-114.

Smyth, M., 1984. Coal microlithotypes related to sedimentary environments in the Cooper Basin, Australia, in R. A. Rahmani and R. M. Flores, eds., Sedimentary of Coal and Coal-bearing Sequences: Special publication of the International Association of Sedimentologists, p. 333-348.

Spackman, W., Dolsen, C. P. and Riegel, W., 1966, Phytogenic sediments and sedimentary environments in the Everglades-Mangrove complex: Paleontographica, 117B, p. 135-152.

Sprunk, G. C. and O'Donnell, H. J., 1942, Mineral matter in coal: U.S. Bureau of Mines, Technical Paper 648, 67 p.

Stach, E., Mackowsky, M.-TH., Teichmuller, M., Taylor, G. H., Chandra,D., and Teichmuller, R., 1982, Stach's Textbook of Coal Petrology: Gebruder Borntraeger, Berlin, Stuttgart, Germany, 553 p.

Stanton, R. W., Moore, T. A., Warwick, P. D., Crowley, S. S. and Flores, R. M., 1989, Comparative facies formation in selected coal beds of the Powder River Basin, in Flores, R. M., ed., Tertiary and Cretaceous coals in the Rocky Mountains, 28th international geological congress, June-July, 1989.

Steadman, N. E., Zygarlicke, C. J., Benson, S. A. and Jones, M. L., 1990, A microanalytical approach to the characterization of coal, ash, and deposits: ASME Seminar on Fireside Fouling Problems, Brigham Young University, Provo, Utah, April, 1990.

Stopes, M. C., 1919, On the four visible ingredients in banded bituminous coal: Proc. Roy. Soc. B, London, v. 90, p. 470-478.

Stopes, M. C., 1935, On the petrology of Banded coal: Fuel v. 14, no. 1, p. 4-13.

Swanson, V. E. and Huffman, C., Jr., 1976, Guideline for sample collection and analytical methods used in U. S. Geological Survey for determining chemical composition: U. S. Geol. Surv. Circular 735, 31 p.

Teichmuller, M., 1950, Zum petrographischen Aufbau und Werdegang der Wiechbraunkohl (mit Berucksichtigung genetischer Fragen der Steinkohlenpetrographie): Geol. Jahrb., v. 64, p. 429-488.

Teichmuller, M., 1952, Vergleichende mikroskopische Untersuchungen versteinerter Torfe des Ruhrkarbons und der daraus entstandenen Steikohlen. C. R., 3rd Congr. Stra. Geol. Carbonif., Maastricht, 2, p. 607-613.

Teichmuller, M. and Thomson, P. W., 1958, Vergleichende mikroskopische und chemische Untersuchungen der niederrheinischen Braunkohle: Fortschr. Geol. Rheinld. Westf., 2, p. 573-589.

Thiessen, R., 1920, Structure in Paleozoic bituminous coals: Bur. Mines Bull. 117, 296 p.

Thiessen, R. and Francis, W., 1929, Terminology in coal research: Fuel, v. 8, p. 385-405.

Triplehorn, D. M., Stanton, R. W., Rupper, L. F. and Crowley, S. S., 1991, Volcanic ash dispersed in the Wyodak-Anderson coal bed, Powder River Basin, Wyoming: Organic Geochem, v. 17, no. 4, p. 567-575.

Warwick, P. D. and Stanton, R. W., 1988, Petrographic characteristics of Wyodak-Anderson coal bed (Paleocene), Powder River Basin, Wyoming, U.S.A.: Organic Geochem., v. 12, no. 4, p. 389-399.

Weisbecker, T., Zygarlicke, C. J. and Jones, M. L., 1992. Correlation of inorganics in Powder River Basin coals in full-scale combustion, in S. A. Benson, ed., Inorganic Transformation and Ash Deposition During Combustion, American Society of Mechanical Engineers, New York, N. Y., p. 699-711.

White, D. and Thiessen, R., 1913, The origin of coals: U. S. Bur. Mines Bull. 38, Washington D.C., 390 p..

Zygarlicke, C. J., 1987, A mineralogy study of the Harmon lignite bed, Bullion Creek Formation (Paleocene), Bowman County, North Dakota: Unpublished M. S. Thesis, University of North Dakota, Grand Forks, N. D., 187p..

Zygarlicke, C.J.; Steadman, E.N., 1990, Advanced SEM techniques to characterize coal minerals: Scanning Electron Microscopy, v. 4 no. 3, p. 579-590.